**Project Title:** One Step Biomass Gas Reforming-Shift Separation Membrane Reactor

**Type of Report:** Final Scientific Report

**Project Period:** February 1, 2007
September 30, 2012

**Principal Authors:** Michael Roberts (GTI), Razima Souleimanova (GTI), Mark Davis (SCHOTT), Bret Howard (NETL), Bryan Morreale (NETL), Jerry Lin (ASU)

**Date of Report:** December 28, 2012
**Award Number:** DE-FG36-07GO17001

**Recipient:** Gas Technology Institute
1700 South Mount Prospect Rd
Des Plaines, IL 60018

**Working Partners:** Gas Technology Institute, National Energy Technology Laboratory (NETL), Pittsburgh, PA; Schott North America, Duryea, PA; ATI Wah Chang, Albany, OR

**Cost-Sharing Partners:** Gas Technology Institute, DesPlaines, IL; National Energy Technology Laboratory (NETL), Pittsburgh, PA; Schott North America, Duryea, PA; ATI Wah Chang, Albany, OR

## Disclaimer

**"This report was prepared as an account of work sponsored by an agency of the United States Government. Neither the United States Government nor any agency thereof, nor any of their employees, makes any warranty, express or implied, or assumes any legal liability or responsibility for the accuracy, completeness, or usefulness of any information, apparatus, product, or process disclosed, or represents that its use would not infringe privately owned rights. References herein to any specific commercial product, process, or service by trade name, trademark, manufacturer, or otherwise does not necessarily constitute or imply its endorsement, recommendation, or favoring by the United States Government or any agency thereof. The views and opinions of authors expressed herein do not necessarily state or reflect those of the United States Government or any agency thereof."**

## Executive Summary

GTI developed a plan where efforts were concentrated in 4 major areas: membrane material development, membrane module development, membrane process development, and membrane gasifier scale-up. GTI assembled a team of researchers to work in each area: Task 1.1 Ceramic Membrane Synthesis and Testing was conducted by Arizona State University (ASU), Task 1.2 Metallic Membrane Synthesis and Testing was conducted by the U.S. National Energy Technology Laboratory (NETL), Task 1.3 was conducted by SCHOTT, and GTI was to test all membranes that showed potential. The initial focus of the project was concentrated on membrane material development. Metallic and glass-based membranes were identified for investigation as hydrogen selective membranes under the conditions of the biomass gasification, temperatures above 700ºC and pressures up to 30 atmospheres. Membranes were synthesized by arc-rolling for metallic type membranes and by incorporating Pd into a glass matrix for glass membranes. Testing for hydrogen permeability properties were completed and the effects of hydrogen sulfide and carbon monoxide were investigated for perspective membranes. The initial candidate membrane, $Pd_{80}Cu_{20}$ was chosen in 2008 for preliminary reactor design and cost estimates.

All ceramic membranes synthesized by ASU during the project showed low hydrogen flux as compared with metallic membranes. The best ceramic membrane showed hydrogen permeation flux of 0.03 SCFH/ft$^2$ at the required process conditions while the metallic membrane, $Pd_{80}Cu_{20}$ showed a flux of 47.2 SCFH/ft$^2$ (3 orders of magnitude difference)

Results from NETL showed the $Pd_{80}Cu_{20}$ alloy membrane had the highest flux; therefore it was chosen as the initial and eventually, final candidate membrane. The criteria considered were high hydrogen flux, long-term stability, and $H_2S$ tolerance.

Results from SCHOTT showed a maximum of 0.25 SCFH/ft$^2$ using glass membranes. Although this is an order of magnitude better than the ceramic membrane, the flux from glass membranes is still two orders of magnitude lower than the metallic membrane.

Although the H2A [1] (Hydrogen Analysis) analysis results indicated a $1.96 cost per gge (gasoline gallon equivalent) $H_2$ based on a 5µm thick Pd-Cu membrane, long-term operation at the required flux to satisfy the go/no go decision was unsuccessful. Further, since the future PSA case yielded a $2.00/gge $H_2$, DOE decided that there was insufficient savings compared with the already proven PSA technology to continue pursuing the membrane reactor design.

A membrane module was designed to be tested with an actual biomass gasifier. Some parts for the module were ordered but the work was stopped as a result of the no go.

**Table of Contents**

## Task 1. Membrane material development

The GTI project team has focused on ceramic, metallic and glass types of membranes and combination of these materials in this task. Under each subtask, the project team synthesized and tested membranes for H2 permeation and investigated thermal and chemical stability An important objective of this task was to select candidate membrane materials for the membrane module design, fabrication and integrated testing with the bench scale biomass gasifier.

### Task 1.1 Ceramic Membrane Synthesis and Testing

A dense thin-ceramic membrane fabricated from mixed protonic and electronic conductors provides a simple and efficient means for the $H_2$ separation from coal derived syngas at high temperature (~900ºC). ASU developed $SrCe_{0.95}Tm_{0.05}O_3$ with improved electronic conductivity of the order of $10^{-2}$ S/cm, which can be improved further to enhance $H_2$ flux. Hence, the objective of this research project is to identify the optimum composition of strontium cerate membranes, with improved electronic and protonic conductivity, and chemical stability.

**Membrane synthesis by the liquid citrate method**

In the liquid citrate method, stoichiometric amounts of the corresponding metal nitrates were mixed with citric acid in distilled water. The amount of citric acid was three times the total molar amount of metal ions present. The transparent liquid was heated to 95-100°C and remained there under reflux and stirring for 4 hours for the polymerization reaction to occur. The lid was then removed and excess water was evaporated off at 100°C leaving the solution a viscous gel. The solution was dried for 24 hours at 110°C and resulting brittle, porous material was heated to 400°C for self-ignition to burn out the presented organics. The material was then grinded with a mortar and pestle for 15 minutes and then calcined at 850°C for 8 hours (ramp rate = 5°C/min). After calcinations, the powder was ground again for 15 minutes using a mortar and pestle. Then powder samples were sintered at 1495°C for 24 hours in a furnace (Thermolyne, 46100) with a ramp rate of 2°C/min. The sintered powder samples were then used for X-ray diffraction analysis. Different membranes were synthesized: $SrCe_{1-x}Tm_xO_{3-\delta}$ (x = 0.0 – 0.5), $SrCe_{0.95-x}Zr_xTm_{0.05}O_{3-\delta}$ ($0.0 < x \leq 0.95$).

In order to improve the stability of $SrCe_{0.95}Tm_{0.05}O_{3-\delta}$ in highly reducing and harsh environments, zirconium (Zr) was chosen as a dopant.

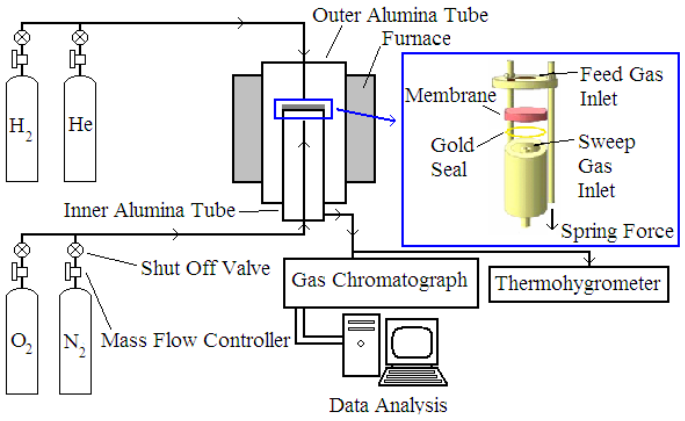


Figure 1. Schematic of high temperature permeation apparatus.

A high temperature permeation setup, as shown in Figure 1, was used to test hydrogen permeation of synthesized membranes. The first step for measuring the hydrogen permeation flux through a membrane is to seal the membrane within the system. The set-up was heated to high temperature (1050°C) to soften the gold seal so the membrane can be pressed into the gold seal ensuring minimal leakage during the $H_2$ permeation flux experiments. After sealing, the set-up was heated to experimental temperature range, the He and Ar gas flows were started once again and the leakage rate was verified before the $H_2$ permeation flux tests were started.

The gases had been introduced and the system was allowed to equilibrate for 3 hours before samples were taken. The relative humidity detected in the sweep gas using a thermohygrometer (Cole Palmer, 37950) was used to determine the flux of $H_2$ through the membrane. The experimental temperature range was 700 - 900°C and temperature ramp rate used during the experiments was 120°C/hour. The system was allowed to equilibrate for 1 hour after a temperature change. Once the gases had been introduced, the system was allowed to equilibrate for 3 hours before samples were taken. The sweep gas was analyzed with a gas chromatographer (Hewlett Packard, 5890 Series II) with a packed column (2836PC, Alltech) and TCD detector. The $H_2$ and He in the sweep were used to quantify the leak through the seal and the flux through the membrane. The experimental temperature range was 700 - 900°C and temperature ramp rate used during the experiments was 120°C/hour. The system was allowed to equilibrate for 1 hour after a temperature change.

## Permeation tests' results

The $H_2$ permeation test was performed with a 1 mm thick gas tight $SrCe_{0.95}Tm_{0.05}O_{3-\delta}$ membrane with 10% $H_2$/He on the feed side and air on the sweep side. Helium leakage through the seal was ~1% and the $H_2$ permeation flux through the seal was corrected accordingly. Figure 2 shows the $H_2$ permeation flux through the $SrCe_{0.95}Tm_{0.05}O_{3-\delta}$ membrane. The highest measured flux was $1.337 \times 10^{-7}$ mol/cm$^2$-s at 900°C.

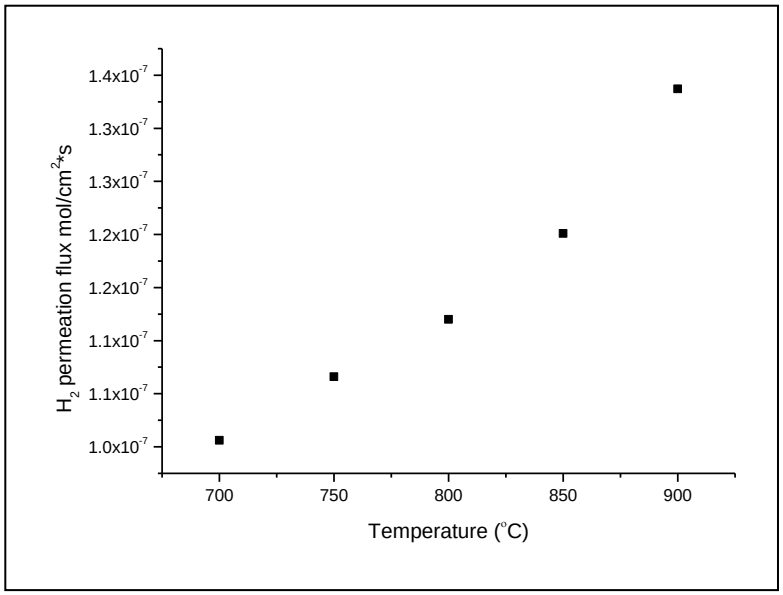


Figure 2. $H_2$ permeation flux through a 1 mm $SrCe_{0.95}Tm_{0.05}O_{3-\delta}$ membrane with a 10% $H_2$/He and air gradient

Figure 3 shows the composition of the sweep gas before, during, and after $H_2$ permeation flux experiments. All leak tests were conducted with a He feed gas and an Ar sweep gas.

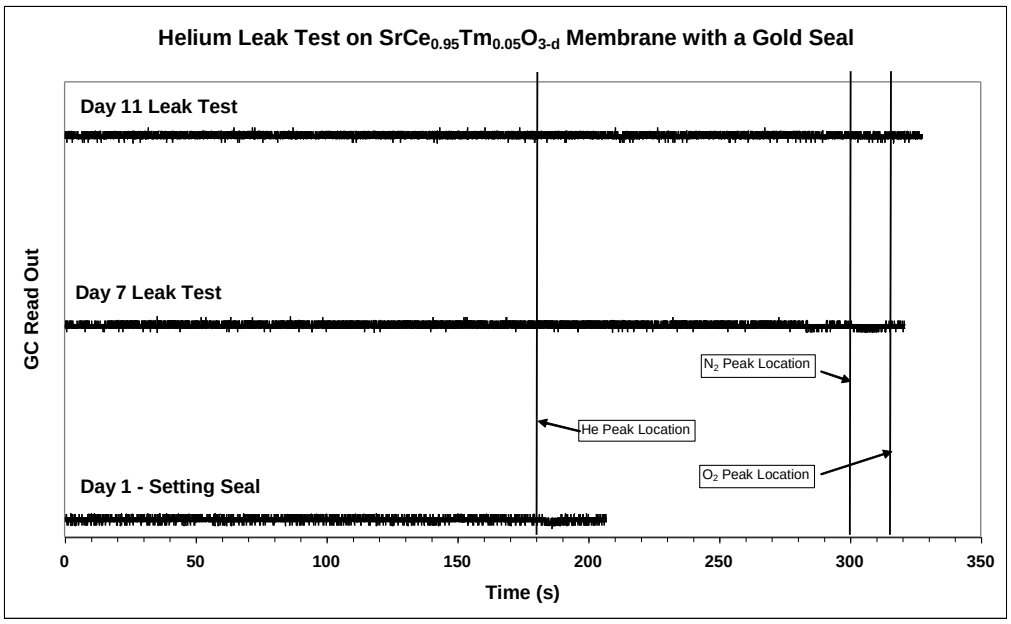


Figure 3. Gold seal leak test

If there was a leak associated with the gold seal, a He peak would be evident at ~180 s. If there was an air leak anywhere in the system, nitrogen and oxygen peaks would be visible at 300 and 315 s, respectively. As shown in Figure 3, the system has no leaks and can maintain a gas tight seal on the membrane for an extended period of time in reducing environments. Figure 4 shows the $H_2$ permeation flux through the membrane with 10% $H_2$/He on the feed side and air on the sweep side. The highest measure flux was $2.43 \times 10^{-8}$ mol/cm$^2$*s (0.036 mL/cm$^2$-min) at 900°C.

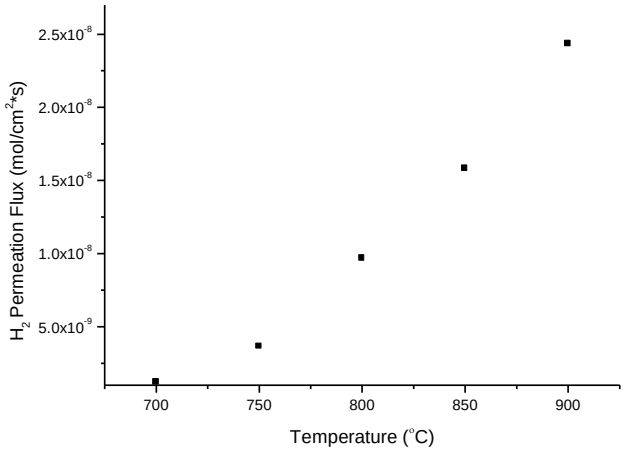


Figure 4. $H_2$ permeation flux through a 1.25 mm $SrCe_{0.95}Tm_{0.05}O_{3-\delta}$ membrane with a 10%$H_2$/He and air gradient

Also, such membranes as 1.2 mm thick $SrCe_{0.95}Tm_{0.05}O_{3-\delta}$, 1.2 mm thick $SrCe_{0.75}Zr_{0.20}Tm_{0.05}O_{3-\delta}$, and a 1.0 mm thick $SrCe_{0.75}Zr_{0.20}Tm_{0.05}O_{3-\delta}$ were tested. Figure 5 compares the $H_2$ permeation flux through each membrane at 900°C with different $H_2$ partial pressures on the feed side and an Ar sweep gas.

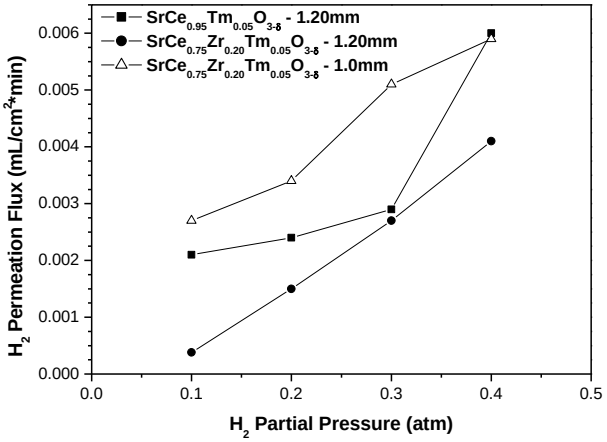


Figure 5. Effect of $H_2$ feed pressure on the $H_2$ permeation flux at 900°C with an Ar sweep gas

The $H_2$ permeation flux increases with increasing $H_2$ partial pressure on the feed side for all membranes tested due to an increase in the driving force. The $H_2$ permeation flux is higher through a $SrCe_{0.95}Tm_{0.05}O_{3-\delta}$ membrane than a $SrCe_{0.75}Zr_{0.20}Tm_{0.05}O_{3-\delta}$ membrane of the same thickness due to the higher conductivity of $SrCe_{0.95}Tm_{0.05}O_{3-\delta}$. Another trend is the $H_2$ permeation flux through $SrCe_{0.75}Zr_{0.20}Tm_{0.05}O_{3-\delta}$ increases proportionally as the membrane thickness decreases, indicating the flux is limited by bulk diffusion of the proton ions only.

Another experiment conducted on all three membranes consisted of a feed composition of 20% $H_2$/He and a 4% CO/Ar sweep. CO was added to the sweep side to observe if a very low $O_2$ partial pressure on the sweep side would have an effect on the $H_2$ flux through the membrane. Figure 6.

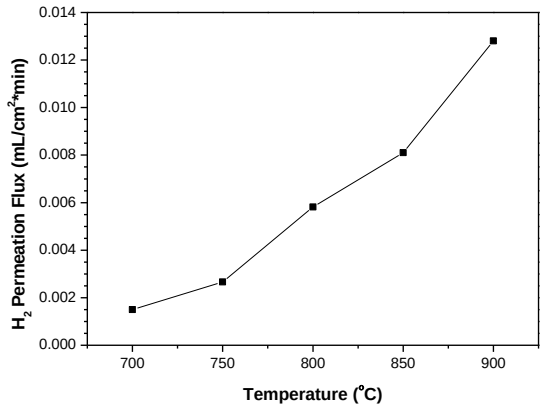


The $H_2$ permeation flux through a 1.2 mm thick $SrCe_{0.95}Tm_{0.05}O_{3-\delta}$ membrane with a 4% CO/Ar sweep gas.

The $H_2$ permeation flux through the $SrCe_{0.95}Tm_{0.05}O_{3-\delta}$ membrane is shown in Figure 6. The $H_2$ permeation flux value at 900°C in Figure 6 (0.013 mL/cm$^2$-min) is higher than the value measured with a 20% $H_2$/He feed gas mixture in Figure 5 (0.0024 mL/cm$^2$-min) for the same $SrCe_{0.95}Tm_{0.05}O_{3-\delta}$ membrane.

When only Ar is used as the sweep gas, the $O_2$ partial pressure in the sweep gas is ~$10^{-4}$ atm, which is dependent on the $O_2$ impurity content of the tank. When CO is introduced on the sweep side, the $O_2$ partial pressure on the sweep side is drastically lower and the total conductivity is higher in the experimental temperature range. A higher total conductivity in this case means a higher electronic conductivity (it has been previously shown that $SrCe_{0.95}Tm_{0.05}O_{3-\delta}$ does not conduct oxygen ions). Therefore, enhanced electronic conductivity at very low $O_2$ partial pressures leads to higher $H_2$ permeation flux values for $SrCe_{0.95}Tm_{0.05}O_{3-\delta}$. $SrCe_{0.75}Zr_{0.20}Tm_{0.05}O_{3-\delta}$ membranes showed lower or $H_2$ permeation fluxes below the detection limit of the data analysis system when 4% CO/He was the sweep gas as the total conductivity of $SrCe_{0.75}Zr_{0.20}Tm_{0.05}O_{3-\delta}$ is lower in extremely low $O_2$ partial pressures than in an Ar environment.

Figure 7 shows the $H_2$ permeation flux through a 1.0 mm thick $SrCe_{0.75}Zr_{0.20}Tm_{0.05}O_{3-\delta}$ membrane with 10% $H_2$/He on the feed side and 20% $O_2$/Ar on the sweep side.

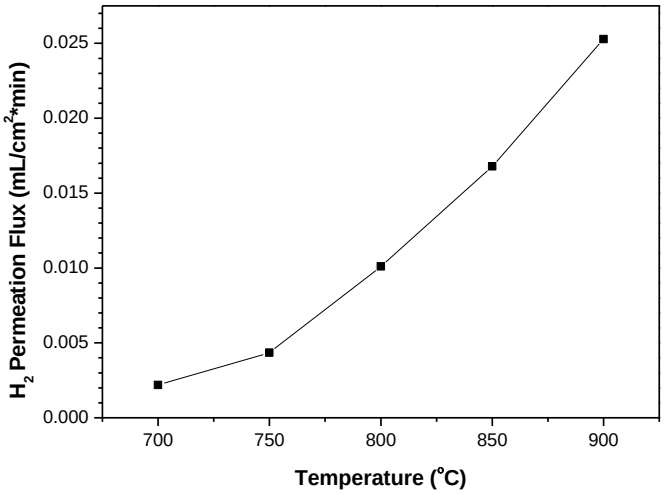


Figure 7. $H_2$ permeation flux through a 1.0 mm $SrCe_{0.75}Zr_{0.20}Tm_{0.05}O_{3-\delta}$ membrane with a 20% $O_2$/Ar sweep

The $H_2$ permeation flux at 900°C in Figure 7 (0.025 mL/cm$^2$-min) is higher than the flux measured with a 10% $H_2$/He feed gas mixture in Figure 5 (0.0027 mL/cm$^2$-min) for the same $SrCe_{0.75}Zr_{0.20}Tm_{0.05}O_{3-\delta}$ membrane. The difference in flux values can be attributed the reaction of the hydrogen that has transported through the membrane with $O_2$ on the sweep side to form water molecules and $SrCe_{0.75}Zr_{0.20}Tm_{0.05}O_{3-\delta}$ has a higher total conductivity in an oxidizing environment. The reaction results in a very low $H_2$ partial pressure on the sweep side so there is a higher driving force with $O_2$ present in the sweep gas and the reaction maintains the large $H_2$ partial pressure difference between the two sides of the membrane. A higher total conductivity for $SrCe_{0.75}Zr_{0.20}Tm_{0.05}O_{3-\delta}$ in an oxidizing environment compared to an inert environment, in this

case, means a higher electronic conductivity as $SrCe_{0.75}Zr_{0.20}Tm_{0.05}O_{3-\delta}$ does not conduct oxygen ions.

The $H_2$ permeation flux through the $SrCe_{0.75}Zr_{0.20}Tm_{0.05}O_{3-\delta}$ membrane at 900°C (0.025 mL/cm$^2$-min) is roughly half of the $H_2$ flux through a $SrCe_{0.95}Tm_{0.05}O_{3-\delta}$ membrane of the same thickness. The difference in the $H_2$ flux is consistent with lower conductivity values in an air environment for the Zr doped membrane compared to the un-doped membrane. The flux values through the $SrCe_{0.95}Tm_{0.05}O_{3-\delta}$ membrane are within experimental error of those reported in literature and the energy of activation was 36.1 kJ/mol.

Both$SrCe_{0.75}Zr_{0.20}Tm_{0.05}O_{3-\delta}$ and $SrCe_{0.95}Tm_{0.05}O_{3-\delta}$ membranes were tested under various experimental conditions. Helium leakage through the seal of the $SrCe_{0.75}Zr_{0.20}Tm_{0.05}O_{3-\delta}$ test averaged 0.000792 mL/cm$^2$·min, which is two orders of magnitude lower than the corrected $H_2$ fluxes when the sweep gas consists of 20% $O_2$/Ar. Figure 8 shows the effect of temperature on the $H_2$ permeation flux through a 1.2 mm thick $SrCe_{0.75}Zr_{0.20}Tm_{0.05}O_{3-\delta}$ with 10% $H_2$/He on the feed side and 20% $O_2$/Ar on the sweep side.

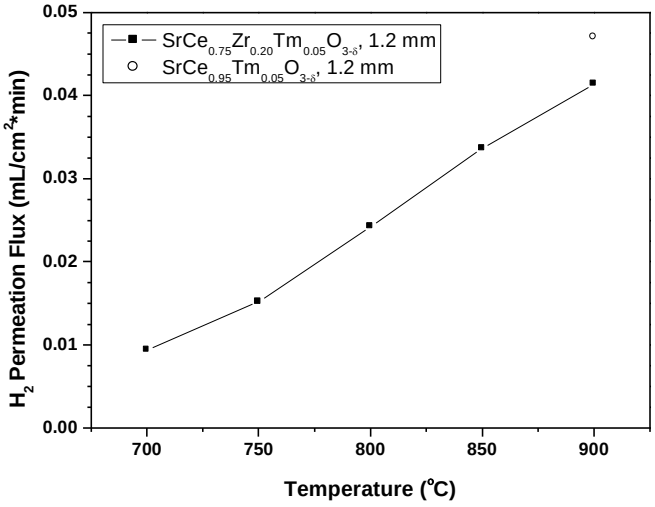


Figure 8. Effect of temperature on the $H_2$ permeation flux through a $SrCe_{0.75}Zr_{0.20}Tm_{0.05}O_{3-\delta}$ membrane with a 20% $O_2$/Ar sweep gas

The activation energy for hydrogen permeation for the $SrCe_{0.75}Zr_{0.20}Tm_{0.05}O_{3-\delta}$ membrane in a 10% $H_2$/He and 20% $O_2$/Ar gradient was 71.2 kJ/mol, which is in fairly good agreement with the $E_a$ of previously tested $SrCe_{0.75}Zr_{0.20}Tm_{0.05}O_{3-\delta}$ membranes under the same experimental conditions. The single $SrCe_{0.95}Tm_{0.05}O_{3-\delta}$ data point from Figure 8 is taken from literature [2] and it shows that $SrCe_{0.75}Zr_{0.20}Tm_{0.05}O_{3-\delta}$ has a comparable $H_2$ permeation flux. The lower flux values are consistent with the lower conductivity values of $SrCe_{0.75}Zr_{0.20}Tm_{0.05}O_{3-\delta}$ compared to $SrCe_{0.95}Tm_{0.05}O_{3-\delta}$.

At 900°C, the $SrCe_{0.75}Zr_{0.20}Tm_{0.05}O_{3-\delta}$ membrane exhibits hydrogen permeation flux equal 0.04 cc/min-cm$^2$. Since hydrogen permeation through ceramic membranes at high temperatures is unlikely limited by the surface reactions (as compared to oxygen permeation), it is expected that

we can improve hydrogen permeation flux to 4 cc/min-cm$^2$ by reducing the thickness of the membrane by 100 times (to less than 14 μm).

For a similar experiment using a 1.0 mm thick $SrCe_{0.95}Tm_{0.05}O_{3-\delta}$ membrane, the He leakage averaged 0.00038 mL/min or 0.00022 mL/cm$^2$-min. Figure 9 shows the effect of temperature on the $H_2$ permeation flux through a 1.2 mm thick $SrCe_{0.95}Tm_{0.05}O_{3-\delta}$ with 10% $H_2$/He on the feed side and 20% $O_2$/Ar on the sweep side.

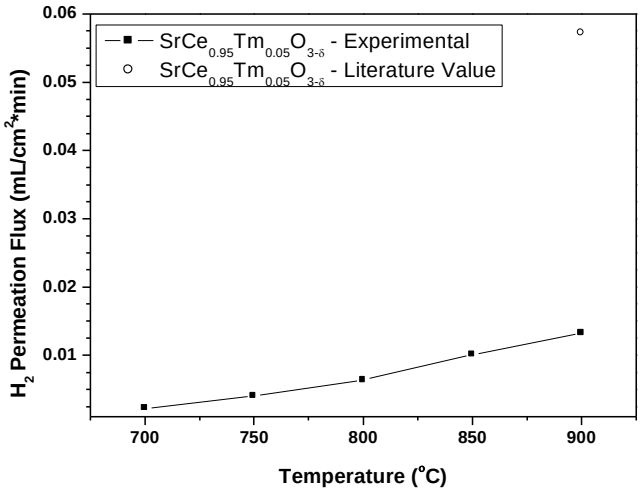


Figure 9. Effect of temperature on the $H_2$ permeation flux through a $SrCe_{0.95}Tm_{0.05}O_{3-\delta}$ membrane with a 20% $O_2$/Ar sweep

In Figure 9, the experimentally measured $H_2$ permeation flux at 900°C is roughly 25% of the literature value shown [2]. Another sign that the $SrCe_{0.95}Tm_{0.05}O_{3-\delta}$ membrane might not be chemically stable under the experimental conditions was the measured activation energy for hydrogen permeation was 84.7 kJ/mol, which is more than double the reported $E_a$ (36.5 kJ/mol) for $SrCe_{0.95}Tm_{0.05}O_{3-\delta}$ [2]. The seal was verified to be intact after the experiments. The feed side of the membrane had been exposed to a highly reducing environment at high temperatures for 48 hours before the experiment shown in Figure 9 was conducted. Therefore, the reduction in $H_2$ flux and drastic increase in the $E_a$ could be due to reactions on the surfaces of the membrane.

In order to determine the chemical stability and the effect of a highly reducing environment on the $H_2$ permeation flux through a 1.0 mm thick $SrCe_{0.95}Tm_{0.05}O_{3-\delta}$ membrane, a long term $H_2$ permeation test was conducted. The feed side consisted of 20% $H_2$/He, the sweep side consisted of 20% $O_2$/Ar, and the temperature of the system was maintained at 900°C for the duration of the experiment. Figure 10 shows the $H_2$ permeation flux through the $SrCe_{0.95}Tm_{0.05}O_{3-\delta}$ membrane at 900°C over time. The $H_2$ permeation flux decreases drastically in the first five hours of the experiment, losing roughly 60% of the initial value. Zuo et al [3] have reported a 48% reduction in the $H_2$ permeation flux through a cermet (ceramic-metal composite) membrane during the first six hours of exposure to a highly reducing environment at 900°C and a continued loss in the $H_2$

permeation flux for up to 80 hours. For $SrCe_{0.95}Tm_{0.05}O_{3-\delta}$, the $H_2$ permeation flux stabilized after the initial loss and maintained a relatively stable flux value for the duration of the experiment.

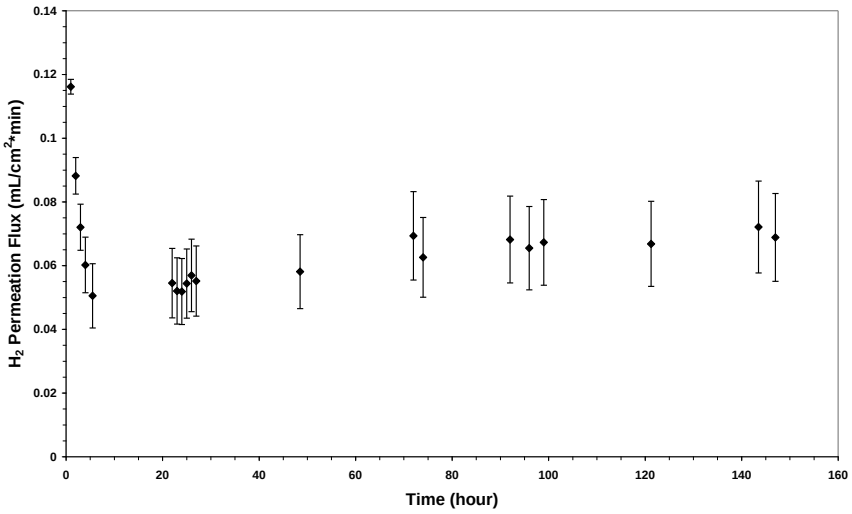


Figure 10. $H_2$ permeation flux through a $SrCe_{0.95}Tm_{0.05}O_{3-\delta}$ membrane at 900°C

In Figure 11, the feed side (the side of the membrane that was exposed to 10 – 40% $H_2$/He) has virtually the same XRD pattern as the fresh membrane. Both the feed and sweep side XRD patterns do not have a peak shift or additional peaks, meaning the membrane was chemically stable over the duration of the experiments. Besides a new peak (indicating the formation of $CeO_2$) on the feed side surface, both the feed and sweep side XRD patterns are in good agreement with the pattern of the fresh membrane. The feed side (side of the membrane exposed to 10 – 40% $H_2$/He)noticeably changed from a light green color before the experiments to brown while the sweep side maintained the green color (see Figure 11). The black marks on either surface are pen markings used to identify the membrane. The color change could indicate a reduction of cerium on the surface of the membrane from $Ce^{+4}$ to $Ce^{+3}$. A surface characterization technique that can determine the elemental composition as well as the electronic state of each element in the surface is x-ray photoelectron spectroscopy (XPS).

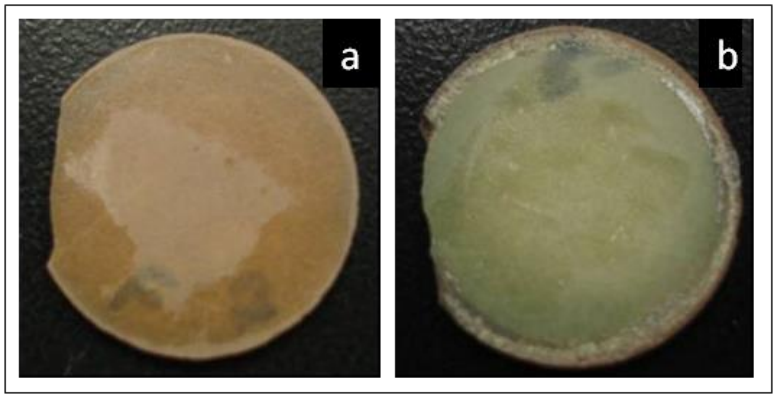


Figure 11. $SrCe_{0.95}Tm_{0.05}O_{3-\delta}$ surface exposed to $H_2$ after experiments (a) and sweep side $SrCe_{0.95}Tm_{0.05}O_{3-\delta}$ surface after experiments

More investigations of color changes during hydrogen permeation experiments are needed.

In conclusion, all ceramic membranes synthesized by ASU during this project showed a low hydrogen flux as compared with metallic membranes. The best ceramic membrane showed hydrogen permeation flux of 0.03 SCFH/FT$^2$ at process conditions while the metallic membrane as $Pd_{80}Cu_{20}$ had a hydrogen flux of 47.2 SCFH/FT$^2$.

**Task 1.2 Metallic Membrane Synthesis and Testing**

The concept envisioned by GTI incorporates a hydrogen-selective membrane within a gasifier for direct extraction of hydrogen from biomass derived syngas. As more than 50~60% of the final hydrogen product is generated in the gasification stage, there is great potential of maximizing hydrogen production by separating this hydrogen directly from the gasifier. By incorporating a hydrogen-selective membrane into a gasification reactor, both gasification reactions and hydrogen separation can be accomplished simultaneously within the gasifier, thus increasing hydrogen production and simplifying process operation.

The main objective of the task performed by NETL was to investigate the feasibility of using Pd-type of membrane for the application of the biomass gasification membrane reactor. Hydrogen permeability in the presence of various $H_2/H_2S$ gas mixtures at relevant gasifier temperatures and pressures was measured. Testing conditions are at high temperatures (750 to 900$^oC$) and high pressures (up 33 atmospheres) to encompass the conditions anticipated in the biomass gasifier. Although the components and composition of the gasifier product stream will vary with the biomass feedstock, some of the key impurities of interest will be compounds of C, N, Cl, and Na. Initial permeability testing of Pd-Cu alloys in the presence of gaseous components such as CO, $CO_2$, $H_2O$ and $NH_3$was evaluated at temperatures and pressures associated with the gasifier.

Several key capabilities were required to successfully develop, test and characterize dense metal-based membranes for application to the gasification process. Although NETL has unique capabilities to accommodate membrane testing and fabrication, including annealing ovens, box furnaces and several test apparatus. Also, NETL has a micro-welding system and a plasma arc-melter, which enhances the sealing and mounting of membranes and allows for the fabrication of alloy combinations that require melting points greater than 1500$^oC$, respectively. The Thermogravimetric Analyzer (TGA) is utilized for determining the corrosion behavior of promising metal membrane components with respect to sulfidation and oxidation environments generated from the gasification of biomass.

NETL was pursuing a new approach for stabilizing Pd alloys for high temperature use. This approach was modeled on a strategy that has been used to strengthen and stabilize certain high performance alloys such as Ni-based super alloys for high temperature applications. This approach utilizes a two-phase microstructure for stabilization. Unlike previous approaches where the additive is concentrated at grain boundaries, the two phases in the system under consideration can form a uniform dispersion of grains rather than be concentrated at grain boundaries. In this scenario, the primary phase transports hydrogen while the secondary phase improves the high temperature strength. A possible difficulty with this approach is that the phase through which the hydrogen would diffuse would undergo a lattice expansion which could impart mechanical stresses on the membrane.

NETL has fabricated several Pd-alloy combinations (80 wt % Pd-Cu, 70 wt % Pd-Cu, 65 wt % Pd-Cu, 69 wt % Pd-Pt, 95 wt % Pd-Au, 94 wt % Pd-Co, 94 wt % Pd-Ni, 98Pd-$Y_2O_3$, 99.5Pd-Si and 55Ni-Pt) and have characterized the performance of these alloys in the presence of neat hydrogen at temperatures consistent with the biomass gasification process. Table 1 details the composition and fabrication status for the alloys interest in this study. In addition to the alloy

combinations listed in Table 1, several other alloys and alloy additives are being considered, which may not contain palladium as a primary component.

Table 1. Alloy composition and fabrication status of current NETL dense metal membranes.

| Alloy Composition (wt%) | Current Fabrication Status |
|---|---|
| 80Pd-Cu | ~100 µm thick foil |
| 70Pd-Cu | ~100 µm thick foil |
| 65Pd-Cu | ~100 µm thick foil |
| 69Pd-Pt | ~100 µm thick foil |
| 95Pd-Au | ~100 µm thick foil |
| 94Pd-Co | ~100 µm thick foil |
| 94Pd-Ni | ~100 µm thick foil |
| 98Pd-$Y_2O_3$ | Fractured during rolling |
| 99.5Pd-Si | ~100 µm thick foil |
| 55Ni-Pt | Partially rolled |

The membrane materials listed in Table 1, which focus on the addition of chemically stable additives (Pt, Au, Cu, Ni, Co, Ag etc) to a highly permeable metal (Pd), has resulted in permeability values comparable to pure palladium in the presence of clean hydrogen, as expected. The initial results with the PdAu alloy in the presence of a $H_2S$-containing gas stream shows significant chemical reactivity in the presence of $H_2S$. Post-test analysis of the PdAu alloy showed significant surface sulfidiation, and negligible Au present.

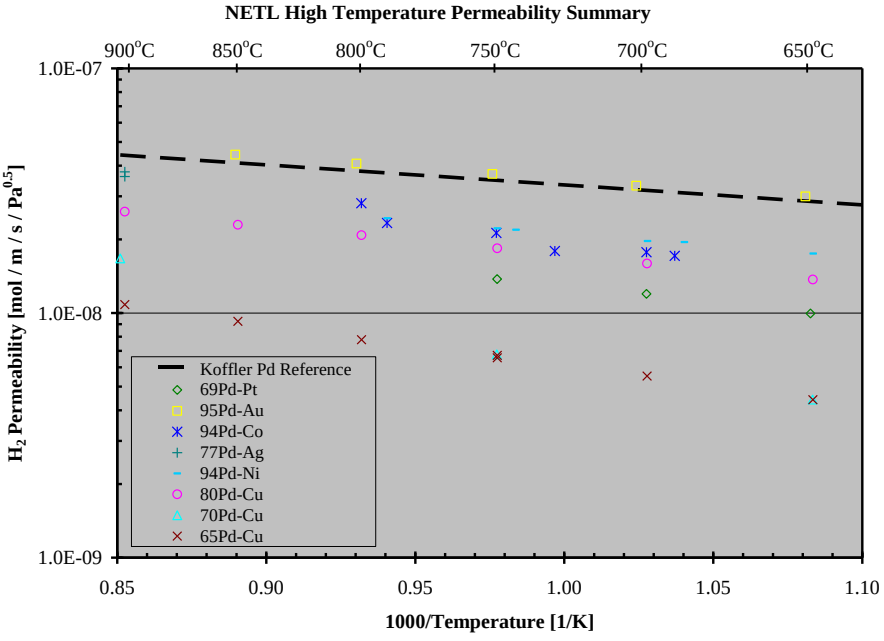

Figure 12. Permeability results of the alloys fabricated and tested at NETL as a function of temperature in the presence a 10%He-$H_2$ balance gas mixture.

Of the alloys listed in Table 1, all of the alloys have been tested in the presence of clean hydrogen except the Pd-$Y_2O_3$. Figure 12 illustrates the results of the metal alloys tested in the presence of in clean hydrogen, which is used as a comparative baseline for tests conducted in the presence of other syngas constituents.

The Pd-Yt complex suffered from cracking during the rolling procedure, and had prevented flux testing of the material. However, SEM analysis of the fabricated foil showed promise, in that the yttria appeared to be highly dispersed (see Figure 13).

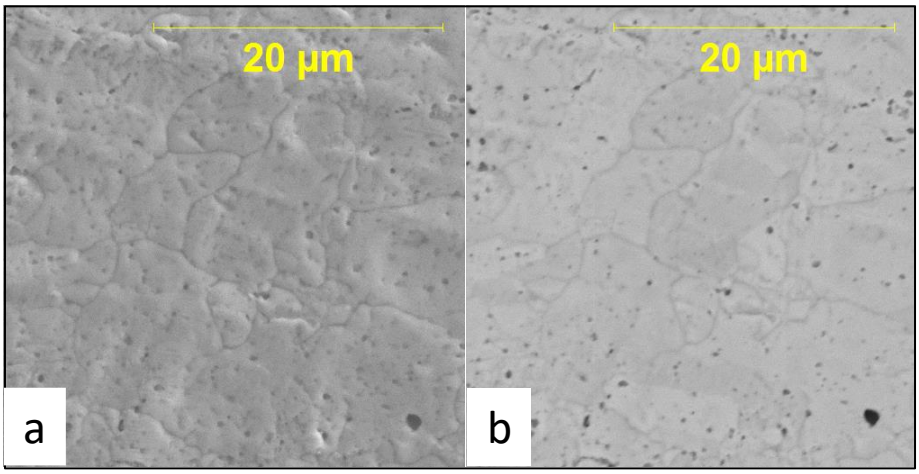


Figure 13. SEM images (a) of the Pd-Yt composite material. Image (b) shows the dispersion of the yttria (black spots) on the surface of the composite.

Fabrication efforts were continued in the fabrication of an oxide-dispersed alloy for hydrogen separation due to the potential of increased mechanical and chemical stability.

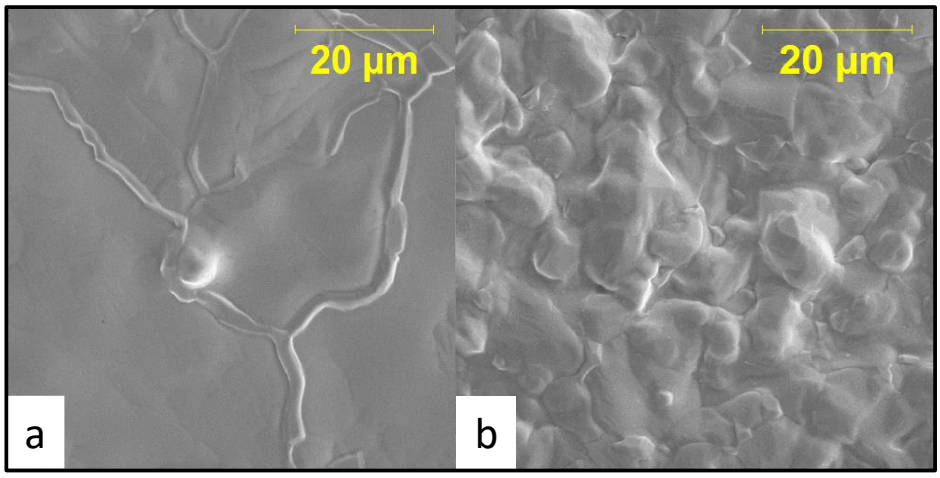


Figure 14. SEM images of the Pd-Aumembrane after testing in 10%He-$H_2$ (a) and 1%$H_2S$-10%He-Balance (b) atmosphere.

SEM and XRD analysis of the post-tested PdAu membrane showed significant surface restructuring/faceting and compositions as a function of gas exposure. The PdAu alloy tested in clean hydrogen (Figure 14a) appears very smooth with pronounced grain boundaries. The same alloy composition tested in the presence of a sour-hydrogen stream appeared to experience significant restructuring, with a significant amount of $Pd_4S$ and negligible Au present (Figure 14b). Efforts were continued in identifying alloy additives that retards the formation and growth of palladium sulfide in Pd-based membranes.

Efforts of cold-rolling the Pd-$Y_2O_3$ composite have halted due to the extreme "hardness" of the mixture. This attribute of the mixture is a property of interest along with the possibility of chemical grain stabilization, which is illustrated in the SEM and elemental mapping in Figure 15. Future focus of the Pd-$Y_2O_3$ composite was on developing other methods (i.e. waffering) to obtain a "testable" membrane sample.

The Pd-Si composite ingot appears much more malleable, and should allow for the development of a testable sample via cold-rolling. Figure 15 illustrates the results of the elemental analysis conducted by SEM/EDS on the ingot. The localization of the Si within the membrane surface shown on SEM image may yield grain-boundary stabilization during elevated temperature operation.

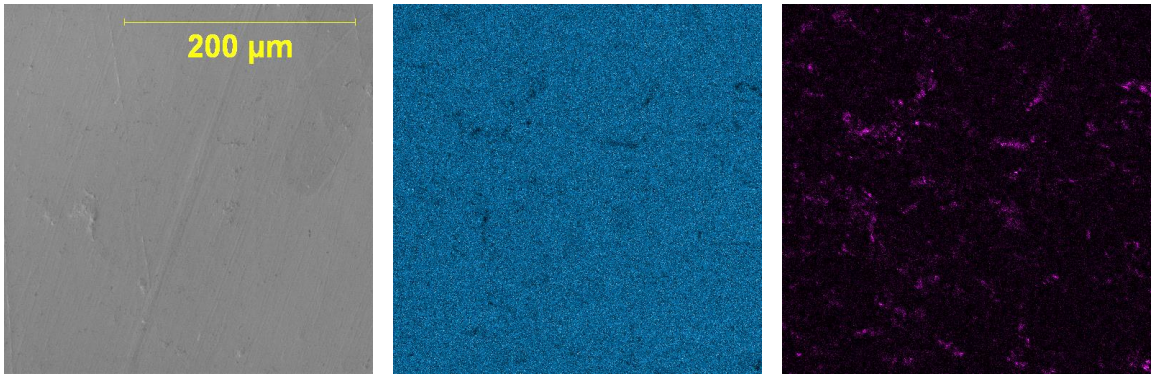


SEM surface image, Pd-$Y_2O_3$ | Pd elemental map | $Y_2O_3$ elemental map

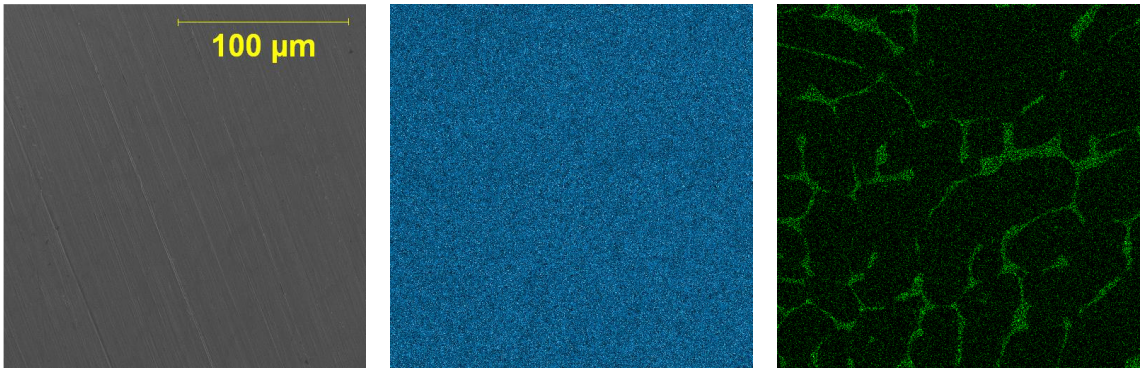


SEM surface image, Pd-Si | Pd elemental map | Si elemental map

Figure 15. SEM and elemental analysis of the 95Pd-Si ingot fabricated at NETL.

Of additional importance in the study, is the influence of $H_2S$-containing gas mixtures on the performance and chemical stability of membrane alloy candidates. Figure 16 summarizes the results of the membrane tests conducted in the presence of $H_2S$ gas mixtures. All of the membrane samples showed relatively high performance upon the introduction of the $H_2S$ gas mixtures. The PdAu alloy has been tested for approximately 25 hours in the presence of a $H_2S$-contining gas mixture at 700°C. Although a ~30% reduction in performance of the PdAu alloy was observed, the stability of the alloy at longer test durations appears very promising. However, none of the membranes tested completed the 120-hour test protocol due to the formation of leaks during testing. NETL researchers were focused on identifying if the leaks were a result of the high temperature operation, the presence of the gas mixture or a combination thereof, but initial inspections show that failure occurred at the grain boundaries.

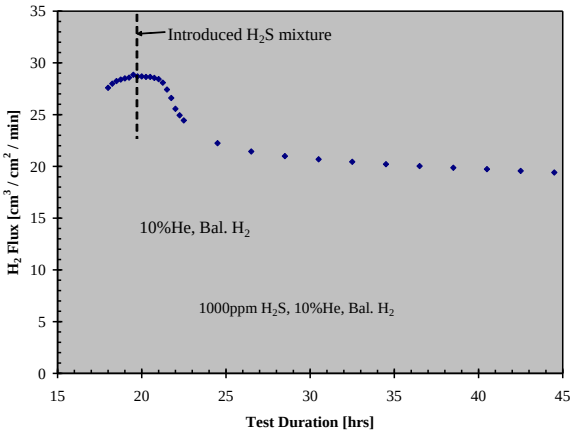


95Pd-Au, 700°C

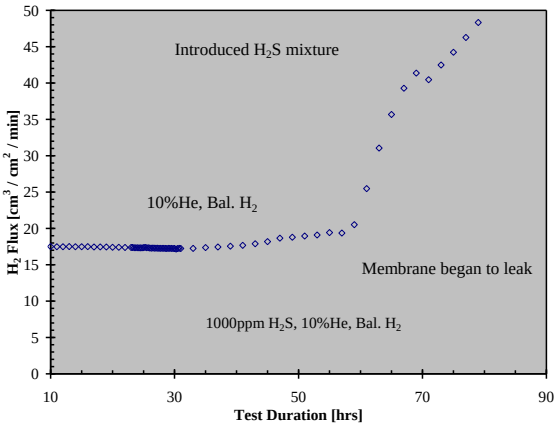


94Pd-Co, 700°C

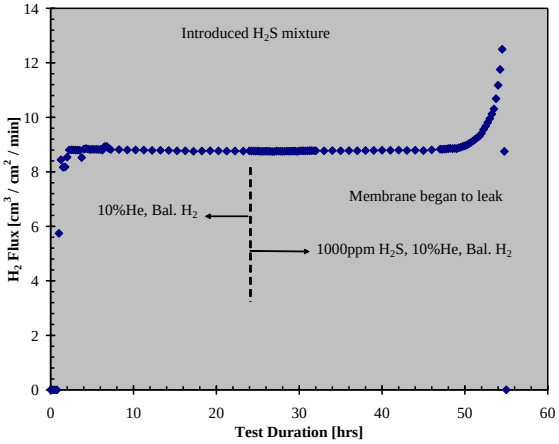


Figure 16. Influence of a 0.1%$H_2S$, 10%He, Bal. $H_2$ gas mixture on the hydrogen flux of several Pd-based alloys.

Several of the membranes of interest (Table 1) have been characterized in the presence of clean hydrogen stream, with Pd-Ag and Au yielding the highest values. Initial testing of the Pd-Pt, -Au, -Co membrane systems in $H_2S$-containing gases showed promise, in that relatively negligible influence on flux was observed. Unfortunately, all of the membranes developed leaks during operation, which appeared to be attributable to grain boundary issues.

The 99.5 Pd-Si ingot was successfully rolled to a ~100 µm foil. The baseline performance of this alloy was tested over the range of 350 to 900°C using 90% $H_2$/10% He; however, at 800°C the membrane failed. The membrane was characterized by SEM/EDS to attempt to determine the cause of failure. The results of the SEM/EDS analysis are shown in Figure 17 along with an image of the membrane surface before use for comparison, Figure 17a. A number of areas of severe pitting were observed, Figure 17b, which probably account for the failure. The pits may have resulted from the formation of a low-melting Pd-Si eutectic resulting from non-uniform Si distribution in the alloy. The Pd-Si phase diagram shows that a composition containing about 5 wt% Si melts near 800°C which supports this conjecture. Additionally, re-examination of the EDS elemental map of a polished area on the original ingot, Figure 17e suggests a non-uniform alloy composition with localized Si enrichment. This localized enrichment could have remained to some extent in the final foil. Figures 17c and 17d show more surface details. The areas labeled were analyzed by EDS. Pd was the only detectable element in the areas indicated by “A”. The deposit at the grain boundary, “B”, contained both Pd and Si as did the surface deposits marked “C”. Until its failure, this alloy exhibited performance about equal to pure Pd.

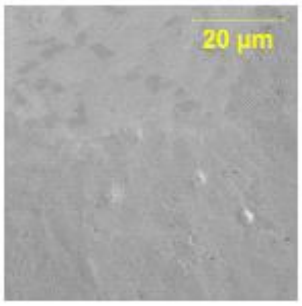


17a. SEM surface image of fresh 99.5Pd-Si foil.

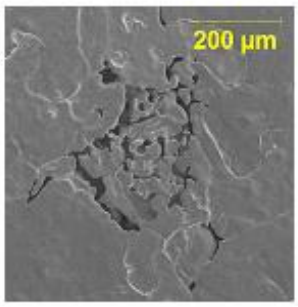


17b. Holes in failed membrane.

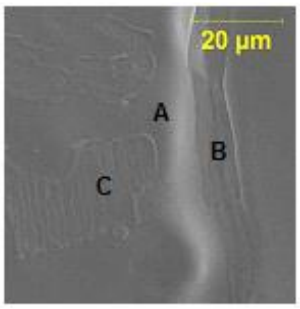


17c. Details of surface and grain boundary.

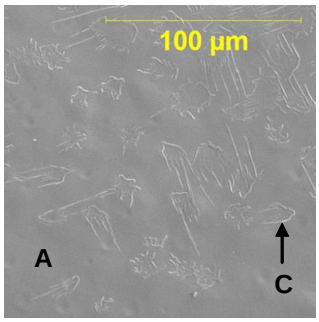


17d. Details of surface.

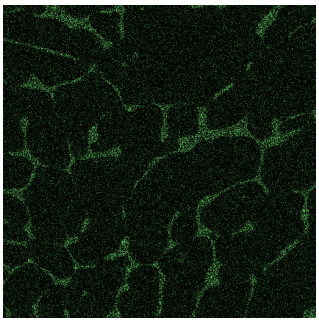

17e. Si elemental map of original alloy ingot (view is ~200 x 200 µm). Brighter areas show Si enrichment.

Figure 17. SEM and EDS analysis of the 95Pd-Si alloy.

The 55 wt% Ni-Pt alloy was successfully rolled and should yield four 0.75 inch diameter membrane disks for testing. XRD indicated a single phase face centered cubic (fcc) solid solution structure as expected based on the phase diagram. SEM showed some defects in the foil such as rolled in silica and minor pits as well as what appear to be bubbles in the foil. These defects are not expected to impact testing. Figure 18 shows permeability of 55wt%Ni-Pt alloy at 600,700 and 800°C. Membrane failed at 800°C.

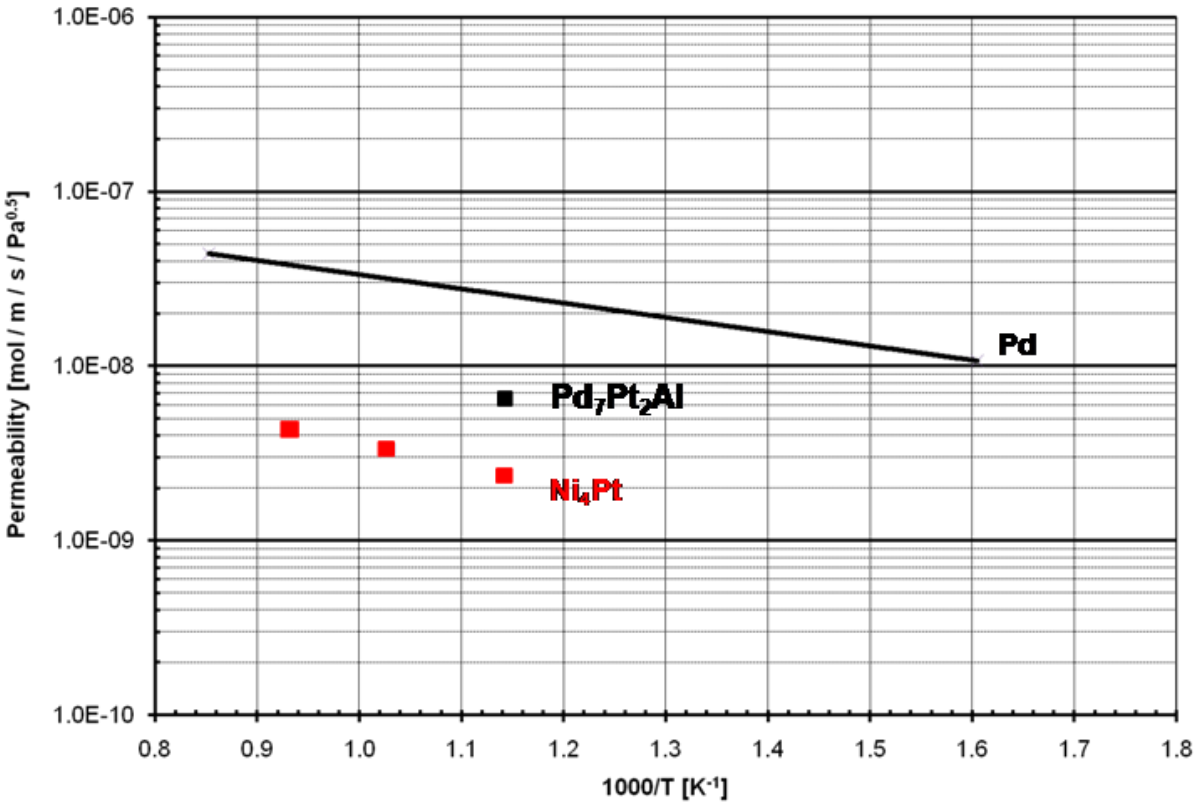


Figure 18. Hydrogen permeability results for Ni-Pt and Pd-Pt-Al alloys.

A second foil, a PdCuPt alloy, was also successfully rolled and should yield eight 0.75 inch diameter membrane disks for testing. Pt was added to this alloy to attempt to improve both strength and sulfur resistance. XRD indicated a single phase fcc solid solution structure for this foil. Baseline hydrogen permeability testing was begun on this sample. Preliminary results show permeability at 700°C of about 5% of that expected for pure Pd.

Also, $Pd_7Pt_2Al$ alloy was synthesized and oxidized to attempt to convert the Al to oxide to stabilize the grain boundaries. Pt added to this alloy possibly can improve strength and sulfur resistance of the membrane. Due to failure of membrane at 700°C there is no data of hydrogen permeability at higher temperatures to see Pt effect on alloy characteristics. SEM micrographs presented on Figure 19 show that Al is located along grain boundaries. So, Al incorporation into alloy with consequent oxidation of Al to $Al_2O_3$ allows Al to be located along grain boundaries. Result of hydrogen permeability for PdAlPt alloy is shown on Figure 18. Unfortunately, both alloys eventually failed during permeability tests.

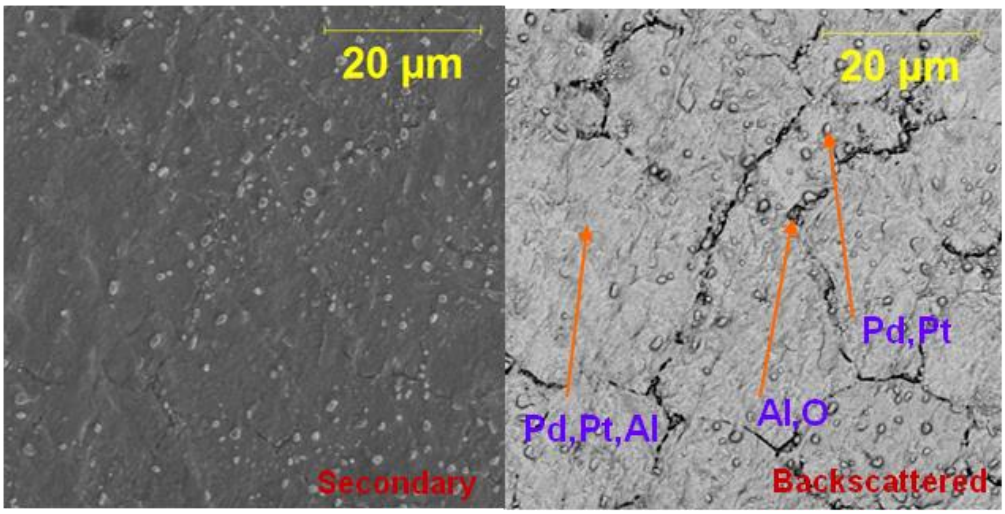


Figure 19. SEM micrographs of secondary and backscattered images for $Pd_7Pt_2Al$ alloy.

Super-permeable alloys have desirable characteristics for hydrogen membrane applications including high permeability, high temperature strength and cost. However, they are very susceptible to poisoning of surface catalytic sites and surface corrosion. A good method to counter these effects is by coating the alloy with a second alloy such as one containing Pd to provide catalytic activity and corrosion protection. Unfortunately, such coatings are likely to be unstable at the temperatures of interest. Therefore, alternative methods of protecting these materials are needed. One possibility being investigated is an inorganic, nonmetallic coating that can protect these alloys at the conditions of interest.

A niobium/tantalum alloy was identified that may offer high temperature stability under the conditions of interest. These alloys offer good resistance to the corrosive conditions of the post-gasifier environment; however, their hydrogen permeability is not known. However, two well-known problems with these types of alloys are susceptibility to surface oxidation and lack of a catalytically active surface. Alloying additions can sometimes help to control these problems.

An alloy, a Pd-Cr composition was tested up to 750°C to investigate its potential application for this project. The test was conducted using 100% $H_2$. Over the range of 650 to 750°C, its permeability was approximately 60% of the permeability of Pd. Figure 20 show hydrogen permeability of Pd-Cr membrane in comparison with pure palladium membrane.

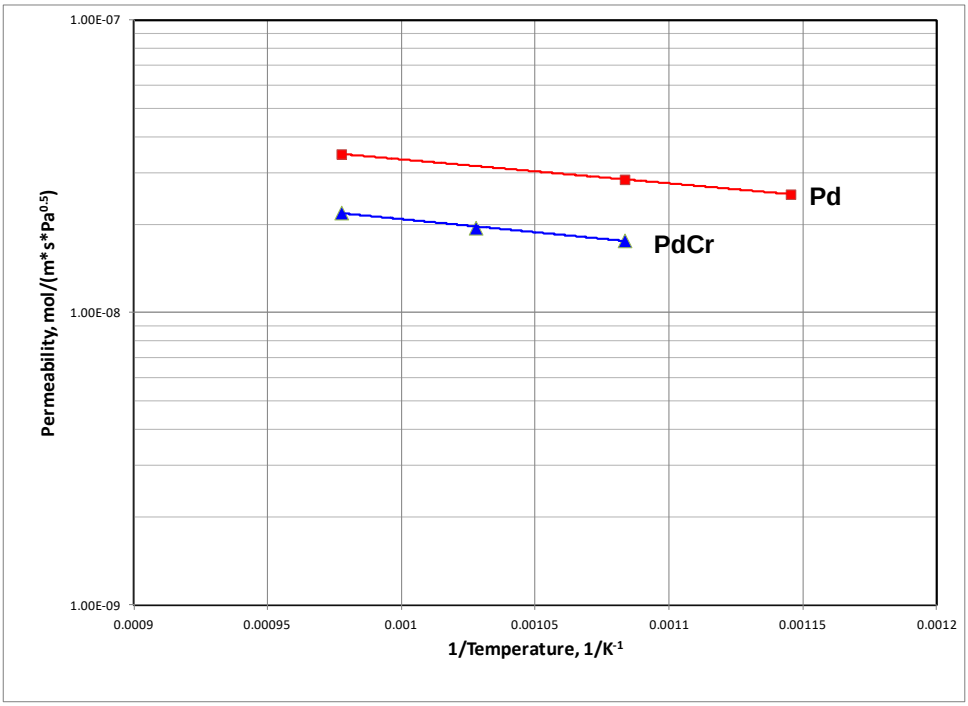


Figure 20. Permeability of Pd-Cr membrane as compared with pure palladium permeability at different temperatures.

Determining the permeability of a new alloy under "clean" conditions is necessary and valuable; however, determining its performance under conditions that are more realistic is critical to evaluating an alloy's potential for scale up and use under actual process conditions. Due to units' relocations, membrane testing facilities had a very limited availability and no membrane testing units with $H_2S$ feed were available during 2010-2012.

In conclusion, the new Pd-based alloys were prepared and tested for hydrogen permeation. Based on permeation properties of synthesized membranes, alloy as $Pd_{80}Cu_{20}$ was chosen as an initial candidate. Criteria for choice were high hydrogen flux, long-term stability together with $H_2S$ tolerance.

**Task 1.3.1 Glass Ceramic Membrane Development**

As part of the project in collaboration with GTI, SCHOTT has investigated synthesis of hydrogen-permeable, glass-ceramic membranes for high-temperature separation purposes.

Relevant work regarding proton conduction in glass-ceramics includes Shelby and Vitko [4] who examined hydrogen transport in a mica-containing, glass-ceramic by noting the time-dependent change in color in the material as a proxy for the diffusion front of protons. For most temperatures, the permeation of hydrogen (~$10^{10}$ molecules/sec/cm/atm) was less than that of helium in this material. Tuzzolo and Shelby [5] examined the development of colloids of reduced metals in oxide glasses due to the permeation of hydrogen. The kinetics of this phenomenon followed a square-root-of-time law, indicating diffusion-limited transport. TEM images show non-connected colloids, suggesting that there should not be a percolative electrical effect in these materials, though such data were not reported. A very broad overview of permeation in glasses is found in Shelby [6] who reports on gas diffusion and permeation for a wide variety of species and glass types and some glass-ceramics.

The following approaches had been identified as avenues to explore:

- Segregation of appropriate metals (e.g., Pd-Ag, Pd-Cu) along grain boundaries during high degrees of crystallization for selected compositions [6-9]
- Combined ion-exchange and heat treatment under a reducing atmosphere [10]
- Co-sintering of glassy powder + metal (e.g., Pd-Ag, Pd-Cu) to produce a high metal content-containing glass-ceramic [11]

A detailed search for data on Ag and, in particular, Pd solubility in glasses was carried out as such data are required for a proper assessment of the likelihood that the segregation approach might be successful. An extensive literature search was conducted using Web of Science to find compositional systems that had reported "significant" Pd solubility in glass-forming systems (e.g., [Pd] > 100 ppm). Typical silicate glass-forming systems have very small Pd solubilities [12, 13]. However, glass-forming systems have been reported in the geologic literature that report [Pd] > 500 ppm [14, 15]. These systems were used to verify these reported high solubilities and, next, to produce Pd-doped glass-ceramics suitable for physical property testing. Glass compositions have been identified in the literature that report sufficiently high Pd solubilities to allow SCHOTT to consider using their "segregation" glass-ceramic approach.

Conventional melting procedures at SCHOTT's facility were used to prepare suitable starting glass samples. Standard analytical techniques were used to determine the crystalline contents in the glass-ceramics. Glass was prepared for solubility tests. SCHOTT had prepared glass-ceramic material for physical property testing, including hydrogen permeation tests to be conducted at GTI.

Both existing SCHOTT glass compositions as well as custom melts (0.5-liter in most cases) were prepared to provide starting material suitable for solubility experiments. In particular, glass cullet was placed into small Pd crucibles (with lids), re-melted for extended time periods, and then analyzed for Pd content. Such measurements, as a function of time and temperature, provide a range of Pd solubility useful as a starting point for composition test.

Five different melts in the $CaO$-$MgO$-$Al_2O_3$-$SiO_2$ (CMAS) system were completed. All compositions were melted in platinum crucibles and were stable glasses. XRF analyses (not

shown) revealed excellent correspondence between input major oxide wt% and measurements on as-cast glass.

The differential thermal analysis (DTA) of synthesized melts shows a clear presence of crystallization exotherms which is consistent with the use of this material as a highly-crystallized glass-ceramic, one necessary condition in the approach. Evaluation of the samples via optical microscopy revealed extensive crystallization of the glass, though concentrated at the bottom interface with the melting vessel (Figure 21). Successful melting of a candidate glass and subsequent testing thereof has yielded a very dark glassy material with suspected high Pd contents.

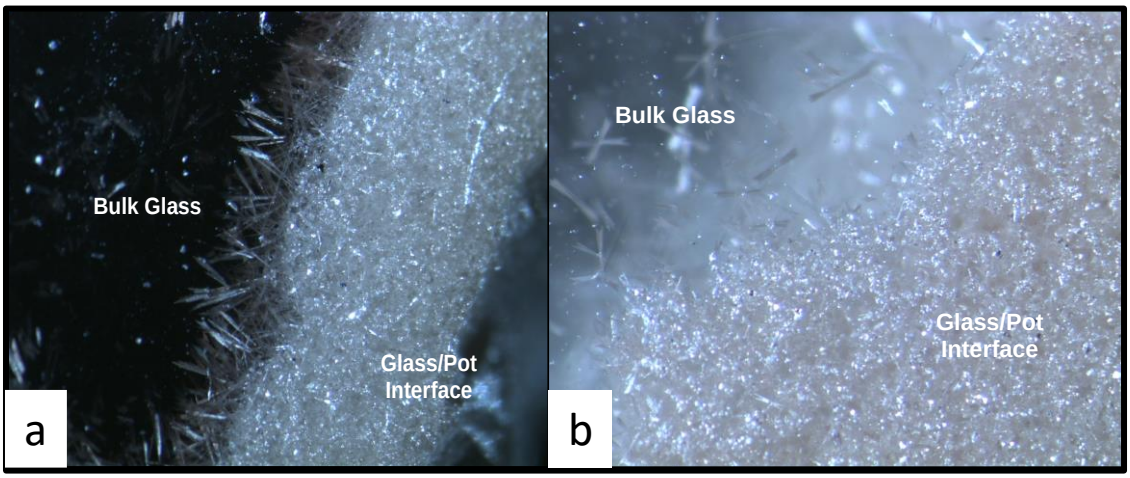


Figure 21. Dark-field optical microscopy view of crystals at bottom of a) Pd and b) Pt pots.

SCHOTT focused on careful analysis of the Pd content in samples, further test melting with suitable Pd compounds (e.g., nitrates) to make large castings, particularly of the CMAS-1 composition, and analysis of these castings to see if equivalent (high) Pd contents were obtained.

Standard in-house test-melting procedures, some of which are proprietary, were used throughout the work. XRF scans of Pd and Pt-bearing samples were performed to confirm and quantify the metal content in CMAS-1, the lead candidate glass. Analysis was performed by ICP-AES, which yielded the results in the Table 2, showing that indeed, high Pd contents were attained (100 X higher than most silicate glasses).

Table 2. Pd content in glass samples

| Sample | Pd (ppm) |
|---|---|
| CMAS-1 Pt pot remelt | < 5 |
| CMAS-1 Pd pot remelt | 592 |

DTA scans of annealed vs. un-annealed patties from the successful Pd batch melt revealed some differences. This difference in peak amplitudes for annealed vs. un-annealed glass for crystallization exotherms is possibly due to crystallization occurring during the annealing cycle. Additionally, the glass-transition temperature is shifted, probably owing to a change in glass composition as a result of crystallization of phases whose composition differs from that of the glass.

Four ceramization trials shown on Table 3 were conducted to produce glass-ceramics from high-Pd containing CMAS-1 glass.

Table 3. Conditions of ceramization trials

| | **Cycle A** | **Cycle B** | **Cycle C** | **Cycle D** |
|---|---|---|---|---|
| **Thermal cycle** | 300°C/hr to 875°C | 300°C/hr to 1100°C | 300°C/hr to 875°C | 300°C/hr to 1100°C |
| **Dwell time (hrs)** | 4 | 4 | 4 | 4 |
| **Atmosphere** | air | air | 95% $N_2$ / 5% $H_2$ | 95% $N_2$ / 5% $H_2$ |

Physical appearances of these samples were notably distinct (Figure 22).Each sample is approximately 20 x 20 x 1 mm in dimension. Cycle D sample is noticeably bluish in natural light.

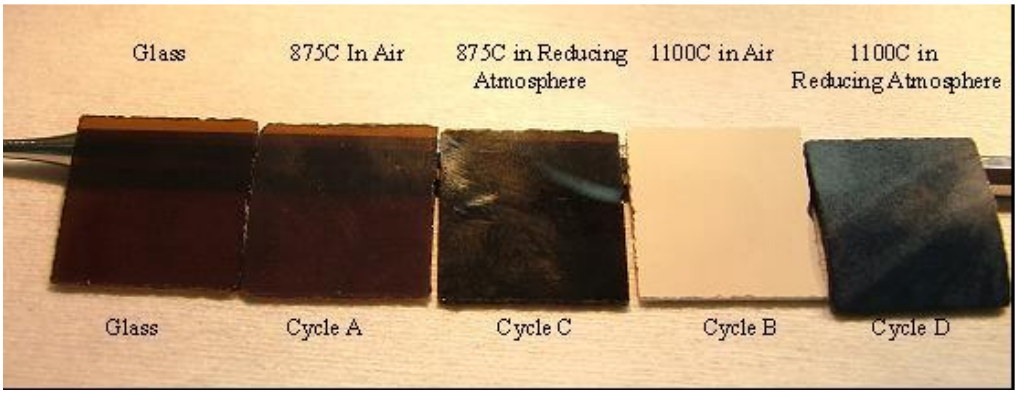


Figure 22. Picture of glass (annealed, at left) and ceramized CMAS-1/2 + Pd samples.

Based on the results it was concluded that furnace atmosphere during ceramization played an important role for physical appearance. The composition CMAS-1 was proven to be crystallizable to a state with essentially no residual glass (amorphous-free by XRD at least). Electrical conductivity measurements taken to date reveals a complex picture, with resistivity values varying by over 7 orders of magnitude (at the same temperature) for the range of samples tested.

Sample was broken in half and cross section analyzed. Cross section analysis revealed a color gradient from the top/bottom of the sample to the center: the color went from dark blue, to gray, to light gray to a white center line (Figure23). The microstructure suggested crystalline alignment perpendicular to the outer sample surface. So, CMAS composition with added reducing agent has

led to markedly different crystallization tendencies. More research is needed to see that these differences are either beneficial or detrimental to electrical conduction and H permeation performance.

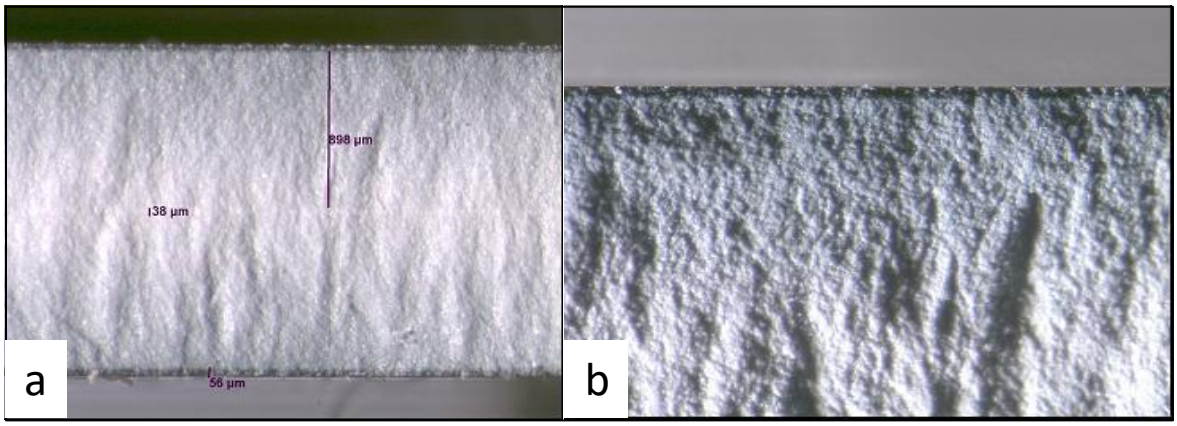


Figure 23. Cross section of ceramized sample (a) and expanded view of the cross-section showing a thin (~30 micron) very dark outer layer along with a thicker, more gradational region extending some 100's of microns into the sample.

Addition of a reducing agent (sugar) may assist hydrogen permeation by further reduction of Pd incorporated in the network. Few formulations with sugar additions were done and total conductivity were measured. Figure 24 show conductivity chart as a function of temperature. The variables among the samples shown are 1) processing conditions; 2) presence or absence of ppm-level Pd metal and 3) addition of sugar. It is clear that when sugar was added to glass total conductivity increased by two orders of magnitude. It is unclear whether or not the addition of a reducing agent (sugar) assists $H_2$ permeation via further reduction of Pd to its metallic state, or whether having reduced Pd in the precursor negatively impacts crystallization. As ceramization typically proceeds in a reducing environment anyway, it may be that having reduced Pd in the precursor glass is unnecessary.

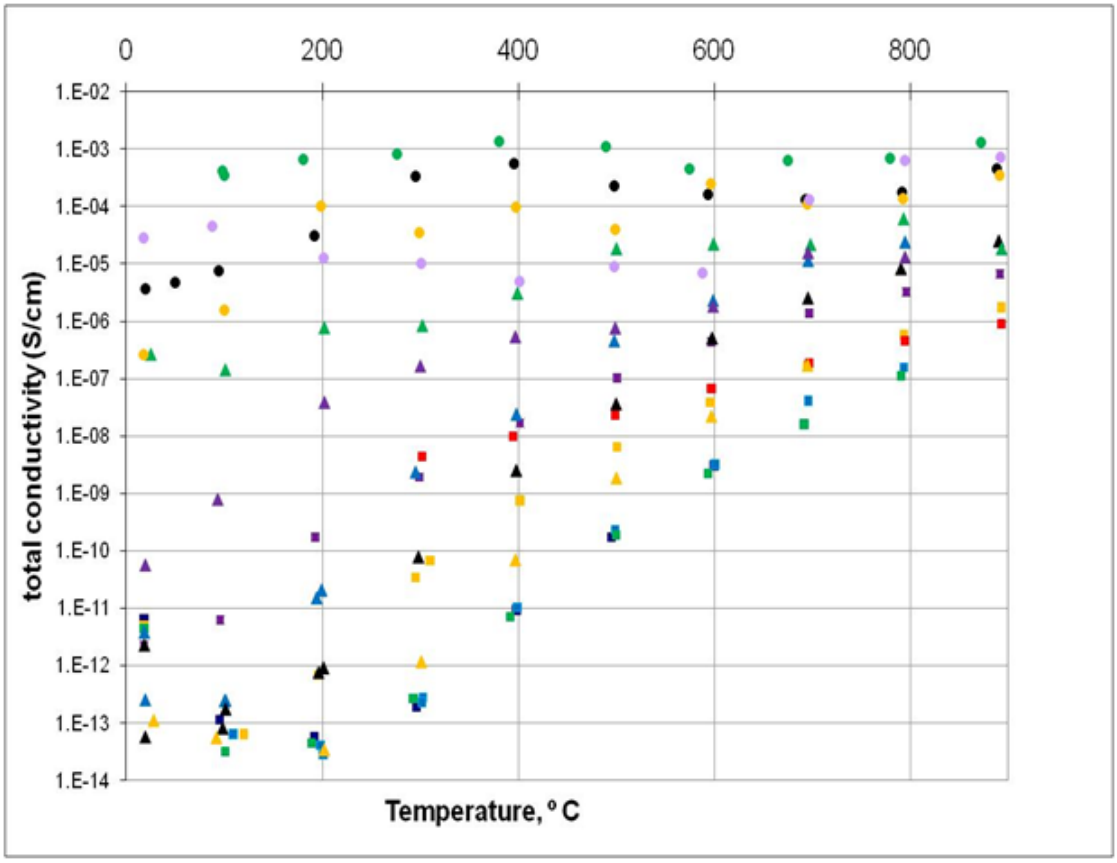


Figure 24. Total conductivity values for all synthesized samples at 25-900°C range.

Main observations from electrical conductivity measurements:

1. Degree of ceramization and treatment atmosphere strongly affects electrical conductivity of synthesized membranes.
2. Initial glasses before ceramization and treatment have similar electrical conductivity.
3. Treatment of glasses with or without Pd at 875°C in air or reducing atmosphere leads to big differences in electrical conductivity as an increase of treatment temperature up to 1100°C in reducing atmosphere too. However, a treatment of glasses at 1100°C in air produces similar results for electrical conductivity.
4. The highest conductivity values were attained for ceramized (in reducing atmosphere) Pd-free samples; these samples also showed remarkably small temperature dependencies, perhaps suggestive of electrical conduction via $Ti^{3+}$ - $Ti^{4+}$ charge transfer.

The membrane from melt CMAS-1 was tested for hydrogen permeation. At T=350°C, hydrogen flux is 0.15 $SCFH/FT^2$ at pressure difference 35.7 psi. At T=850°C, hydrogen flux is 0.25 $SCFH/FT^2$ at pressure difference 12 psi. These results were very encouraging for potential use of Pd-based glass membranes.

In order to reproduce the positive result, the same melting/processing protocol was used to synthesize a new glass batch (CMAS-1/4). Ceramization was completed under forming gas of CMAS-1/4 glass batch. Sample preparation was completed, including samples for electrical conductivity measurements by SCHOTT as well as samples suitable for H permeation testing by GTI. Electrical conductivity results indicated SCHOTT has fabricated highly-conducting samples; however, this is likely a necessary condition, though not sufficient, to ensure hydrogen permeation.

Three additional CMAS melts were completed. Two melts were analyzed for all batch components except the Pd content. Major oxides are within acceptable bounds, but various samples of these two melts show differences in color due, potentially, either to inhomogeneous Pd contents or inhomogeneous palladium and/or titanium redox state.

Figure 25 shows synthesized melts and membranes obtained from this melt.

Figure 25. Example of polished disk

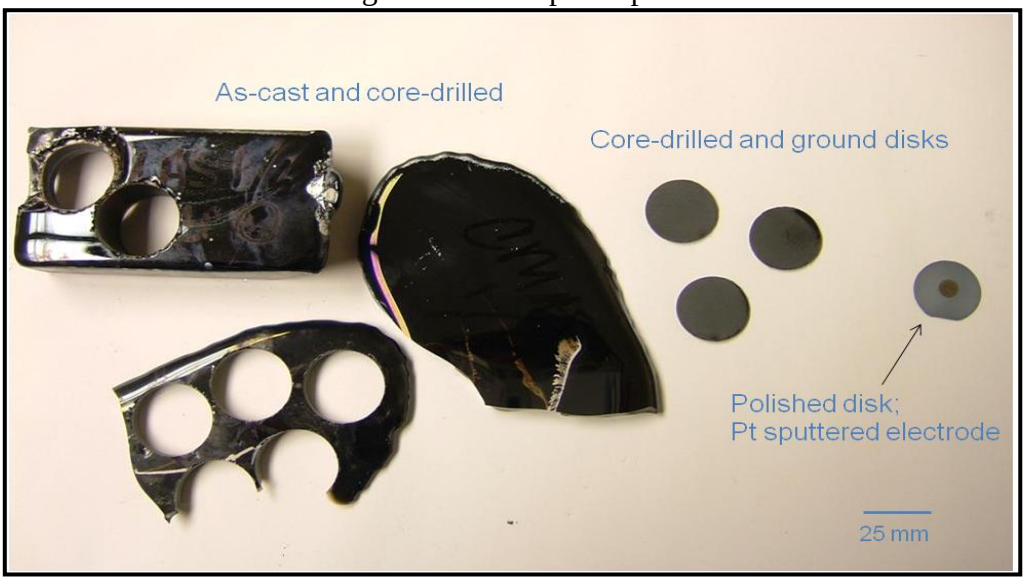


Samples from melt CMAS-1/4 were ceramized under reducing conditions (95% $N_2$/5% $H_2$ "forming gas"), ground and polished, and were sent to GTI for permeation testing. These samples were reported by GTI to be not permeable, unlike our earlier CMAS-1/2 D. Therefore, two more melts, CMAS-1/5 and CMAS-1/6, were produced to try to repeat the performance of CMAS-1/2D. However, the physical appearance of newer melts was different from our earlier melts: CMAS-1/5 was much lighter in color than CMAS-1/6, and CMAS-1/4 (Figure26). The initial thought was that the color difference was due to the retained Pd in the glass. ICP-AES analysis was done to determine the amount of Pd in each glass (Table 4). The analysis shows that the ppm of Pd in CMAS-1/5 was indeed lower, by about half, of that shown in CMAS-1/4 and CMAS-1/6. Thus, melt CMAS-1/5 was not considered for further testing. Samples from melt CMAS-1/6 were produced, ceramized under reducing conditions, ground and polished, and sent to GTI for analysis. Resistance measurements of the ceramized CMAS-1/6 glass were made and the results were comparably low as the ceramized glass of CMAS-1/2 (about $10^4$ ohm cm at room temperature).

Figure 26. Photo of glass "patty" samples, CMAS-1/4, CMAS-1/5, CMAS-1/6, respectively, from left to right. Largest patty in center is approximately 60 x 100 mm in dimension.

Table 4. Summary of Pd contents obtained by ICP-AES after digestion of the glass samples with HF and $HNO_3$. The sample labeled "LE Bar" refers to a roughly 150 x 40 x 10 mm glass piece poured separately from the "patty" samples.

| **Sample** | **Pd content (ppm)** |
|---|---|
| CMAS-1/4 Patty | 91 |
| CMAS-1/5 Patty | 52 |
| CMAS-1/5 LE Bar | 45 |
| CMAS-1/6 Patty | 117 |
| CMAS-1/6 LE Bar | 116 |

Two "alloy" melts were also produced to see what the effects of introducing another metal in addition to the Pd into the base glass had on the performance of the glass. These melts, CMAS-21 and CMAS 22 produced reasonably stable glasses, although CMAS-21 revealed evidence of small crystals in the as-cast glass as suggested by a somewhat matte-like appearance, instead of a purely glassy surface (see Figure 27). The crystals could be either unmelted material or crystals that formed during the casting and annealing process. All samples were then ceramized under reducing conditions, ground, polished and sent to GTI for hydrogen permeation testing.

Figure 27. Photo of CMAS-21 and CMAS-22, respectively, from left to right. Slightly matte-like appearance of CMAS-21 likely due to retained small crystals in the as-cast glass.

Although the Pd contents of melt CMAS-1/6 was lower than expected, it still is far higher than that obtainable in most silicate base compositions. Typical Pd contents are on the order of ppb, not hundreds of ppm, as this particular base composition allows. The solubility maximum for this composition is approximately 600 ppm. Attempts were made to produce nominally identical samples with our CMAS-1/6 melt to allow some measure of repeatability of the permeation results. Further, the Ag-Pd and Cu-Pd compositions might shed some light as to whether "alloy" metal additives have some promise towards the overall goal of significant hydrogen permeation in a robust, temperature-stable, refractory membrane.

Based on permeation test results, glass membranes synthesized by SCHOTT have highest hydrogen permeation equal 0.25 $SCFH/FT^2$, which are at least two orders of magnitude at least less than metallic membranes.

**Task 1.3.2 Select Initial Candidate Membrane**

The goal of this subtask was to develop composite inorganic membranes that have the characteristics of multiphase, multilayer and multi-function to have sufficient hydrogen permeability, chemical and mechanical stability and potentially catalytic capability. GTI coordinated the research results from subtasks 1.1, 1.2 and 1.3.1. The main objective of this task was to select candidate membrane materials for the membrane module design, fabrication and integrated testing with the bench scale biomass gasifier.

*Pd-Cu alloy membranes*

$Pd_{60}Cu_{40}$ foils

Hydrogen fluxes were successfully measured for the $Pd_{60}Cu_{40}$ membrane foils with a thickness of 0.1 mm. Figure 28 shows the hydrogen permeability at 1 atmosphere pressure and temperatures from 300 to 950°C. Hydrogen/helium mixture with a 50/50 mole fraction was used for the feed side while the permeated hydrogen was swept by nitrogen in the permeate side. The flux increased with temperature up to about 600°C, and then abruptly dropped. This was due to the transition of the $Pd_{60}Cu_{40}$ alloy from bcc (body-centered-cubic) phase to fcc (face-centered-cubic) phase when the temperature was increased. The activation energies of hydrogen permeation for the $Pd_{60}Cu_{40}$ membrane were calculated to be 9.3 and 68.9 kJ/mole/K for the bcc phase and fcc phase respectively, as shown in Figure 29.

Hydrogen permeation data for $Pd_{60}Cu_{40}$ alloy at different pressures and 850°C are shown in Figure 30. The data follow Sievert's law very well, indicating that hydrogen permeation in $Pd_{60}Cu_{40}$ alloy is mainly controlled by the bulk diffusion of hydrogen through the membrane foil, not by surface reaction of hydrogen dissociation or other external mass transfer resistance.

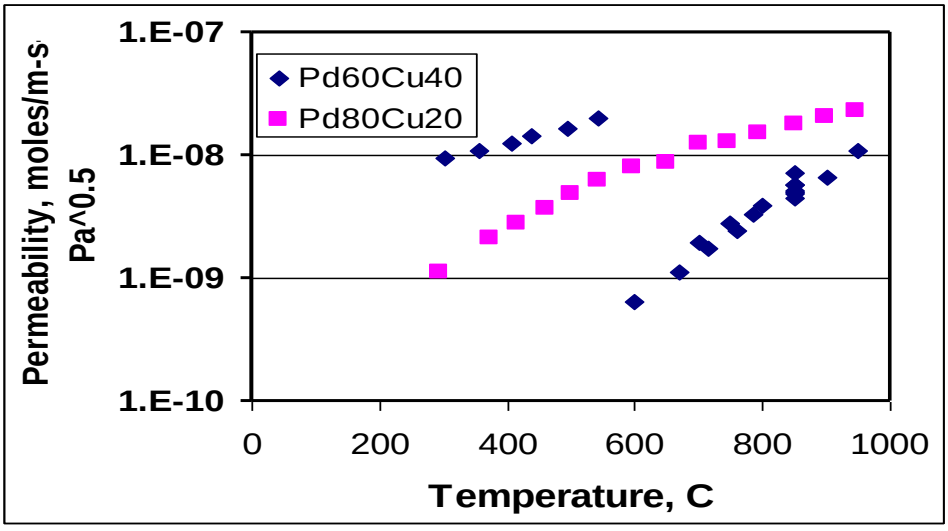


Figure 28. Hydrogen permeability of Pd-Cu alloy membranes at different temperatures

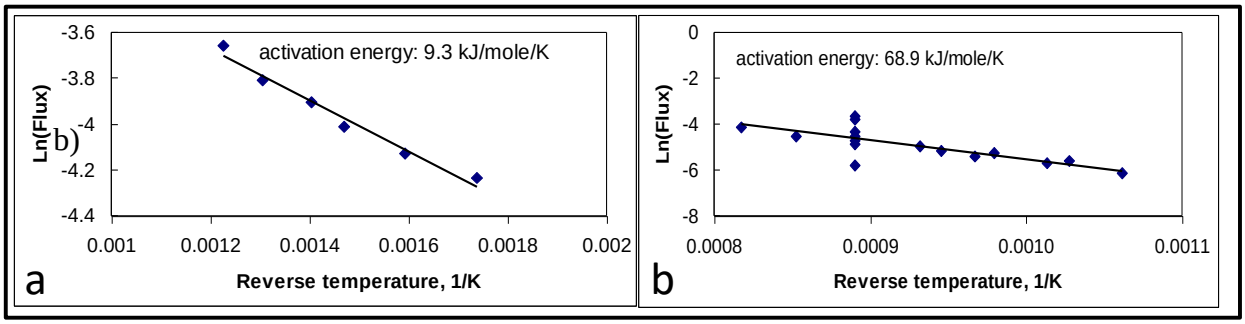


Figure 29. $Pd_{60}Cu_{40}$ membrane shows two activation energies for (a) bcc phase, 300~600ºC, and (b) fcc phase, 600-950°C.

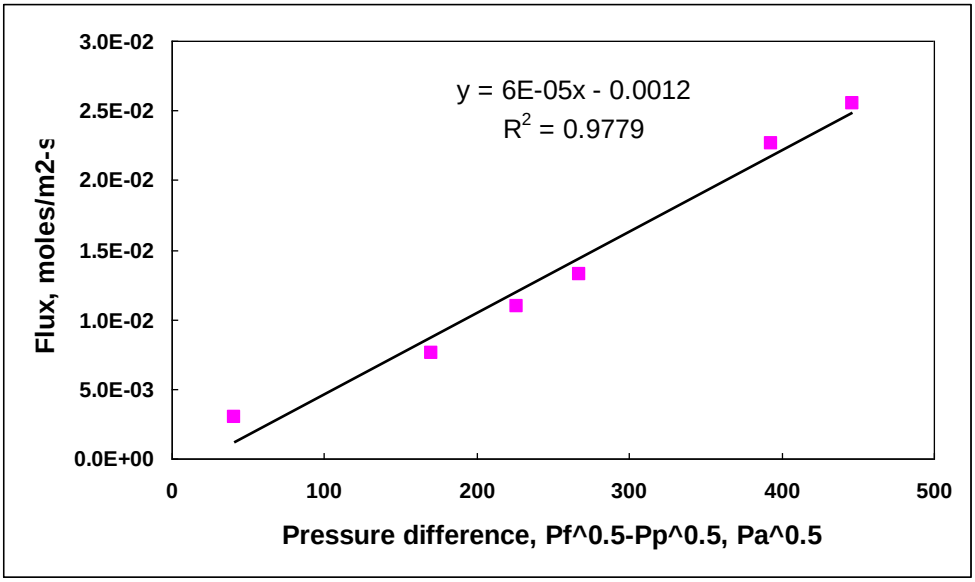


Figure 30. Hydrogen flux follows Sievert's law for $Pd_{60}Cu_{40}$ foil, T=850°C

$\underline{Pd_{80}Cu_{20}}$ foils

Hydrogen fluxes were also measured for the $Pd_{80}Cu_{20}$ membrane foils at temperatures from 300 to 950ºC and 1 atmosphere with 50/50 hydrogen/helium in feed and nitrogen sweep gas in the permeate side. The thickness of the $Pd_{80}Cu_{20}$ membrane was 0.1 mm. The results are plotted in Figure 28. In comparison with the $Pd_{60}Cu_{40}$ data, the $Pd_{80}Cu_{20}$ foil does not have a phase transition during hydrogen permeation. $Pd_{80}Cu_{20}$ alloy is of fcc phase from 300 to 950ºC. Its activation for

the entire temperature range tested is 22.7 kJ/mole-K (Figure 31). Furthermore, $Pd_{80}Cu_{20}$ shows higher hydrogen flux than $Pd_{60}Cu_{40}$ at temperatures higher than 600°C, which is the temperature range of interest for the current project.

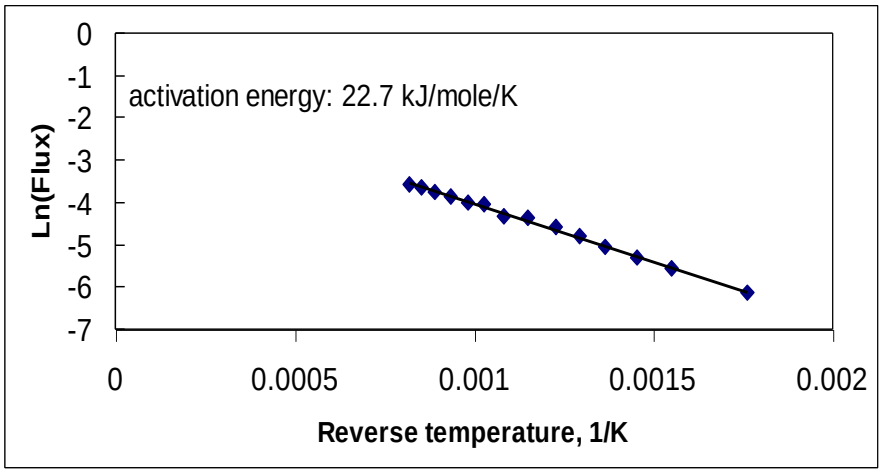


Figure 31. $Pd_{80}Cu_{20}$ membrane shows one single activation energy for fcc phase from 300 to 950°C

*Durability testing of Pd-Cu alloys*

Pd-Cu membranes are typically used in the temperature range of 200 to 600°C based on the reports and publication from the literature [16-23]. If the Pd-Cu alloys are to be used for hydrogen separation from the syngas generated from biomass gasification or steam methane reforming process, the membrane needs to be operated in the temperature range of 700 to 900°C. To ensure that the membranes have good thermal stability in this temperature range, long term hydrogen permeation testing for both Pd-Cu alloy membranes over a period of about two weeks were conducted. Figure 32 shows the hydrogen flux of $Pd_{60}Cu_{40}$ membrane at 850°C and 1 atmosphere with 100% hydrogen in the feed side and nitrogen in the permeate side. The same membrane actually had been tested at 850°C for about a week to generate the data in Figure 30 for the effect of pressure. Therefore, the time scale of Figure 32 starts from the 150th hour. There was a slight decline of hydrogen flux, but no drastic deactivation was observed over an additional 170 hours testing.

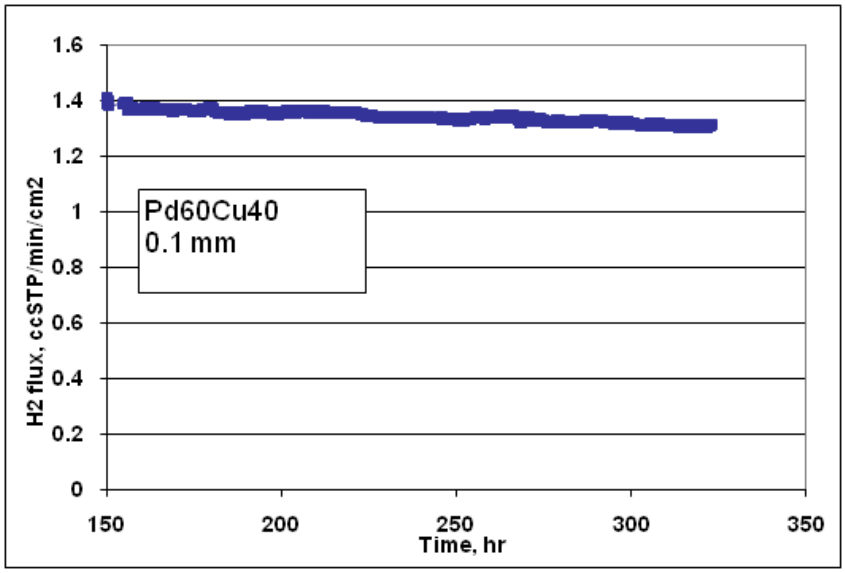


Figure 32. Long term hydrogen permeation testing for $Pd_{60}Cu_{40}$ membrane at 850°C

The long term testing results of $Pd_{80}Cu_{20}$membrane is shown in Figure 67 for a 1mm thickness of membrane, at 850°C and 1 atmosphere with 100% hydrogen in the feed side and nitrogen in the permeate side. The membrane did not show any deactivation over a 12-day period. Figures 32 and 33 show that the Pd-Cu alloy membranes look promising for hydrogen separation applications at temperatures greater than 800°C.

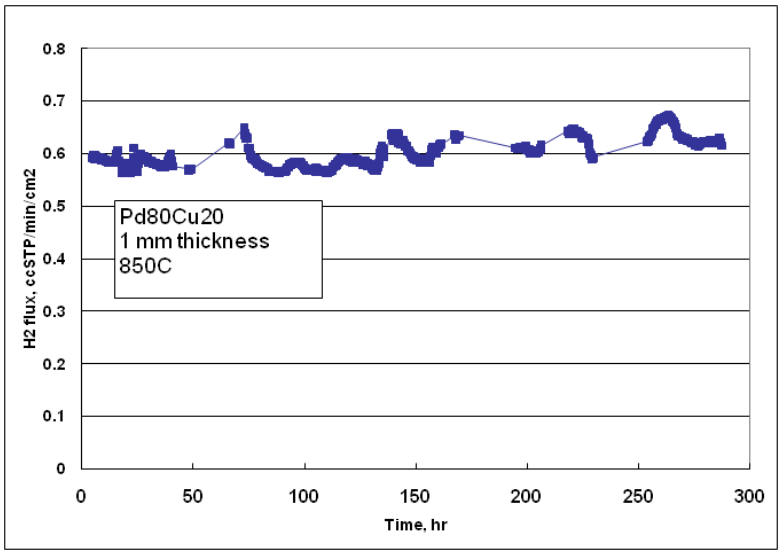


Figure 33. Long term hydrogen permeation testing for $Pd_{80}Cu_{20}$ membrane at 850°C

Permeation testing was done using simulated biomass-derived syngas at temperature equal 850ºC and feed pressure equal 30 atmosphere. Syngas mixture consists from 20 % of hydrogen, 20% of carbon monoxide, 10% of carbon dioxide and 10% of water steam balanced by helium. Small decrease (8% from initial value) of hydrogen permeation was observed (see Figure 34).

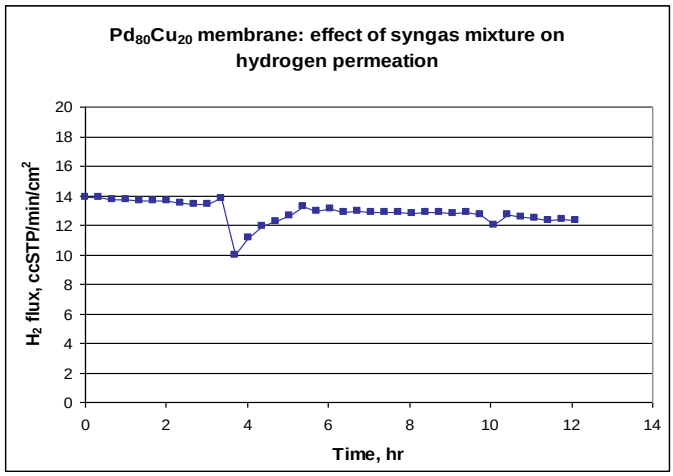


Figure 34. Effect of syngas mixture on hydrogen permeation through Pd-Cu membrane. Pressure-30 atmospheres, T=850ºC

Long-term durability testing using syngas mixture was conducted. Syngas mixture consists of 20 % hydrogen, 20% carbon monoxide, 10% carbon dioxide and 10% of water steam with balance of helium. Figure 35 shows long-term permeability experiment using syngas mixture at T=850ºC and atmospheric pressure. The first 7 hours of the experiment show hydrogen flux at pressure equal to 30 atmospheres, but due to a leak, the experiment was continued at atmospheric pressure.

Figure 35. Long term durability testing with simulated biomass-derived syngas, Pressure-

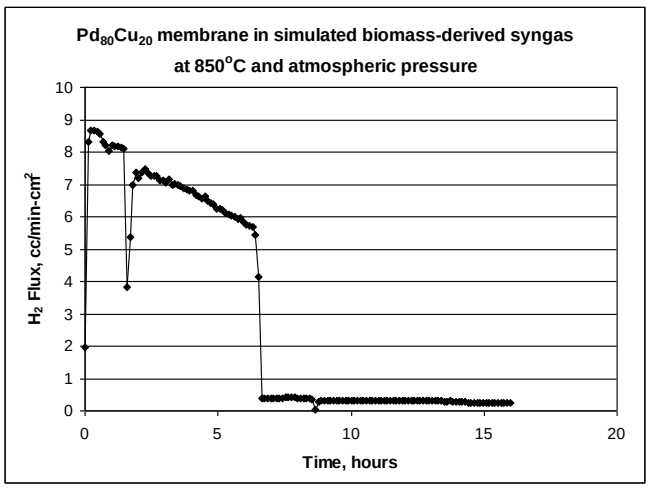


atmospheric, T=850ºC

Figure 36 demonstrates results of hydrogen permeation testing at high pressure (30 atmospheres). It can be seen that Pd-Cu membrane after 24 hours lost half of its initial activity for hydrogen separation. At the same time, previous experiments show that the membrane exhibits hydrogen sulfide resistance and has a moderate hydrogen flux at high temperature and pressure. Pd-Cu membrane was the initial candidate membrane due to the high permeability.

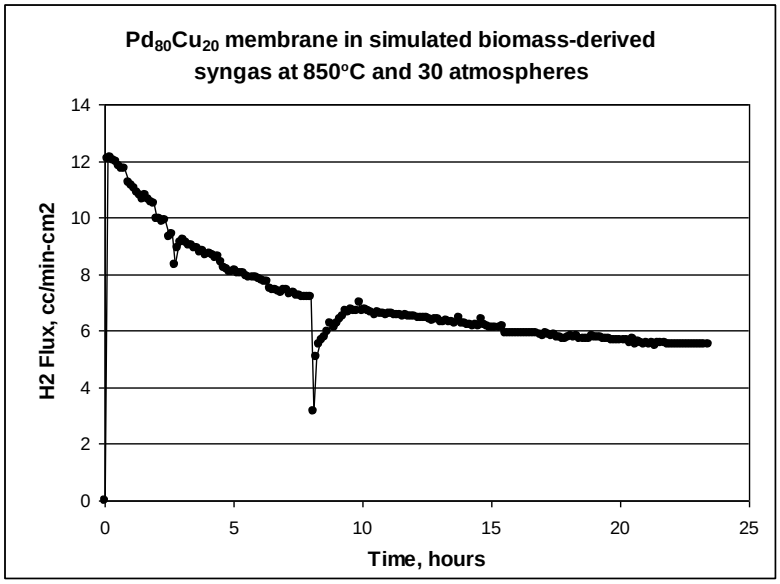


Figure 36. Long term durability testing with simulated biomass-derived syngas, Pressure-30 atmosphere, T=850ºC

*Effect of $H_2S$ on Pd-Cu membrane*

Hydrogen sulfide is a typical contaminant in the syngas generated from solid-fuel gasification systems. For biomass gasification systems, depending on the feed stocks, the $H_2S$ content is generally below 1000 ppm. Hydrogen permeation tests in the presence of hydrogen sulfide were also conducted for the Pd-Cu membrane at different temperatures. The tests were conducted with a 50/50 $H_2$/He feed containing 1000 ppm of $H_2S$ at ambient pressure. Figure 37 shows the hydrogen flux before and after the introduction of 1000 ppm $H_2S$ for a $Pd_{80}Cu_{20}$ membrane of 1 mm thickness at 850ºC. As can be seen, there was no effect on the hydrogen permeation after the membrane had been exposed to $H_2S$ for about eight hours.

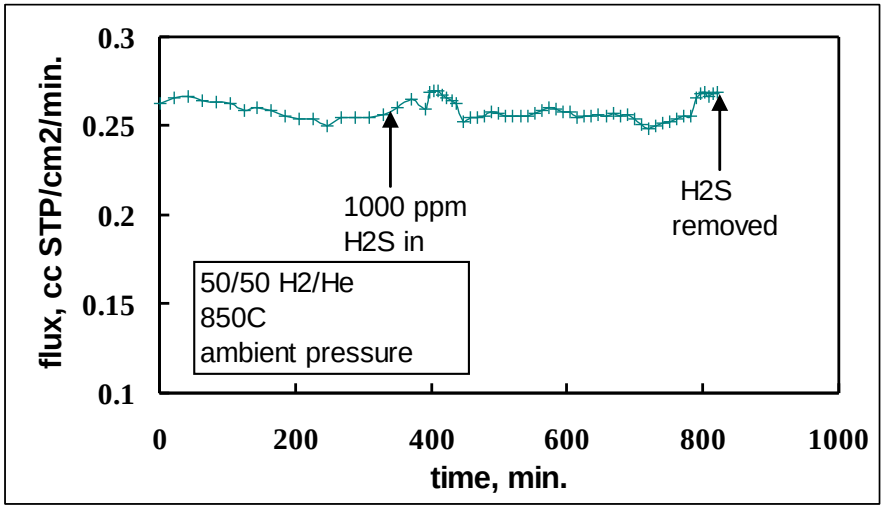


Figure 37. Effect of $H_2S$ on $Pd_{80}Cu_{20}$ alloy membrane at 850°C

*Pd-V-Pd membrane*

Pd-based membranes have shown good permeability properties along with high mechanical, chemical and thermal stability. Also, refractory metals may be used as hydrogen permeation membranes. Several metals, including vanadium, niobium, and tantalum have much higher permeability properties than palladium. The refractory metals have several other advantages over palladium as well. They are much cheaper per unit volume and have greater strength at high temperatures. These metals are not normally used for hydrogen permeation because of poor surface properties, particularly surface oxide layers that slow the hydrogen transport. When palladium or palladium alloys are applied over the surface of refractory alloys, the surface barriers are removed and hydrogen permeation approaches high levels.

Vanadium foil from Alfa-Aesar Company was electroplated by palladium. The foil was polished, the surface oxide layer was removed by reduction, and palladium was deposited by the subsequent electroplating. The membrane showed high hydrogen flux at moderate temperatures but at high temperature, the hydrogen flux decreased and it disappeared with time due to such phenomena as intermetallic diffusion. This phenomenon becomes important at high temperatures. Due to palladium diffusion into vanadium, hydrogen flux disappeared with time since there was no palladium left on the surface to dissociate hydrogen molecules into atoms. Intermetallic diffusion may be reduced if alloys of vanadium are employed.

*Pd-Ag membrane*

Palladium alloys are more practical for use as hydrogen-selective membranes because alloys alleviate the α-β phase transformation that leads to structural distortion and embrittlement in pure palladium. Alloys of Pd and Ag have been the most widely studied, largely because they form a solid solution over the entire composition range, and exhibit a maximum in hydrogen permeability at compositions near 75 % Pd/ 25% Ag.

A membrane with this composition was checked for hydrogen permeation at high temperature. The results show hydrogen flux comparable to that through 80 % Pd-20 % Cu membrane. Figure 38 shows hydrogen flux through the membrane. The increase in hydrogen permeability at time less than 40 hours is due to higher sweep nitrogen flow rate. The significant drop in hydrogen flux (80% from initial value) resulted from carbon monoxide introduction. When a carbon monoxide was removed from the feed side, membrane performance was restored. Carbon deposition was observed on the membrane surface after the experiment. The membrane is still a candidate because when the membrane is subjected to high pressure, the carbon monoxide effect can be very negligible due to unfavorable adsorption of carbon monoxide at these conditions.

$Pd_{75}Ag_{25}$ foil then was tested for hydrogen permeation (127 microns in thickness) at high feed pressure. It exhibits high permeation flux (20 cc/min-cm$^2$ at P=30 atmosphere and T of 850ºC using mixture consisting of 20% $H_2$ and 80% He). When syngas mixture was introduced, there was almost no effect on permeability of the membrane. Hydrogen sulfide did reduce hydrogen permeation flux by 25% as compared with initial value for hydrogen permeation. Pd-Ag membranes have a higher hydrogen flux than Pd-Cu membranes, while hydrogen sulfide presence affects performance of both membranes at about the same degree.

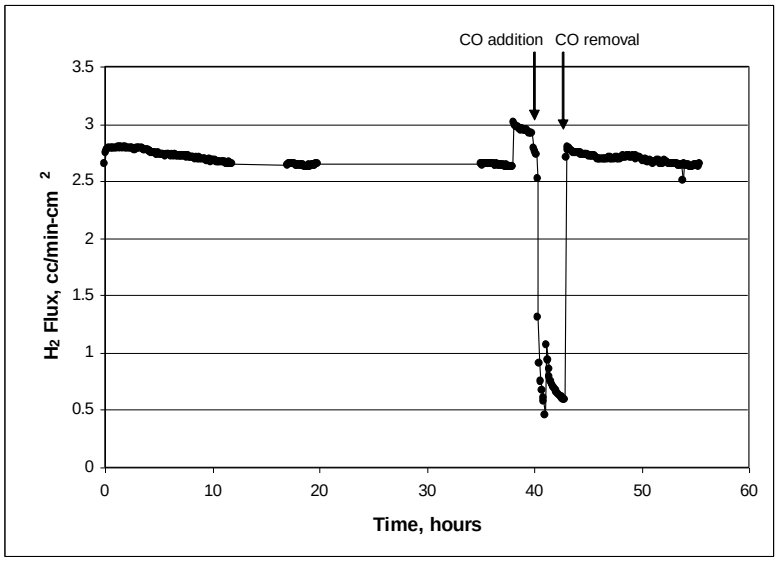


Figure 38. Hydrogen permeability of Pd-Ag alloy membranes at T equal 850ºC and CO effect on permeation flux of hydrogen.

*Refractory metal and alloy membranes*.

Pure refractory metals themselves do not make good membranes, because they become brittle at room temperature in the presence of hydrogen. However, several alloys of these metals do not become embrittled making them good candidates for hydrogen purification membranes. Titanium alloys can be divided into three groups: α-alloys, α/β alloys and β-alloys. Since the solubility of

hydrogen is very low in the α-phase, metal hydrides can form at stress concentrators at very low hydrogen concentrations and these can cause embrittlement [24]. But in stable β-Ti alloys, the hydrogen concentration can exceed 50 atomic % without hydride formation [25].

Ti-based foils as Ti 99.85-Pd 0.15 and Ti 77.5/Mo 12/Zr 6/Sn 4.5 were tested for hydrogen permeation at high temperatures and high pressures. When hydrogen was introduced the Ti-Pd membrane broke down immediately. This breakdown may be the result of hydrogen embrittlement. The hydrogen solubility in titanium is high therefore as hydrogen is incorporated into the metal lattice of the membrane, it weakens and destroys the membrane. This may be solved by palladium deposition on the membrane surface. Another try on testing of Ti-alloy (99.85%Ti-0.15%Pd) membrane show no hydrogen permeation flux when it was plated by palladium layer or used as it is. Palladium was electroplated on the surface of β-Ti alloy (Ti 77.5/Mo 12/Zr 6/Sn 4.5) and the membrane was tested. Unfortunately, when hydrogen was introduced, no hydrogen permeation was observed. It may be explained by incomplete reduction of the surface oxide layer, which is impermeable to hydrogen.

Electroplating by palladium of Ti-based alloy as 90% Ti-65 Al-4% V and V-Ni alloy were done. Ti-alloy with V and Al show low hydrogen flux (0.04 cc/cm$^2$-min) at pressure difference equal to 10 atmospheres and at 850ºC. Membrane consisted from Pd layers and 93%Ni-7%V alloy have higher hydrogen permeability 0.3 cc/cm$^2$-min at pressure difference 4 atmospheres and 850ºC. As compared with Pd-Cu membrane all these tested membranes have 1-2 orders of magnitude lower permeability for hydrogen. A membrane consisting of a Pd layer and 93%Ni-7%V alloy was tested for carbon monoxide stability. Unfortunately, even at high feed pressures of 15 atmospheres carbon monoxide introduction decreased hydrogen permeation flux dramatically down to 33 % from initial value.

*Perovskite membrane*

Membrane $LaFe_{0.57}Co_{0.38}Pd_{0.05}O_3$ was synthesized by solid state reaction and was calcinated to make a dense membrane. The membrane was successfully sealed and tested for hydrogen permeation. Hydrogen flux was low as compared to Pd-Cu metallic membrane due to low palladium content (5% atomic %). A membrane with higher palladium content may have higher hydrogen flux.

*Pd-based membranes*

Testing of alloy Pd-Ni membranes (40% Pd-60% Ni) for hydrogen permeation was done. The membrane has a low hydrogen permeability, ten times less than the Pd-Cu membrane. At the same time, the membrane shows resistance to carbon monoxide (17% in the feed) and hydrogen sulfide (1000 ppm). Figure 39 shows the results of this experiment.

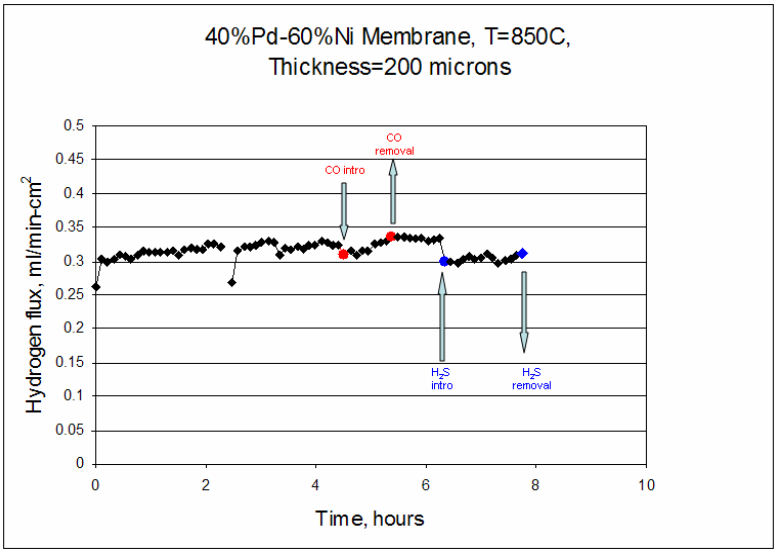


Figure 39. Effect of carbon monoxide and hydrogen sulfide on hydrogen permeation through Pd-Ni membrane. Pressure-atmospheric, T=850ºC.

*Pd-Au membrane*

Pd-Au (50% Pd-50%Au) foil shows good hydrogen permeability but the presence of $H_2S$ decreased hydrogen flux by 20 % from the initial value. As compared with Pd-Cu membrane, Pd-Au has lower hydrogen permeability (see Figure 40).

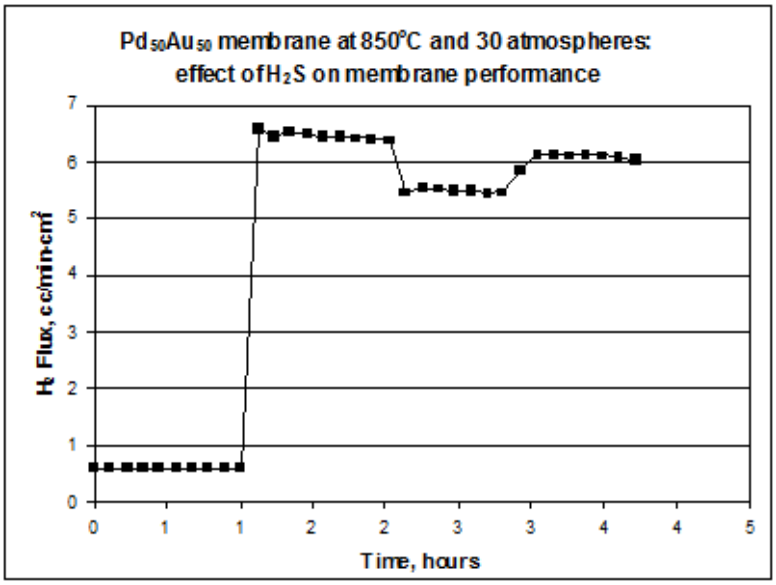


Figure 40. Effect of hydrogen sulfide on Pd-Au membrane performance

*Co plated by Pd membrane*

Co (127 microns thickness) and Pd plated Co foils exhibit low permeation flux (0.2 cc/min-cm$^2$ at P=30 atm and T = 850ºC using a mixture consisting of 20% $H_2$ and 80% He). When a syngas mixture was introduced, there was no effect on the permeability of the membranes. Hydrogen sulfide did reduce hydrogen permeation flux by 15% in the case of the Co membrane. But when Co foil was plated by Pd, hydrogen sulfide didn't affect hydrogen permeability flux. The Pd-Co alloy may have a good resistance to carbon monoxide and hydrogen sulfide.

*Ta, Ti and V-based membranes*

Ta and Ti foils (127 microns in thickness) were plated by Pd using electrodeposition technique and then the membranes were checked for hydrogen permeability. The flux is very low as compared with permeability of Pd-Cu membranes (2 orders of magnitude lower). This can be explained by surface oxide layer resistance. This can occur due to incomplete reduction prior to plating or non-continuous layer of deposited Pd and, as a result, reformation of surface oxide layer during air exposure.

Also, Ta90-W10 and V foils were electroplated and a Pd layer was deposited. The Ta-based membrane was tested for hydrogen permeation. Flux of hydrogen was found to be 0.3 SCFH/FT$^2$ at pressure difference 0.8 atm and temperature of 850°C. A Pd plated vanadium membrane showed that hydrogen flux decreased and completely disappeared with time due to hydrogen embrittlement.

*Ni-based alloy membranes*

Ni-based alloy ($Ni_{77}Fe_{14}Cu_5Mo_4$, 127 microns in thickness) was electroplated by palladium and tested for hydrogen permeation. Hydrogen flux is equal 0.8 cc/min-cm$^2$ at P=30 atmosphere and T=850ºC. When a mixture containing 20% hydrogen, 20% carbon monoxide, 10% carbon dioxide, 10% water steam, 1000 ppm hydrogen sulfide with a balance of helium, was introduced the membrane showed little reduction (5% from initial value) in hydrogen permeation flux.

Ni-based alloy ($Ni_{67}Cu_{33}$, 510 microns in thickness) was electroplated by palladium to test hydrogen permeability properties. Hydrogen flux at P=30 atmosphere and T=850ºC equals 0.3 cc/min-cm$^2$. Normalized permeability (due to different thicknesses of membranes) is still lower than for Pd-Cu membrane. Presence of hydrogen sulfide together with syngas components reduced permeability by 12 %.

Ni metallic foil was also tested for hydrogen permeation. However, a leak developed during heating due to a large difference of thermal expansion coefficients between the support (stainless steel) and the Ni foil.

*Pd and Cu electroplating of support.*

Stainless steel support was electroplated by Pd and Cu metals consecutively. After a few hours of plating some pores were still open. There was preferential hydrogen permeation so additional electroplating is needed to prepare a dense membrane. Also, other metals such as Ni, Fe, Co, Ag, and Au can be deposited by layer and thermal treatment leads to alloy formation.

*Ceramic membranes synthesized by Schott*

Pd-based ceramic membrane was obtained from SCHOTT and tested for hydrogen permeation. At T=350°C, hydrogen flux is 0.15 SCFH/FT$^2$ at pressure difference 35.7 psi. At T=850°C, hydrogen flux is 0.25 SCFH/FT$^2$ at pressure difference 12 psi. These results are very encouraging for potential use of Pd-based glass membranes.

*Porous supports*

Permeability of membranes is inversely proportionate to thickness. Therefore, to have a higher hydrogen flux thinner foil is needed. Mechanical stability for these thin membranes may be provided by using porous supports. Porous supports of stainless steel, ceramics and titanium were bought and tested for use in a membrane module. Stainless steel (SSL-316) and titanium supports withstood high pressure and temperature without any obvious changes while the ceramic support was destroyed due to high pressure. To facilitate choosing between these supports additional experiments should be conducted. Metallic supports are mechanically strong but intermetallic diffusion between the membrane and support became a concern at long-term operations. Ceramic substrates have good thermal and chemical stability then mechanical stability may be improved by using a thicker support or an additional metal layer.

To develop a design for the membrane support structure, experiments with and without support were conducted. To prevent intermetallic diffusion between Pd-Cu membrane and SS porous substrate, porous cement was deposited on the surface of substrate. Figure 41 shows there is no transport resistance for SS porous support (20 microns pore size) coated by cement.

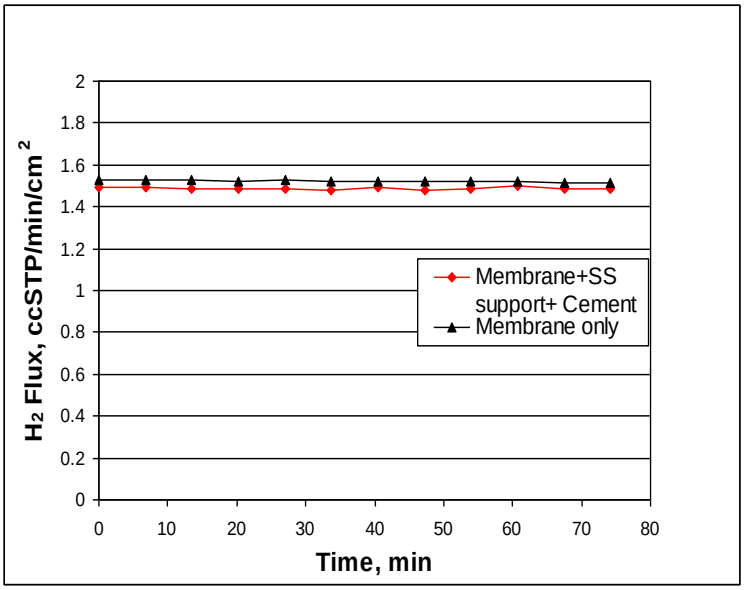


Figure 41. Experiments with and without porous support to check transport resistance of substrate. Pressure-atmospheric, T=850ºC

*Sealing for high temperature and high pressures*

Sealing of membranes is a critical step. Metals such as silver, gold or copper may be used for sealing due to softness of the material. Due to failure of copper O-rings for pressures higher than 4 atmospheres, thicker O-rings and O-rings coated by carbon were tested. Leak-free sealing was achieved up to 8 atmospheres at high temperature, but success was not 100%. As a result a new reactor design was made and finalized. This design incorporates copper O-rings fitting into groves to allow tight sealing at high pressures.

*Catalysts for tar cracking,reforming and shift reactions.*

Based on literature, two forms of catalysts, nonmetallic and metallic, have proven effectiveness for tar conversion in biomass gasification. Dolomites are the most widely used nonmetallic catalysts for tar conversion, while olivine, another naturally occurring mineral has also demonstrated tar conversion activity. Metallic catalysts as nickel-based catalysts have proven to be very effective for tar destruction and reforming. Also, they have some water-gas shift activity. Some studies have also shown that nickel catalyzes the reverse ammonia reaction thus reducing the amount of ammonia in gasification product gas. A limitation for nickel catalysts is rapid deactivation, which leads to short catalysts lifetime. The catalyst used in tar reforming, steam reforming and methane reforming should be able to operate at elevated temperatures. A nickel-based catalyst by BASF Company was chosen for tar and methane reforming. Also, it is known that Pd has high catalytic activity for water-gas shift reactions at high temperature. So, if the selected membrane contained some amount of palladium, there may be no need for additional shift catalyst.

During the milestone meeting, GTI identified the procedure used to downselect the metals to be evaluated for an initial candidate membrane. As shown in Figure 42, four series of metals were identified and tested based on a literature review. Each metal series is shown in a different color: red, green, blue, and purple. The red series (PdCu, PdAg, and PdAu) showed the highest permeability. Each of the color series in sequence showed a decreased permeability (order of magnitude) for the green, blue, and the lowest permeability for the purple series.

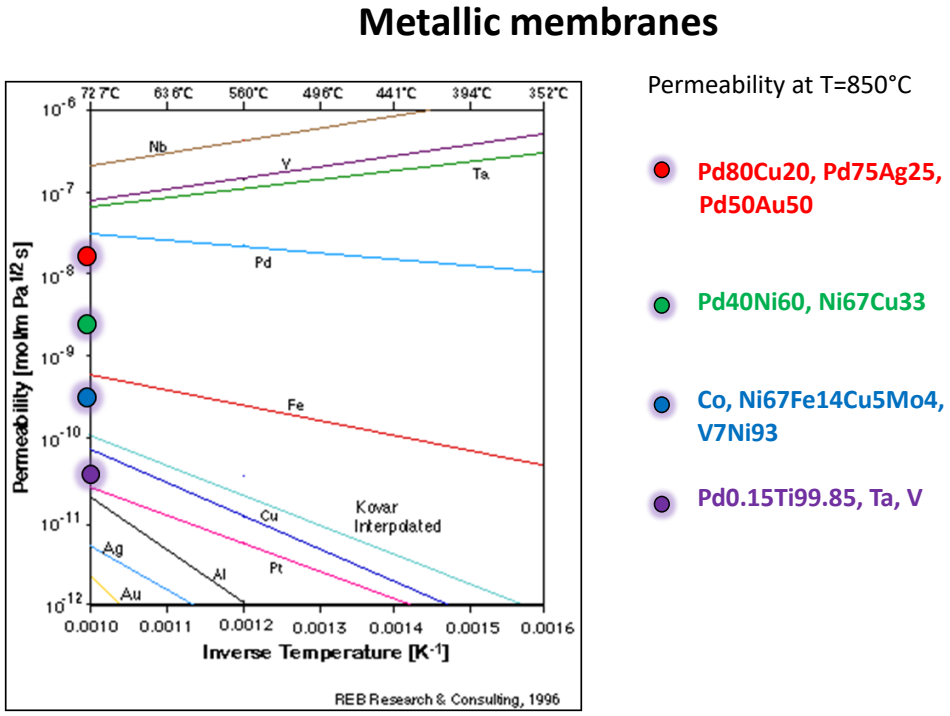


Figure 42. Permeability of metallic membranes together with literature data.

Table 5 show most successful membranes in every area synthesized by GTI, NETL, Arizona State University and Schott Company.

CONCLUSION

- Based on experimental data presented on Table 5, Pd-Cu membrane was chosen as the initial candidate.
- SS porous support with 20 microns pore size coated with cement was selected for the membrane support.
- A Ni-based catalyst was initial choice for tar cracking, reforming and shift reactions

Table 5. Properties of membranes tested during Task 1.3.2: Select Initial Candidate Membrane

| Membrane & Thickness | $H_2$ Flux, SCFH/FT$^2$ | Temperature,$^o$ C | ΔP $H_2$,psi | Effect of $H_2S$ | Effect of Syngas (CO, $CO_2$, $H_2O$) |
|---|---|---|---|---|---|
| GAS TECHNOLOGY INSTITUTE | | | | | |
| 50Pd50Au - 200µm | 12.8 | 850 | 86.7 | 15% decrease | n/a |
| 80Pd20Cu - 120µm | 47.2 | 850 | 216.2 | 7% decrease | n/a |
| 80Pd20Cu - 120µm | 25.6 | 850 | 85.1 | n/a | 7% decrease |
| 75Pd25Ag – 127µm | 36.8 | 850 | 52.9 | 15% decrease | 5% decrease |
| NATIONAL ENERGY TECHNOLOGY LABORATORY | | | | | |
| 69Pd31Pt - 100µm | 24.5 | 750 | 79.3 | 18% decrease | n/a |
| 95Pd5Au - 100µm | 81.9 | 750 | 79.8 | 35% decrease | n/a |
| 77Pd23Ag - 111µm | 36.0 | 700 | 78.0 | n/a | n/a |
| 94Pd6Ni - 100µm | 40.5 | 750 | 79.6 | n/a | n/a |
| 80Pd20Cu - 140µm | 27.7 | 900 | 80.5 | n/a | n/a |
| ARIZONA STATE UNIVERSITY | | | | | |
| $SrCe_{0.95}Tm_{0.05}O_3$-1 mm | 0.03 | 850 | 1.47 | n/a | n/a |
| SCHOTT North America | | | | | |
| <1%Pd-glass- 1.5mm | 0.15 | 350 | 35.7 | n/a | n/a |
| <1%Pd-glass- 1.5mm | 0.25 | 850 | 12.0 | n/a | n/a |

## Task 2. Process Development and Economic Analysis

The objective of Task 2"Gasification membrane reactor process development and economic analysis" in Phase 1 was to perform a preliminary techno-economic analysis to determine the potential economic viability of hydrogen production from biomass gasification using an initial candidate membrane chosen in Task 1.2. A process system for producing the lowest cost hydrogen from biomass incorporating the gasification membrane reactor was developed in this task. Different process schemes and operating conditions were evaluated in a commercial flowsheet simulator, HYSYS, which also calculates mass and energy balances of the system. Process variations depend on how the non-permeable gas from the gasification membrane reactor is processed in the downstream steps. Energy efficiency and economic analysis was performed to evaluate the cost of each process option. The modeling approach was used to calculate the membrane area requirement for close-coupling with the biomass gasification and hydrogen separation for a conceptual design of the membrane gasification reactor.

The results of this task set the targets for the performance and the cost of the membrane materials. It was expected that certain iterations between Tasks 1.5 and 2 would be needed to determine the optimal process and the best material. Estimating the costs of the process compared to the conventional technology can determine the economic feasibility of a project. Also the analysis was useful in directing research toward areas in which improvements will result in the greatest cost reductions. The expected deliverable from this task was a biomass gasification membrane reactor system that verifies the technology and meets the DOE's cost target of \$1.60/kg $H_2$, based on the feasibility study of the membrane materials and initial conceptual process design.

### Process Design

The central hydrogen production technologies considered in this analysis comprise biomass gasification and hydrogen production without carbon capture. For this project, the RENUGAS® biomass gasification technology was utilized. Biomass gasification is the partial oxidation of biomass feedstocks to produce a combustible low-calorific-value (LCV) fuel gas. This chemical transformation can take place in fixed, moving, or fluidized beds or entrained flow gasifiers at temperatures of 1400 to 1800°F and pressures from 1 to 30 atmospheres. The RENUGAS® technology uses a single fluidized-bed gasification vessel to achieve high carbon conversion to gas. Fluidized-bed operation also allows the utilization of fine (dusty) feedstocks, and is tolerant to feedstock variations due to its large inventory in the gasifier. These characteristics provide the following benefits: (1) the ability to convert a wide range of biomass feedstocks to fuel gas; (2) the ability to produce an excellent biomass-to-fuel gas conversion efficiency; and (3) the production of a fuel gas that is very low in tar content, minimizing cleanup costs.

Some of the basic biomass gasification reactions are as follows:

$C\ (biomass) + O_2 \rightarrow CO_2$

$C\ (biomass) + \frac{1}{2}\ O_2 \rightarrow CO$

$H\ (biomass) + \frac{1}{4}\ O_2 \rightarrow \frac{1}{2}\ H_2O$

$Biomass \rightarrow CO + CO_2 + H_2 + H_2O + CH_4 + C_xH_y + oils\ \&\ tars$

$C\ (biomass) + H_2O \rightarrow H_2 + CO$

$CO + H_2O \rightarrow \ H_2 + CO_2$

$C + CO_2 \rightarrow \ 2\ CO$

$C_xH_y + x\ H_2O \rightarrow \ x\ CO + (x+y/2)\ H_2$

The first step in the gasification process is to reduce the moisture level of the biomass to between 10 and 20 percent. The biomass is brought from the dryer to the gasifier via appropriate solids handling equipment. The solids' handling equipment delivers biomass to the gasifier through the feeding system. The gasifier is fed with steam and oxygen (or air) to produce a hot syngas. The syngas flows through a cyclone that removes particulates in the syngas (Figure 43).

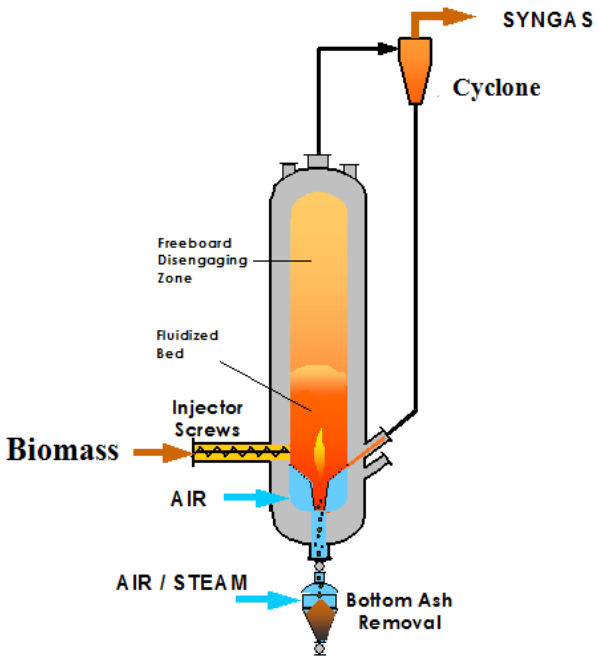


Figure 43. Simplified Cross-Section of RENUGAS® Gasifier

The downstream process flow designs for three cases were developed using the HYSYS® process design and simulation program. In the first two process options, the membrane module and the reformer catalysts were integrated into a single unit such that various processing steps (tar reforming, methane steam reforming, shift conversion and hydrogen purification) necessary

forefficient hydrogen production occur in a single reactor. But in the first configuration, the membrane reactor is located inside the biomass gasifier, while in the second case the membrane module is located outside of the gasifier after the cyclone. In the third configuration, conventional hydrogen production, the components downstream are placed in order: tar reformer, syngas cooler, low-temperature water-gas shift reactor, $H_2S$ and $CO_2$ physical absorption units, and pressure swing adsorption. Feedstock for the biomass gasification was chosen based on its cost and information availability.

Since the biomass gasification reactor operates at elevated temperatures (800 to 900°C), it is necessary to also have the membrane module operate at elevated temperatures. The palladium-copper alloy as an initial candidate membrane was tested for high pressure and elevated temperature operation.

Also, additional hydrogen can be formed by the reactions:

$$CH_4 + 1/2O_2 \rightarrow CO + 2H_2 \text{ (Partial Oxidation)}$$

$$CH_4 + H_2O \rightarrow CO + 3H_2 \text{ (Reforming)}$$

$$H_2O + CO \rightarrow H_2 + CO_2 \text{ (Shift)}$$

A catalyst is incorporated in the membrane module to promote the reactions. The catalyst used in tar reforming, steam reforming and methane reforming should be able to operate at elevated temperature. A nickel-based catalyst by BASF Company was chosen for tar and methane reforming. Also, nickel is active as a catalyst in the water-gas shift reaction. In the membrane module, partial oxidation, reforming and shift reactions and the hydrogen separation take place. Hydrogen is transported to the permeate side of the membrane by the partial pressure difference driving force. When hydrogen is removed from the reaction zone, more hydrogen is formed by these reactions. Significant amounts of hydrogen are recovered from the reaction zone by transport through the membrane to the permeate side. Eventually, a partial pressure difference (driving force) between the reaction zone and the permeate side is reached, limiting the amount of hydrogen that can be recovered.

For the conventional process, tar reforming and methane steam reforming occur in one reactor and the water-gas shift reaction occurs in the low-temperature regime in a separate reactor. A commercially available CuO/ZnO catalyst is used.

In the first two options (membrane module inside gasifier and closely-coupled membrane module) purified hydrogen will be obtained at low pressure so a compressor is needed. For the third case, the conventional process, hydrogen will be extracted at high pressure so there is no need for additional compression.

Figure 44 shows the schemes of modeling for process development. RENUGAS® modeling software results as syngas composition, temperature, pressure, etc were used as input data for the HYSYS software. Results of HYSYS such as hydrogen flux, temperature, pressure, membrane area, gas composition were used as input for the AspenPlus Software to determine the potential economic validity of the process. The Hydrogen Analysis [1] (H2A) production models provide

cost analysis methodology for the production of hydrogen with process design assumptions. Required input to the models includes capital and operating costs for the hydrogen production process, fuel type and use, and financial parameters such as the type of financing, plant life, and desired internal rate of return. The models use a standard discounted cash flow rate of return analysis methodology to determine the hydrogen selling cost for the desired internal rate of return.

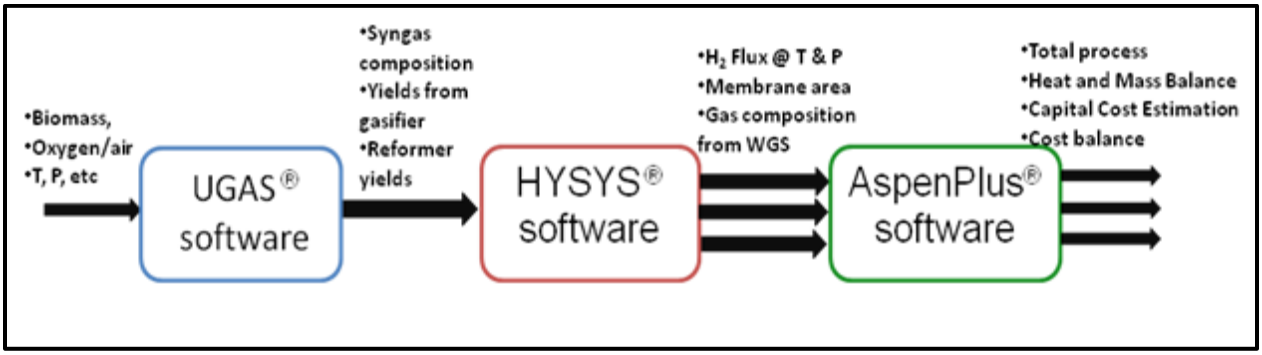


Figure 44. Process Modeling Scheme.

**Gasifier Modeling**

Fluidized bed gasifier required a feed to have moisture level between 10 and 20 percent. The gasifier is fed with dried biomass, steam and oxygen (or air) to produce a hot syngas. The syngas passes through a cyclone section to remove particulates in the syngas. The feedstock used for this analysis is hybrid poplar wood chips delivered at 50 wt% moisture. The properties of the feed used in this study are given in Table 6.

Table 6. Proximate and Ultimate analysis results for hybrid poplar wood chips

| Proximate Analysis | |
|---|---|
| Moisture, % | 20.00 |
| Volatile Matter, % | 66.19 |
| Ash, % | 0.90 |
| Fixed Carbon, % | 12.91 |
| Ultimate Analysis | |
| Ash,% | 0.92 |
| Carbon, % | 50.88 |
| Hydrogen, % | 0.04 |
| Nitrogen, % | 0.17 |

| | |
|---|---|
| Sulfur, % | 0.09 |
| Chlorine, % | 0.00 |
| Oxygen, % | 41.90 |

In the process, the gasification reactor produces 193,410 $Nm^3$/hr of syngas with the following major constituents: 14.6% $H_2$, 8.7% $CH_4$, 7.9% CO, 21.8% $CO_2$, and 42.0% $H_2O$. A summary of the parameters for the gasifier reactor is in Table 7.

Table 7. Summary of parameters for gasification reactor.

| | |
|---|---|
| feed, lb/hr | 229,648 |
| oxygen feed, lb/hr | 65869 |
| steam feed to gasifier, lb/hr | 112162 |
| transport gas, lb/hr | 22965 |
| syngas flow rates, lb/hr | 426396 |
| Hydrogen,% | 14.6 |
| Carbon monoxide,% | 7.9 |
| Carbon dioxide,% | 21.8 |
| Water steam,% | 42.0 |
| Methane,% | 8.7 |
| Higher hydrocarbons,% | 0.3 |

The design was based on a biomass feed of 2000 TPD (dry) using wood chips. GTI's RENU-GAS® fluidized bed was used for the gasifier, operating at 30 bars and 927° C. Oxygen, instead of air, was used for the gasifier oxidant. Air separation was based on the conventional cryogenic process. In addition to the gasifier, oxygen was also used for the combustion of the waste gas for steam or power generation. The simulation also focused on the heat recovery to generate additional power from the steam cycle.

**Downstream Processes Modeling**

The composition of syngas obtained from RENUGAS® modeling was input into a HYSYS® model to study the effect of process conditions. For a closely-coupled membrane with gasifier case, shown in Figure 45, the gasifier gas was first cracked to remove tars (in the vessel with a C on it in the left of the figure), and this also serves to increase the hydrogen concentration in the gas. Next, the gas was brought to equilibrium concentrations at a variety of temperatures from 1000º F to 2000º F, reflecting possible heating or cooling of the reformed gas stream. Next, a series of five steps where hydrogen is removed by the membrane followed by re-equilibration of the gas composition was performed so that an accurate profile of the hydrogen partial pressure driving force across the membrane was obtained. The amount of hydrogen permeating in each of these five stages was set so that their areas were about equal when a 100-micron thick membrane was used with a 1 bar permeate pressure at a starting temperature of 1800º F. The HYSYS® model also included several stages of compression for the hydrogen product, so that a variety of permeate pressures could be evaluated.

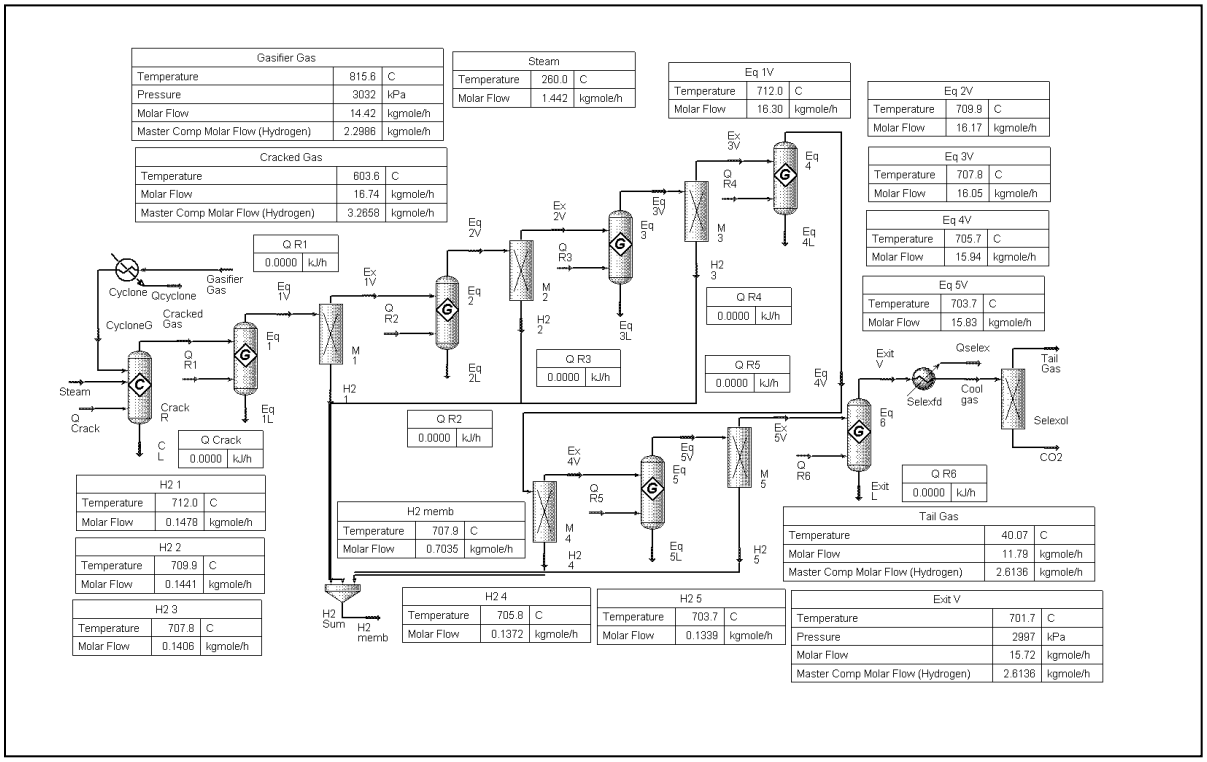


Figure 45. Flow Diagram of Closely-Coupled Membrane with Gasifier Case for Process Condition Optimization Study

Based on the equations for membrane permeation rate as a function of thickness, temperature, and differential hydrogen partial pressure that were obtained from laboratory data, areas were calculated for each of the five zones in the model, and were summed to give the required membrane area for the chosen process conditions. Increasing the temperature increased the flux rate, and thus reduced membrane area. Temperature dependence was investigated and results are shown in Figure 46.

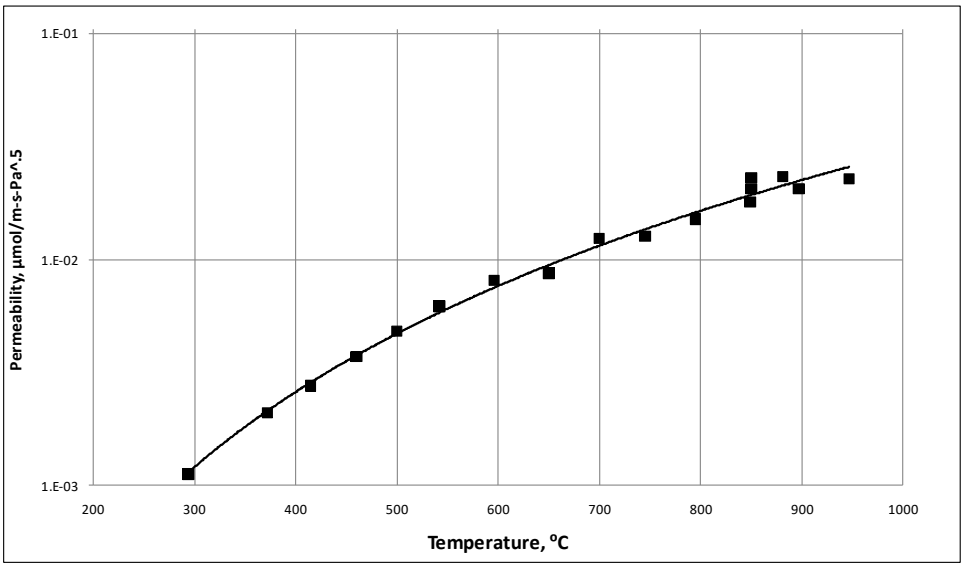


Figure 46. Hydrogen permeability as a function of temperature.

Increasing the permeate pressure decreased the flux by decreasing the driving force, but also decreased the amount of hydrogen compression needed to deliver a hydrogen product at 300 psi.

Figure 47 shows the dependence of membrane permeance from feed pressure.

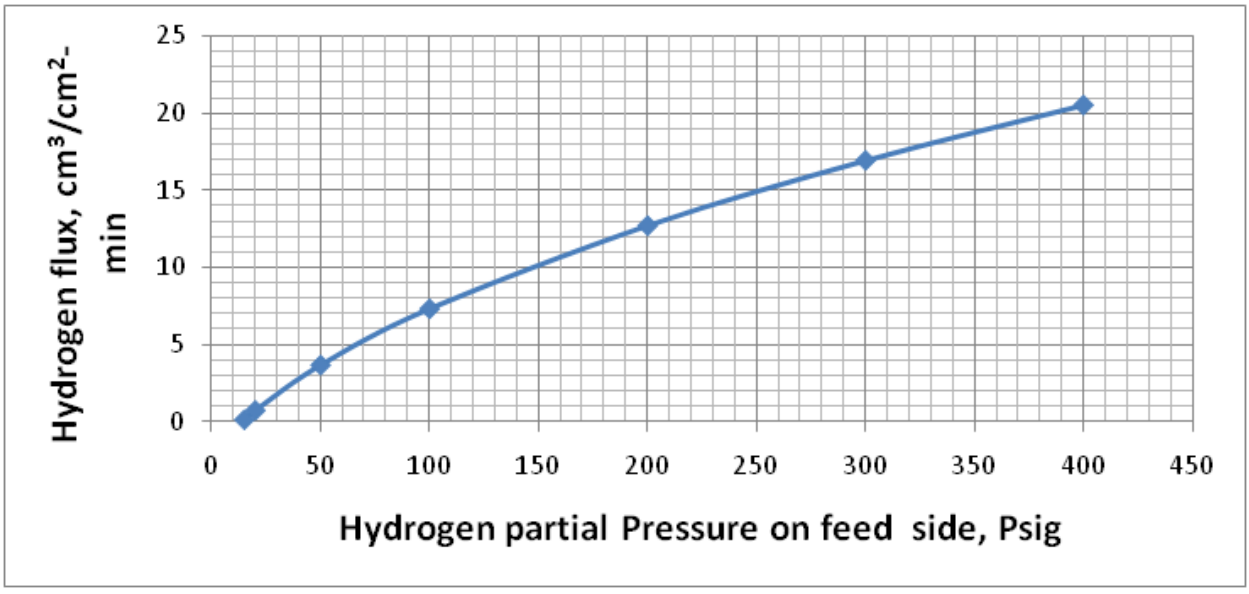


Figure 47. Effect of feed pressure on hydrogen flux of $Pd_{80}Cu_{20}$ membrane.

Hydrogen permeation flux increases with thinner membranes. The dependence of permeation flux with thickness is shown in Figure 48.

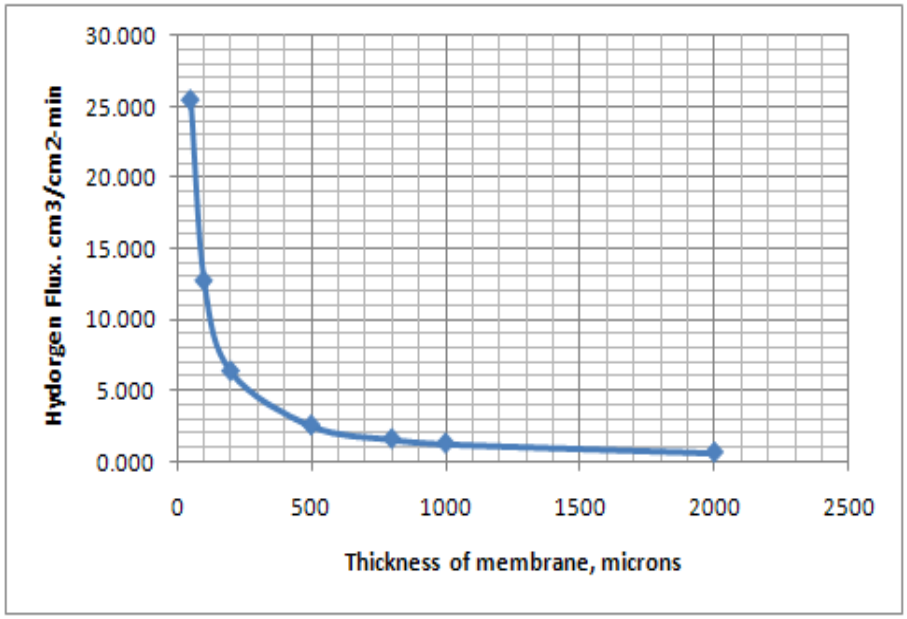


Figure 48. Effect of membrane thickness on hydrogen flux through $Pd_{80}Cu_{20}$ membrane

To determine the optimum process conditions, first a membrane investment cost was obtained by multiplying the membrane area by its cost ($21,500/m$^2$ at 100 microns thickness; $12,000/m$^2$ at 50 microns thickness; and $7,000/m$^2$ at 25 microns thickness). The capital costs of the compressors were obtained by using a scaling-law equation. To these capital costs, an operating cost for 4 years operation of the compressors was added to reflect a levelized cost approximation. The results of these studies for the 50-micron membrane are shown in Figure 49. The inlet temperature is given on the x-axis while the levelized cost is given on the y-axis, with different permeate pressures (in bars) shown in the legend.

With a 0.4 bar permeate pressure the optimum temperature is approximately 1700º F. However, levelized costs are reduced as the permeate pressure is reduced down to about .05 atm. Further reduction in permeate pressure results in a levelized cost increase. At these lower permeate pressures, the optimum temperature is the maximum temperature studied.

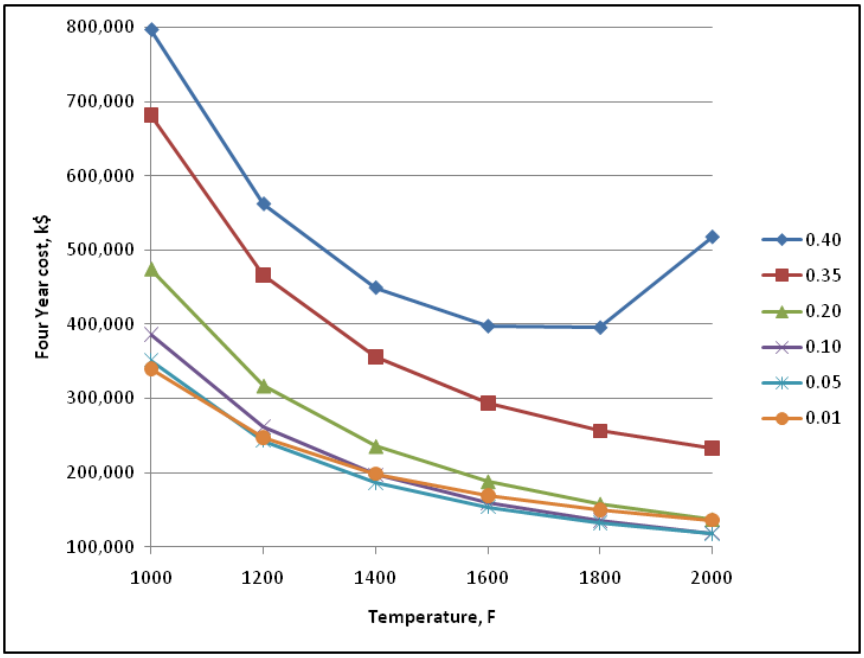


Figure 49. Levelized Cost with 50-Micron Membrane

The levelized cost analyses for the 25-micron thick membrane are shown in Figure 50. Overall levelized costs are lower than with the 50-micron thick membrane. But with this membrane, the optimum permeate pressure is about 0.2 bar.

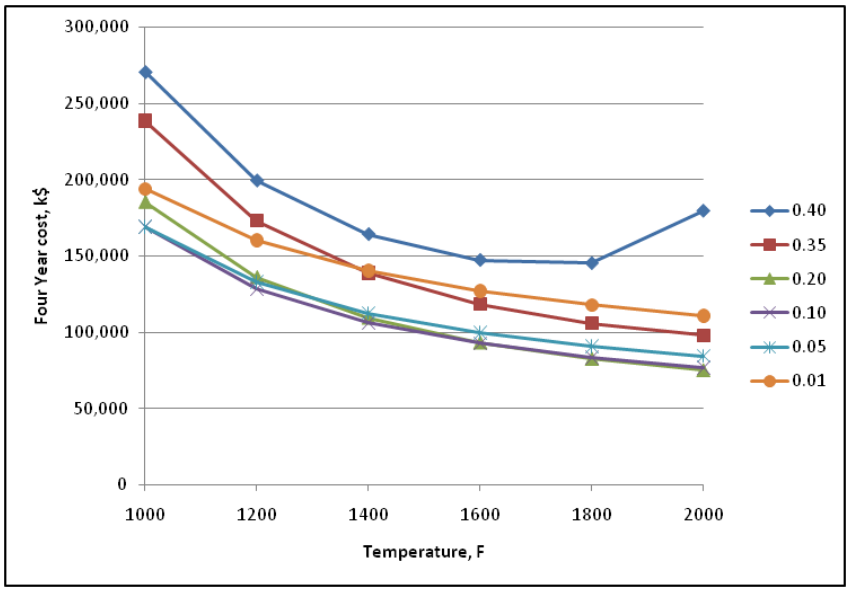


Figure 50. Levelized Cost with 25-Micron Membrane.

For the conventional case shown in Figure 51, the gasifier gas passed through a tar reformer and then gas cleaning using a cyclone. The syngas was cooled through heat exchange with the steam cycle and additional cooling via water scrubbing. Low water-gas shift reaction is a next step to maximize hydrogen concentration. Removal of $CO_2$ and $H_2S$ was accomplished using the Selexol technology. Clean and cooled gas was directed to pressure-swing absorption where hydrogen was separated and tail gas was directed to generate power. Because this process is commercially available, no process optimization was done.

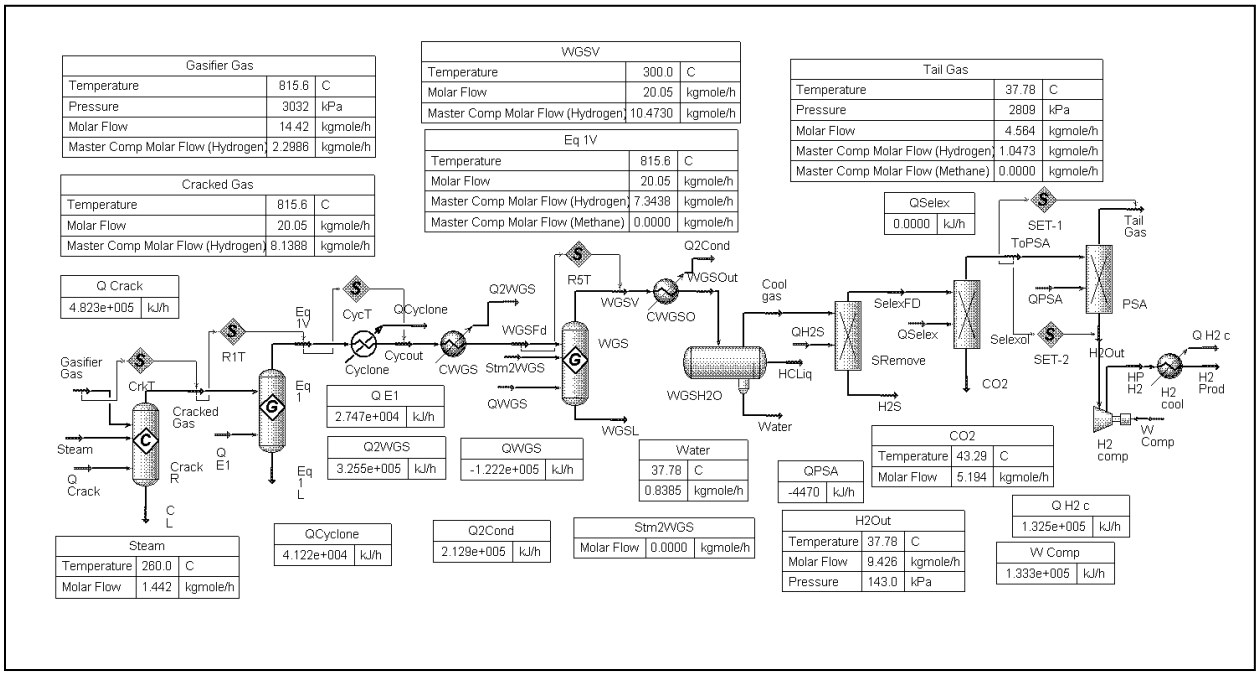


Figure 51. Flow Diagram of Conventional Hydrogen Production with PSA Case.

## H2A Analysis

A preliminary techno-economic analysis was performed to determine the potential economic viability of hydrogen production from biomass gasification using an initial candidate membrane-$Pd_{80}Cu_{20}$ foil 100 microns thick. Estimating the costs of the process compared to the conventional technology can determine the economic feasibility of a project. Also the analysis was useful in directing research toward areas in which improvements will result in the greatest cost reductions. As the economics of a process are evaluated throughout the life of the project, advancement toward the final goal of commercialization can be measured.

H2A production models provide cost analysis methodology for the production of hydrogen with process design assumptions. Required input to the models includes capital and operating costs for the hydrogen production process, fuel type and use, and financial parameters such as the type of financing, plant life, and desired internal rate of return. The models use a standard discounted cash

flow rate of return analysis methodology to determine the hydrogen selling cost for the desired internal rate of return.

To compare the metallic membrane with the PSA process, an Aspen Plus model was formulated of an entire plant to correspond to the PSA Target Case Economics study [26]. Since PSA is a commercial process, it was assumed that the design conditions for PSA have been optimized. The capital cost for the PSA section of the plant has been reduced to 17 million$ from 30 million$ in the Current Design Case. The Process Flow Diagram for the metallic membrane case is shown in Figure 52.

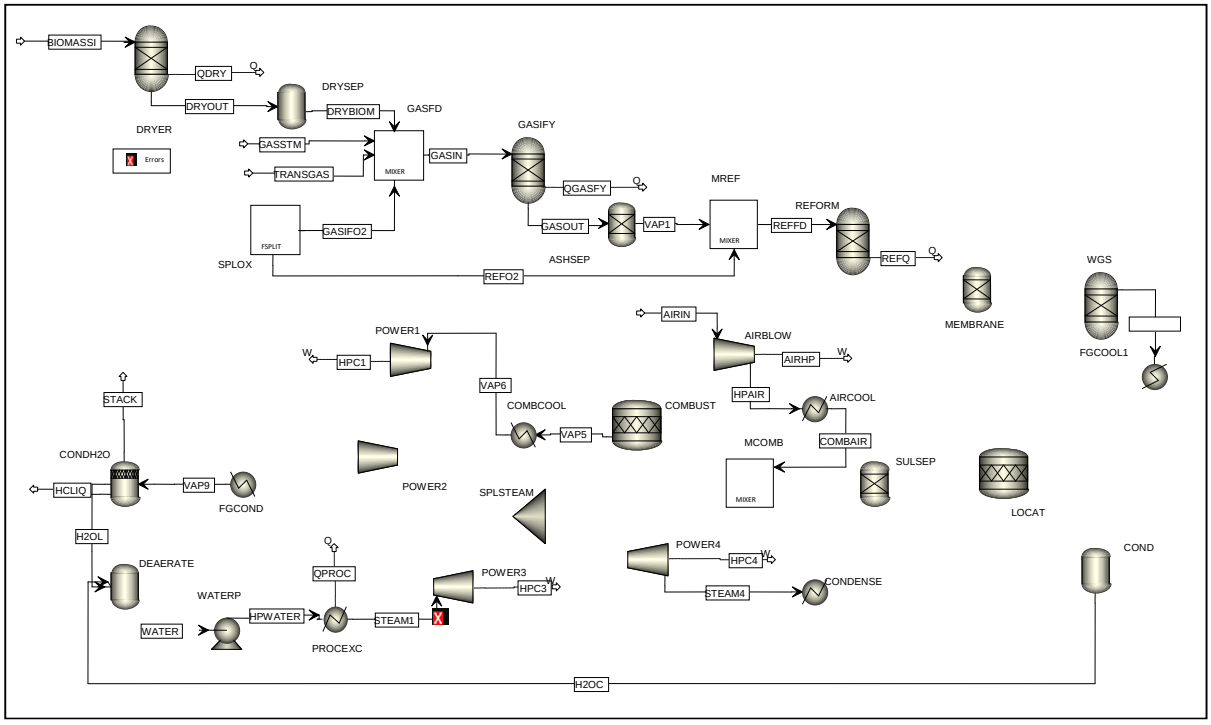


Figure 52. Process Flow Diagram of Metallic Membrane Process

To be consistent with what was done for the published H2A study with PSA, the same hybrid poplar wood chip feed was chosen at a rate of 2000 tons per day (dry basis). First, the feed is dried to 20% moisture from 50% and then ground for feeding to the gasifier. Next, steam, oxygen and transport gas are mixed with the dried biomass and fed at 28.9 atm to the gasifier. Next, the ash is removed and there is provision to add oxygen to heat the reformer feed to higher temperatures. In this study, none was added, but external heat exchange was used to raise the reformer temperature to 982º C. The metallic membrane is installed in the freeboard space of the reformer. In the PFD, this is shown as separate hydrogen removal and composition equilibration steps, as was done in the HYSYS model. Because the GTI gasifier can operate at 28.9 atm, no syngas compression is needed, as in the PSA process. Next, the gas is cooled and fed to a LO-CAT for conversion of hydrogen sulfide to elemental sulfur for removal. Because there are no catalytic shift steps needed

in this process, the ZnO bed that is needed in the PSA process can be eliminated. Next air is compressed and the cleaned fuel gas is combusted to produce power and steam. Finally, the flue gas is cooled and sent to the stack. Any water condensed from the flue gas is used in a steam cycle to convert excess process heat into additional power.

A case for hydrogen production using PSA was designed and economic analysis was done by P. Spath et al [26] and the flow diagram is shown in Figure 53.

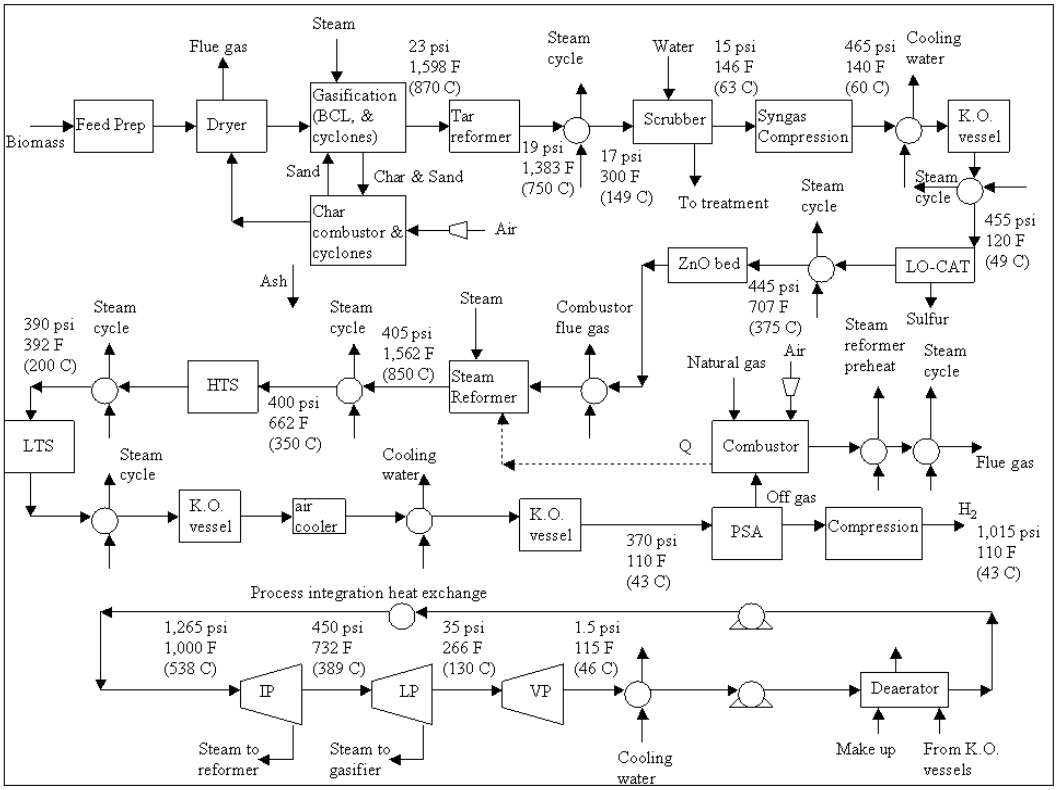


Figure 53. Process Flow Diagram of Hydrogen Production with PSA

Product gas from the biomass gasifier was directed to a tar reformer followed by syngas cooling, compression, sulfur removal, steam methane reforming, and high and low temperature water-shift reactions. The syngas is cooled through heat exchange with the steam cycle and the scrubber removes impurities such as particulates and ammonia together with any residual tars. The syngas is compressed using a centrifugal compressor. The syngas exiting the gasifier contains $H_2S$, so sulfur removal is needed due to the potential for WGS catalyst poisoning. The steam reformer is fueled by the pressure swing adsorption (PSA) off-gas.

A PSA unit is used to separate the hydrogen from the other components in the shifted gas stream, mainly $CO_2$, and un-reacted CO, $CH_4$, and other hydrocarbons. For a 70 mol% hydrogen PSA feed, a hydrogen recovery rate of 85% is typical with a product purity of 99.9 vol%. Finally, the hydrogen is compressed prior to shipment through a pipeline. The steam cycle produces power in

addition to providing steam for the gasifier and reformer operations. The steam cycle is integrated with the biomass-to-hydrogen production process. Steam is supplied to the reformer and gasifier from the intermediate and low pressure turbine sections of the extraction steam turbine/generator, respectively. A cooling water system is also included in the Aspen Plus model to determine the requirements of each cooling water heat exchanger within the hydrogen production system as well as the requirements of the cooling tower.

The full plant design for the membrane case has not yet been completed to the level of detail needed for H2A analysis. To get a preliminary value for the economics, the plant inputs and outputs were compared with just the gasification, reforming and hydrogen removal steps considered. The results are compared in Table 8. The wood feed rates for both processes are the same, but the membrane process uses oxygen for the gasifier while the PSA process uses air. The PSA process produces more hydrogen because a hydrogen shift at low temperature is used. However, the membrane process produces more by-product gas. The by-product gas was valued at ½ the value of hydrogen in this evaluation. However, the PSA by-product gas is needed for the gasification and reforming heat duties, while these steps are adiabatic with the membrane process. So there is potential for the membrane process to give better economics when the final heat integration is accomplished.

Table 8. Preliminary Scoping Economics

| | Cost Basis | | Flow rate, lb/hr | | MM$/yr | |
|---|---|---|---|---|---|---|
| | | | PSA | Membrane | PSA | Membrane |
| Feed | | | | | | |
| Wood | 30 | $/ton | 367437 | 367437 | -43.45 | -43.45 |
| Oxygen | 35 | $/ton | 0 | 65869 | 0.00 | -9.09 |
| Product | | | | | | |
| Hydrogen | 7.10 | $/MMBtu | 15322 | 11931 | 40.75 | 34.43 |
| Fuel gas | | | 230694 | 414465 | | |
| HHV, MMBtu/hr | 3.55 | $/MMBtu | 349 | 690 | 9.78 | 19.30 |
| LHV, MMBtu/hr | | | 305 | 641 | | |
| Less process use | | | 349 | | -9.78 | 0 |
| | | | | | | |
| Total | | | | | -2.70 | 1.19 |

The main conclusions for preliminary cost analysis were:

- Identified process cost dependence from main features of the membrane candidate.
- Completed flow sheet simulation for hydrogen production based on the proposed membrane reactor processes to compare to the conventional process.

- The proposed membrane reactor process could potentially decrease the hydrogen cost from the conventional biomass to hydrogen process, based on a preliminary economic analysis.

Process development and optimization is essential to realize the maximum performance from the selected membrane materials and achieve the overall cost effectiveness. The developed membrane gasifier technology will be validated through a series of bench, pilot and commercial demonstration units.

Based on economic analysis results, optimization of variables such as gasifier temperature, steam/carbon ratio, membrane temperature, membrane area was continued. Table 9 shows main cost constituents for 5 different cases, where gasifier temperature, membrane temperature, hydrogen recovery, membrane area were changed.

Table 9. Cost of Production for Hydrogen ($/kg)

| **Case** | **PSA** | **Membrane** | | | | |
|---|---|---|---|---|---|---|
| | | **Case 3A** | **Case 3B** | **Case 3C** | **Case 4A** | **Case 4B** |
| Gasifier T | | 1562 | 1562 | 1562 | 1472 | 1472 |
| Membrane T | | 1562 | 1562 | 1472 | 1472 | 1472 |
| Steam/Carbon | | 0.6 | 0.6 | 0.6 | 0.6 | 0.6 |
| Air excess | | 5% | 5% | 5% | 5% | 5% |
| $H_2$ Recovery | 81% | 100% | 96% | 100% | 100% | 90% |
| Area, $m^2$ | Adv | 7423 | 6973 | 8723 | 8796 | 7665 |
| Wood | 0.40 | 0.44 | 0.46 | 0.43 | 0.42 | 0.46 |
| Oxygen | 0.00 | 0.15 | 0.16 | 0.15 | 0.13 | 0.15 |
| Power | 0.05 | -0.21 | 0.26 | -0.25 | -0.23 | 0.27 |
| Fuel | 0.03 | 0.00 | 0.00 | 0.00 | 0.00 | 0.00 |
| MTIO | 0.10 | 0.14 | 0.14 | 0.14 | 0.14 | 0.14 |
| Capital | 0.38 | 0.52 | 0.51 | 0.53 | 0.51 | 0.54 |
| Salaries+OH | 0.07 | 0.08 | 0.09 | 0.08 | 0.08 | 0.09 |
| Cat & Chem | 0.10 | 0.06 | 0.06 | 0.06 | 0.06 | 0.06 |
| Water | 0.03 | 0.03 | 0.04 | 0.03 | 0.03 | 0.04 |
| Total excluding hydrogen compression | 1.17 | 1.22 | 1.19 | 1.17 | 1.14 | 1.22 |

Next step was to increase level of details simulation to have a better idea of equipment size of the process. Figure 54 shows that the scope of the membrane process includes feed drying, gasification, reforming with hydrogen recovery, heat recovery, gas clean-up, combustion, and

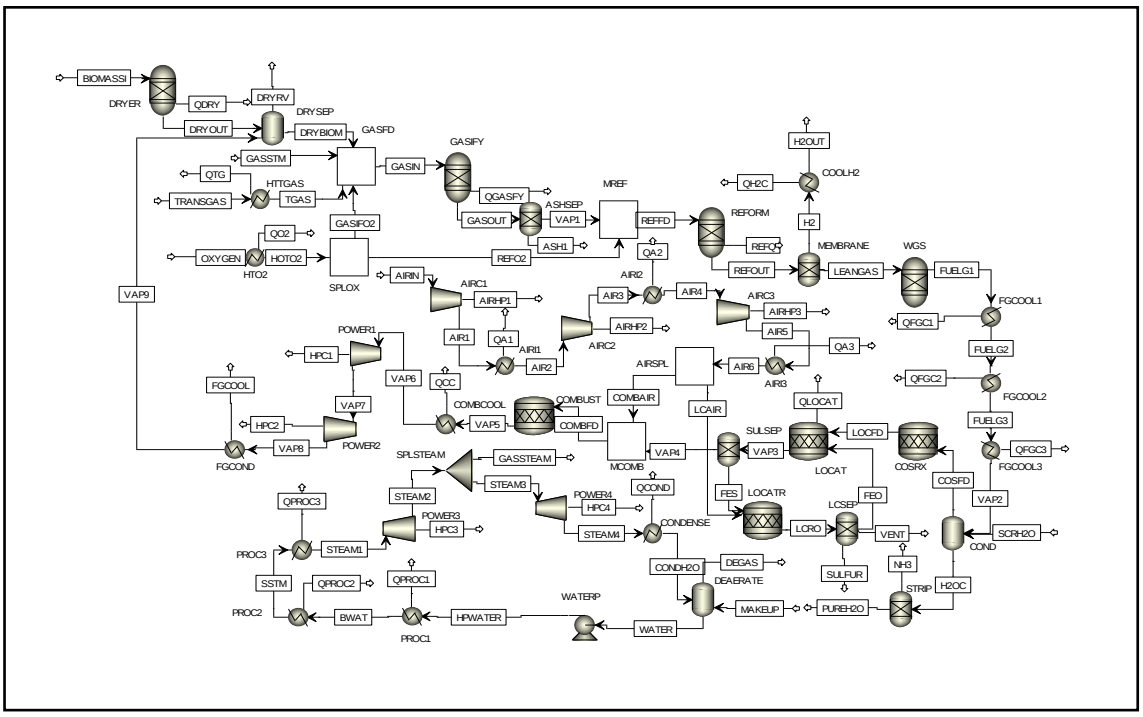


Figure 54. Aspen-Plus Process Flow Diagram of Membrane Process

power generation. Also, PINCH analysis was incorporated into the evaluation to size heat exchangers in the process. Figure 55 shows pinch analysis, which was used to determine the appropriate level of heat integration and steam generation for each case. Use of detailed simulation allowed estimates of capital costs by scale. Table 10 shows capital cost for case 4A as defined in Table 9.

Table 10. Capital Cost for Case 4A

| | 1472ºF Membrane Case 4A | | | | | | | |
|---|---|---|---|---|---|---|---|---|
| | MMBtu/hr | lb/hr | P2/P1 | Scaling | Base | Install F | 2002$ | 2005$ |
| Flue Exchanger | 0.80 | | | 0.60 | 18900 | 2.47 | 46760 | 49620 |
| Dryer | | 367440 | | 0.75 | 7627500 | 2.47 | 18839800 | 19993000 |
| S100 | | | | | | | 18886600 | 20042600 |
| Reform exchanger 1 | 2.70 | | | 0.65 | 14000 | 2.47 | 34500 | 36700 |
| Reform exchanger 2 | 162.00 | | | 0.6 | 884900 | 2.47 | 2185800 | 2319600 |
| Gasifier & blower | 0.00 | | | 0.65 | 0 | 2.47 | 0 | 0 |
| Renugas | | | | | | 2.47 | 23000000 | 24407800 |

| | | | | | | | | |
|---|---|---|---|---|---|---|---|---|
| Reformer/ regenerator | | 100000 | | 0.65 | 1387500 | 2.47 | 3427200 | 3636900 |
| S200 | | | | | | | 28647500 | 30400900 |
| Water cooler | 0.90 | | | 0.44 | 12400 | 2.47 | 30650 | 32530 |
| LOCAT heater | | 314200 | | 0.60 | 2800 | 2.47 | 6840 | 7260 |
| ZnO heater | 51.59 | 0 | | 0.44 | 74200 | 2.47 | 183400 | 194600 |
| Syngas compressor | | 0 | | 0.80 | 0 | 2.47 | 0 | 0 |
| Reformer blower | | 383000 | | 0.59 | 44700 | 2.47 | 110300 | 117000 |
| Sludge pump | | 1000 | | 0.33 | 7800 | 2.47 | 19320 | 20500 |
| LOCAT vessel | | 0 | | 0.65 | 0 | 2.47 | 0 | 0 |
| ZnO beds | | 0 | | 0.56 | 0 | 2.47 | 0 | 0 |
| Precompr KO | | 0 | | 0.60 | 0 | 2.47 | 0 | 0 |
| Postcompr KO | | 0 | | 0.60 | 0 | 2.47 | 0 | 0 |
| Sludge tank | | 21700 | | 0.60 | 11700 | 2.47 | 28800 | 30600 |
| S300 | | | | | | | 379300 | 402500 |
| Shift and PSA | | | | | 0 | 2.47 | 0 | 0 |
| Membrane | | 8800 | m2 | | | | 58020700 | 61572000 |
| HT Shift | | 383000 | | 0.56 | 486600 | 2.47 | 1201900 | 1275500 |
| Compr intercool | | 14600 | 2.05 | 0.60 | 171800 | 2.47 | 424300 | 450300 |
| Compr air cool | | 14600 | 2.05 | 0.60 | 175800 | 2.47 | 434300 | 460800 |
| Compr $H_2O$ cool | | 14600 | 2.05 | 0.44 | 43200 | 2.47 | 106800 | 113400 |
| H2 compr | | 14600 | 2.05 | 0.80 | 4114400 | 2.47 | 10162600 | 10784700 |
| Precompr KO | | 14600 | | 0.60 | 13600 | 2.47 | 33500 | 35500 |
| Post KO | | 14600 | | 0.60 | 14200 | 2.47 | 35000 | 37100 |
| S500 | | | | | | | 11196500 | 11881800 |
| Blowdown cool | | 166600 | | 0.60 | 1950 | 2.47 | 4820 | 5120 |
| Water cooler | | 82500 | | 0.44 | 6620 | 2.47 | 16340 | 17340 |
| Boiler & pumps | | 166600 | | 0.60 | 3666900 | 2.47 | 9057200 | 9611600 |
| S600 | | | | | | | 9078300 | 9634000 |
| S700 | | | | | 1381500 | 2.47 | 3412300 | 3621200 |
| Bldg & structure | | | | | | | 5983100 | 6368000 |
| Plant | | | | | | | 1368062200 | 145198600 |

| | | | | | | | | |
|---|---|---|---|---|---|---|---|---|
| Plant ex H2 compr | | | | | | | 125609700 | 133316700 |

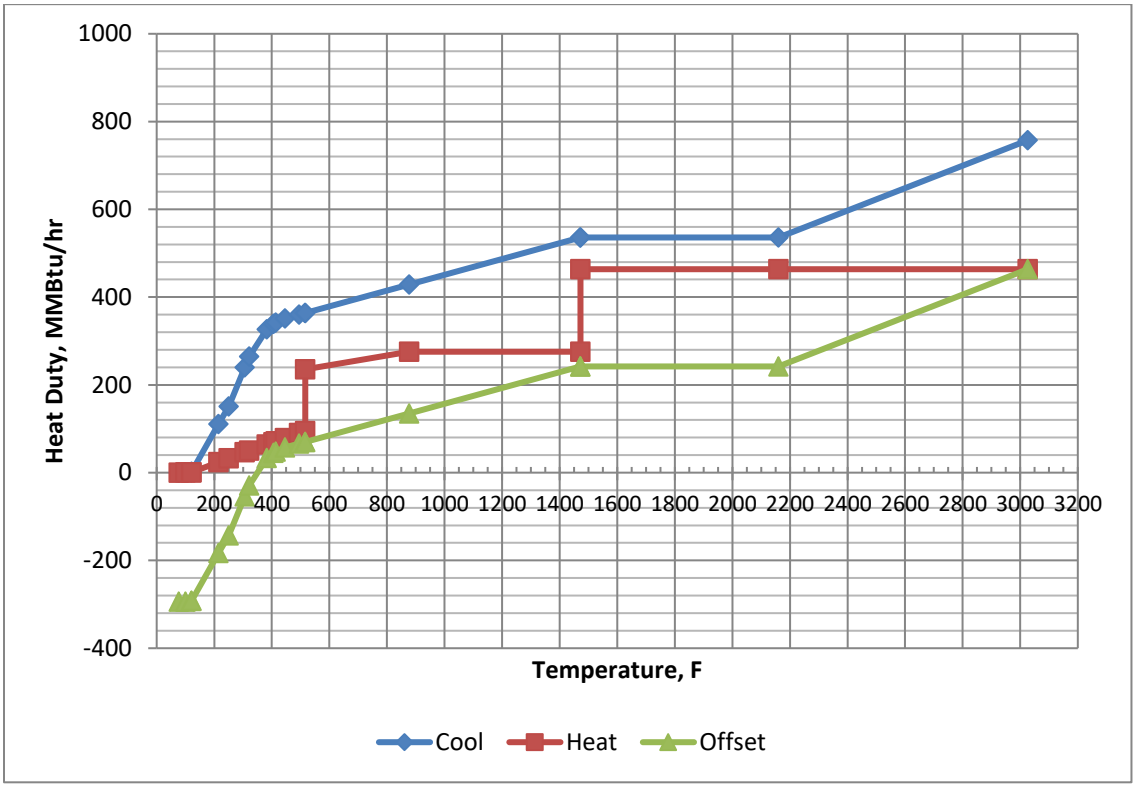


Figure 55. Pinch Analysis for Case 4A

Economic optimization was conducted for the variables of reforming (membrane) temperature, permeate pressure, and hydrogen recovery level for membranes 5 microns in thickness. The HYSYS model of the process was used to determine the membrane area needed at the specified process conditions for a given level of hydrogen recovery. The Aspen model of the process was then used to determine the stream flow rates and/or process heat duties for all the process steps so that equipment sizes could be estimated. The capital cost basis was taken from the PSA Advanced Case, and capital cost requirements were scaled from that for the membrane cases. In all the cases, hydrogen compressors were included to raise the pressure of the permeate hydrogen to 300 psi for consistency with the PSA cases.

Nine cases (denoted 6A to 6I) were simulated at 1472ºF reforming temperature; with all combinations of three permeate pressures (0.1, 0.2, and 0.3 bar) and three hydrogen recovery levels (90%, 95%, and 100% of the hydrogen entering). Because of the water gas shift reaction, the hydrogen in the stream was never depleted, even at 100% recovery of the hydrogen originally present. However, at higher recovery levels, the partial pressure driving force across the membrane went down, requiring more surface area. These same nine sets of recovery parameters were also simulated at 1382ºF in Cases 7A to 7I.

Figure 56 shows the effect of permeate pressure and hydrogen recovery level on the cost of hydrogen production. The dashed lines indicate the production cost at a pressure of 315 psi, while the solid lines indicate the production cost at 1000 psi pressure. The PSA Advanced case had a cost of production of $1.22/kg, so some of the membrane cases evaluated this quarter match the cost of production using PSA. The figure shows that higher levels of hydrogen recovery lead to lower cost of production, up to the 100% that was the maximum studied. Higher recovery levels will be evaluated next quarter to find the optimum. The optimum permeate pressure was between 0.2 and 0.3 bar. An additional case 7J was simulated at 0.25 bar to confirm that the optimum permeate pressure was closer to 0.2 bar than 0.3 bar. More stages of hydrogen compression were needed for the lower permeate pressures, and more studies are needed to define the optimum conditions accurately. Figure 57 shows that the lower reforming temperature was more economic for all cases studied.

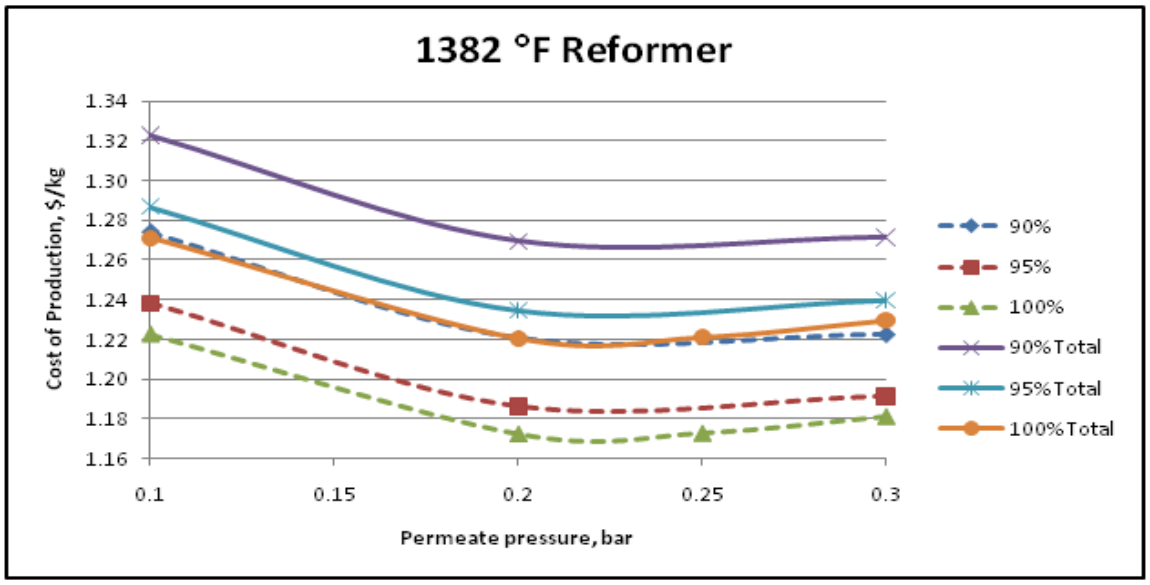


Figure 56. Effect of permeate pressure and hydrogen recovery level on the cost of hydrogen production.

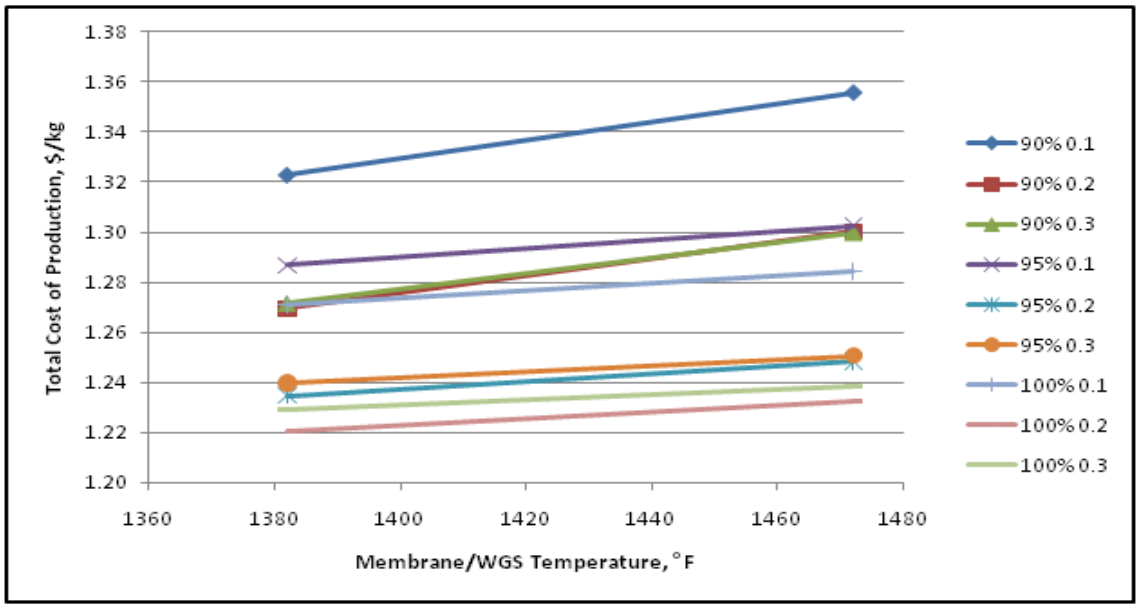


Figure 57. Effect of water-gas shift and hydrogen recovery level on the cost of hydrogen production.

The preliminary process design for a plant to produce hydrogen from a biomass feed using a hydrogen permeable membrane that was previously completed was subjected to a PINCH Analysis to optimize the heat integration and to minimize external heating and cooling demands. A Heat Exchange Network (HEN) analysis then allowed individual heat exchangers to be specified and sized so that the exchanger capital cost estimation could be updated. The pressures in the various pieces of equipment in the process were then updated to make sure that pressure drop driving forces were available for these heat exchangers and all other equipment, and the sizes of the pumps and compressors in the process were updated. The updated process design was documented in a set of twelve drawings to show all the required process equipment. Figure 58 below shows part of a diagram wherein a hydrogen membrane module is incorporated into the process.

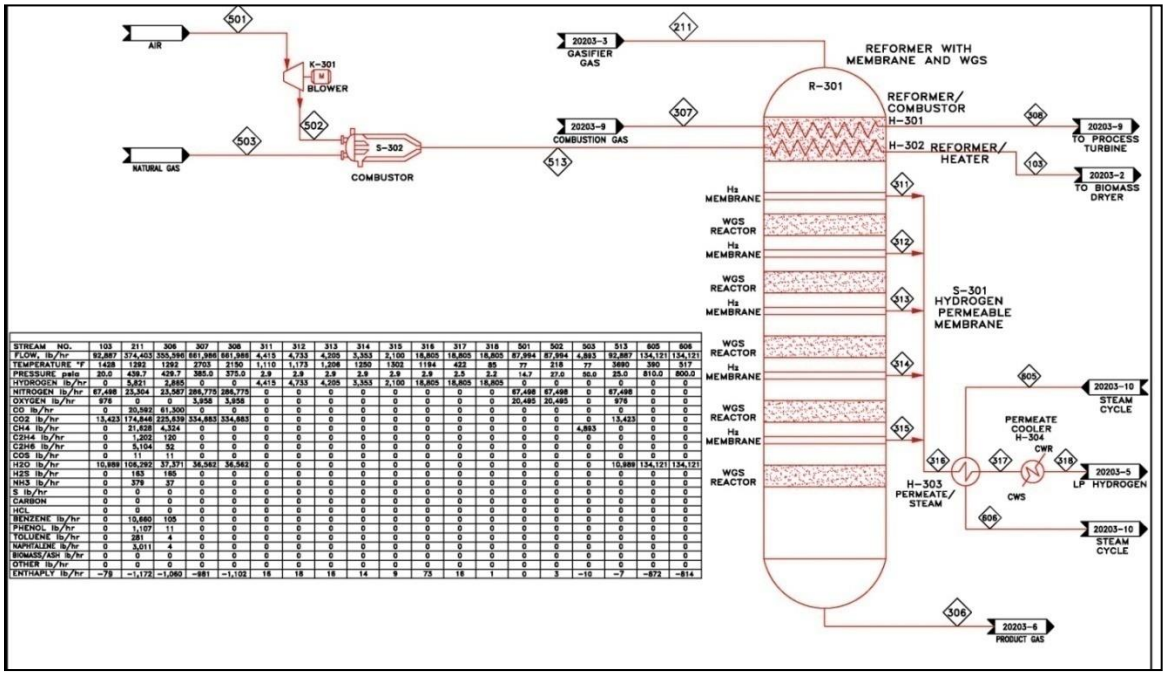


| STREAM NO. | 103 | 211 | 306 | 307 | 308 | 311 | 312 | 313 | 314 | 315 | 316 | 317 | 318 | 501 | 502 | 503 | 513 | 805 | 806 |
|---|---|---|---|---|---|---|---|---|---|---|---|---|---|---|---|---|---|---|---|
| FLOW, lb/hr | 92,887 | 374,453 | 355,596 | 681,268 | 681,268 | 4,415 | 4,733 | 4,205 | 3,353 | 2,100 | 18,805 | 18,805 | 18,805 | 87,994 | 87,994 | 4,893 | 92,887 | 134,121 | 134,121 |
| TEMPERATURE °F | 1428 | 1292 | 1292 | 2703 | 2150 | 1,110 | 1,173 | 1,206 | 1250 | 1302 | 1184 | 422 | 85 | 77 | 318 | 77 | 3690 | 390 | 517 |
| PRESSURE psig | 20.0 | 439.7 | 429.7 | 385.0 | 375.0 | 2.9 | 2.9 | 2.9 | 2.9 | 2.9 | 2.9 | 2.5 | 2.2 | 14.7 | 27.0 | 80.0 | 25.0 | 810.0 | 800.0 |
| HYDROGEN lb/hr | 0 | 5,921 | 2,885 | 0 | 0 | 4,415 | 4,733 | 4,205 | 3,353 | 2,100 | 18,805 | 18,805 | 18,805 | 0 | 0 | 0 | 0 | 0 | 0 |
| NITROGEN lb/hr | 67,498 | 23,304 | 23,587 | 286,775 | 286,775 | 0 | 0 | 0 | 0 | 0 | 0 | 0 | 0 | 67,498 | 67,498 | 0 | 67,498 | 0 | 0 |
| OXYGEN lb/hr | 976 | 0 | 0 | 3,958 | 3,958 | 0 | 0 | 0 | 0 | 0 | 0 | 0 | 0 | 20,495 | 20,495 | 0 | 976 | 0 | 0 |
| CO lb/hr | 0 | 20,592 | 61,300 | 0 | 0 | 0 | 0 | 0 | 0 | 0 | 0 | 0 | 0 | 0 | 0 | 0 | 0 | 0 | 0 |
| CO2 lb/hr | 13,423 | 174,846 | 225,439 | 334,883 | 334,883 | 0 | 0 | 0 | 0 | 0 | 0 | 0 | 0 | 0 | 0 | 0 | 13,423 | 0 | 0 |
| CH4 lb/hr | 0 | 21,628 | 4,324 | 0 | 0 | 0 | 0 | 0 | 0 | 0 | 0 | 0 | 0 | 0 | 0 | 4,893 | 0 | 0 | 0 |
| C2H4 lb/hr | 0 | 1,302 | 120 | 0 | 0 | 0 | 0 | 0 | 0 | 0 | 0 | 0 | 0 | 0 | 0 | 0 | 0 | 0 | 0 |
| C2H6 lb/hr | 0 | 5,104 | 52 | 0 | 0 | 0 | 0 | 0 | 0 | 0 | 0 | 0 | 0 | 0 | 0 | 0 | 0 | 0 | 0 |
| COS lb/hr | 0 | 11 | 11 | 0 | 0 | 0 | 0 | 0 | 0 | 0 | 0 | 0 | 0 | 0 | 0 | 0 | 0 | 0 | 0 |
| H2O lb/hr | 10,889 | 106,292 | 37,371 | 36,562 | 36,562 | 0 | 0 | 0 | 0 | 0 | 0 | 0 | 0 | 0 | 0 | 0 | 10,889 | 134,121 | 134,121 |
| H2S lb/hr | 0 | 183 | 185 | 0 | 0 | 0 | 0 | 0 | 0 | 0 | 0 | 0 | 0 | 0 | 0 | 0 | 0 | 0 | 0 |
| NH3 lb/hr | 0 | 379 | 37 | 0 | 0 | 0 | 0 | 0 | 0 | 0 | 0 | 0 | 0 | 0 | 0 | 0 | 0 | 0 | 0 |
| S lb/hr | 0 | 0 | 0 | 0 | 0 | 0 | 0 | 0 | 0 | 0 | 0 | 0 | 0 | 0 | 0 | 0 | 0 | 0 | 0 |
| CARBON | 0 | 0 | 0 | 0 | 0 | 0 | 0 | 0 | 0 | 0 | 0 | 0 | 0 | 0 | 0 | 0 | 0 | 0 | 0 |
| HCL | 0 | 0 | 0 | 0 | 0 | 0 | 0 | 0 | 0 | 0 | 0 | 0 | 0 | 0 | 0 | 0 | 0 | 0 | 0 |
| BENZENE lb/hr | 0 | 10,660 | 105 | 0 | 0 | 0 | 0 | 0 | 0 | 0 | 0 | 0 | 0 | 0 | 0 | 0 | 0 | 0 | 0 |
| PHENOL lb/hr | 0 | 1,107 | 11 | 0 | 0 | 0 | 0 | 0 | 0 | 0 | 0 | 0 | 0 | 0 | 0 | 0 | 0 | 0 | 0 |
| TOLUENE lb/hr | 0 | 381 | 4 | 0 | 0 | 0 | 0 | 0 | 0 | 0 | 0 | 0 | 0 | 0 | 0 | 0 | 0 | 0 | 0 |
| NAPHTALENE lb/hr | 0 | 3,011 | 4 | 0 | 0 | 0 | 0 | 0 | 0 | 0 | 0 | 0 | 0 | 0 | 0 | 0 | 0 | 0 | 0 |
| BIOMASS/ASH lb/hr | 0 | 0 | 0 | 0 | 0 | 0 | 0 | 0 | 0 | 0 | 0 | 0 | 0 | 0 | 0 | 0 | 0 | 0 | 0 |
| OTHER lb/hr | 0 | 0 | 0 | 0 | 0 | 0 | 0 | 0 | 0 | 0 | 0 | 0 | 0 | 0 | 0 | 0 | 0 | 0 | 0 |
| ENTHAPLY lb/hr | -79 | -1,172 | -1,060 | -881 | -1,102 | 18 | 18 | 18 | 14 | 9 | 75 | 18 | 1 | 0 | 3 | -10 | -7 | -872 | -814 |

Figure 58. Part of Piping and Instrumentation Diagram with membrane module reactor.

Next step was focusing on engineering design and costing of the process plant that fed 2000 tons/day of biomass and delivered high-pressure hydrogen product using a hydrogen permeable membrane. Optimum values for gasification temperature, reforming temperature and permeate pressure were used, based on optimization studies previously completed. The Aspen model of the process was then used to determine the stream flow rates and/or process heat duties for all the process steps so that equipment sizes could be estimated. A PINCH Analysis and HEN analysis was completed so that individual heat exchangers could be sized. The sizes of pumps, vessels, conveyors, compressors, reactors, etc. were based on the flow rates and heat balance from the Aspen model. This analysis resulted in a listing of the sizes for all major pieces of equipment in the process plant.

A capital cost estimate was then generated from the detailed equipment list. The capital cost basis for each piece of equipment was taken from the PSA Advanced Case, in-house GTI commercial designs, and other literature sources, as needed. As in the PSA Advanced Case, hydrogen compressors were included to raise the pressure of the permeate hydrogen to 20.4 atm for in-plant storage, and then to 1000 psi for delivery to an outside customer, if needed. Table 11 summarizes the new capital cost estimate.

This compares with a total of 121.5 MM$ previously estimated from a less complete process design basis, with hydrogen delivered at 68 atm. If hydrogen is produced at 20.4 atm, the new capital cost is 120.4 MM$, compared with the old estimate of 118.0 MM$. Based on this small change, we expect that the hydrogen membrane process will continue to have an equal or lower cost of hydrogen production than in the PSA Advanced Case.

Table 11. Capital Cost Estimate

| **Plant Section** | **Capital Cost, MM$ 2005** | |
|---|---|---|
| | **Old Basis** | **New Basis** |
| Section 100- Feed Crushing & Dryer | 18.8 | 20.3 |
| Section 200 - Gasifier | 12.0 | 12.9 |
| Section 300 – Gas Processing (including reformer, gas treating, and hydrogen compression to 300 psi) | 14.7 | 18.9 |
| Section 300 - Membrane | 30.3 | 29.6 |
| Section 400 – Air Compression | 21.9 | 23.6 |
| Section 500 – Hydrogen Compression to 1000 psi | 3.3 | 3.5 |
| Section 600 – Steam & Power | 4.9 | 5.3 |
| Section 700 - OSBL | 11.4 | 12.2 |
| Section 800 - Buildings | 6.4 | 6.4 |
| **Total** | **123.7** | **132.7** |

The more accurate costing increased the capital cost somewhat. If hydrogen is produced at 20.4 atm, the new capital cost is 129.2 MM$, compared with the old estimate of 120.4 MM$.

The new capital and operating costs for the membrane process were input into version 3 of the H2A program. This version updates the base year of the analysis from 2005 to 2007. A revised cost of hydrogen production of $1.82/kg was obtained, as detailed in Table 12.

Table 12. Hydrogen Cost of Production Estimate

| **Cost Component** | **H2 Cost, $ 2007 /kg** |
|---|---|
| Capital Cost | 0.675 |
| Decommissioning | 0.001 |
| Fixed O& M | 0.199 |
| Feedstock Cost | 0.511 |
| Other Raw Material | 0.109 |
| By-Product Credits | 0.000 |
| Other Variable Costs | 0.320 |

| | |
|---|---|
| **Total** | **1.816** |

A tornado diagram was prepared to show the sensitivity to several key process variables as shown in Figure 59.

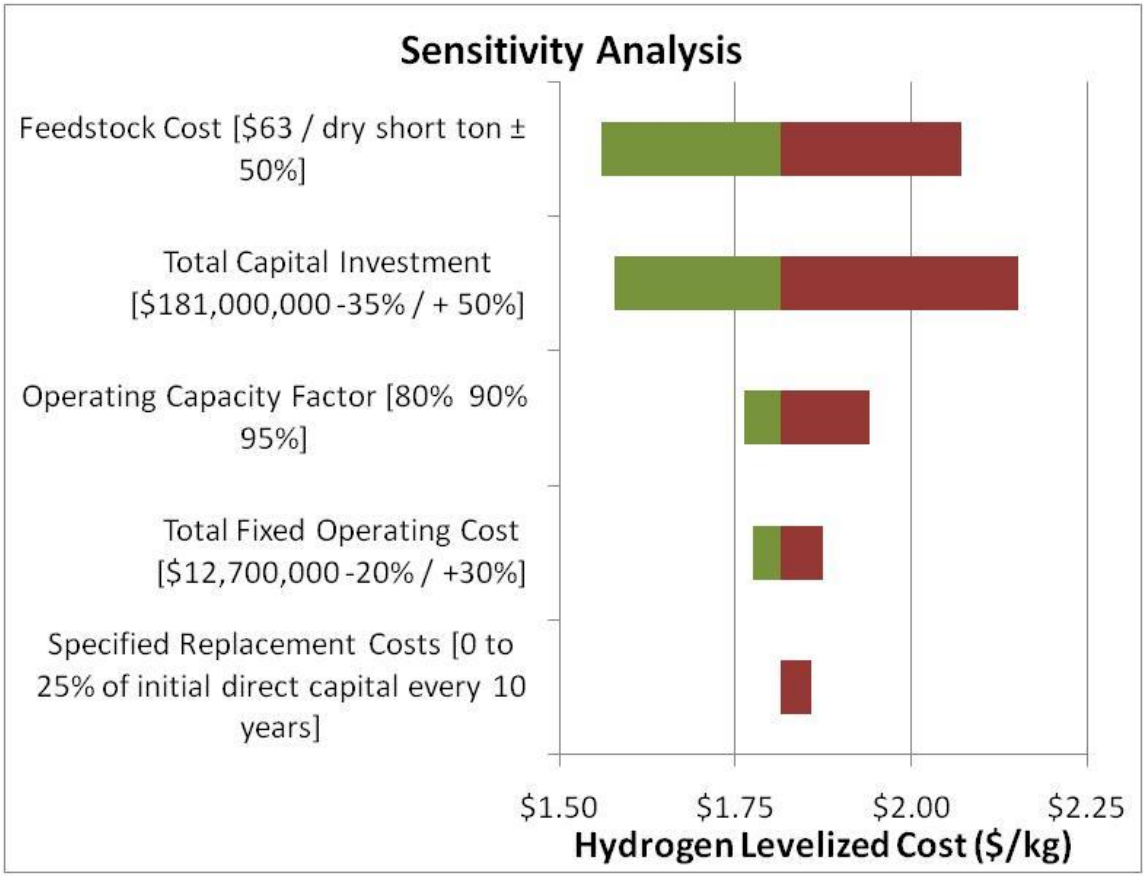


Figure 59. Sensitivity Analysis for Hydrogen Cost of Production

A process design was redone in Aspen and HYSYS using only process temperatures in the gasifier and reformer which have been experimentally demonstrated. Previous optimization studies had shown that lower operating temperatures gave better hydrogen production costs, as reported last quarter. A capital cost estimate was generated from the revised detailed equipment list using in-house GTI commercial designs, the PSA Advanced Case and other literature sources, as needed. As in the PSA Advanced Case, hydrogen compressors were included to raise the pressure of the permeate hydrogen to 300 psi for in-plant storage, and then to 1000 psi for delivery to an outside customer, if needed. Table 13 summarizes the new capital cost estimate which was developed this quarter. The biggest change in this Case 9 from the previous design is that less hydrogen is produced at the higher gasifier and reformer temperature. Somewhat compensating is that is that less membrane area is needed to recover the reduced amount of hydrogen. Case 9 assumes a 5 micron thick membrane, which has been fabricated, but not yet tested in the laboratory.

Table 13. Capital Cost Estimate

| **Plant Section** | **Capital Cost, MM$ 2005** | |
|---|---|---|
| | **Old Basis** | **Demonstrated Temperatures** |
| Section 100- Feed Crushing & Dryer | 20.3 | 20.3 |
| Section 200 – Gasifier | 12.9 | 13.1 |
| Section 300 – Gas Processing (including reformer, gas treating, and hydrogen compression to 300 psi) | 18.9 | 19.6 |
| Section 300 – Membrane | 29.6 | 28.0 |
| Section 400 – Air Compression | 23.6 | 24.5 |
| Section 500 – Hydrogen Compression to 1000 psi | 3.5 | 3.1 |
| Section 600 – Steam & Power | 5.3 | 7.2 |
| Section 700 – OSBL | 12.2 | 13.2 |
| Section 800 – Buildings | 6.4 | 6.4 |
| **Total** | **132.7** | **135.3** |

The new capital and operating costs for the membrane process were input into version 3 of the H2A program. This version uses the base year of the analysis of 2007. A revised cost of hydrogen production of $1.96/kg was obtained, as detailed in Table 14.

Table 14. Hydrogen Cost of Production Estimate

| **Cost Component** | **H2 Cost, $ 2007 /kg** | |
|---|---|---|
| | **Old Basis** | **Demonstrated Temperatures** |
| Capital Cost | 0.675 | 0.721 |
| Decommissioning | 0.001 | 0.001 |
| Fixed O& M | 0.199 | 0.220 |
| Feedstock Cost | 0.511 | 0.613 |
| Other Raw Material | 0.109 | 0.109 |

| | | |
|---|---|---|
| By-Product Credits | 0.000 | 0.000 |
| Other Variable Costs | 0.320 | 0.292 |
| **Total** | **1.816** | **1.955** |

This is lower than the cost of production target of $2/kg. If the membrane thickness is restricted to that which has been demonstrated in the laboratory, ten times as much membrane area would be needed for the same hydrogen flux and the estimated cost of production would be $3.32/kg. This would not meet the project performance milestone.

**Task 3. Bench Scale Biomass Gasifier Design and Construction**

In this task, GTI was supposed to build a bench-scale biomass gasifier in combination with the prototype membrane module from Tasks 4 or 5 to demonstrate direct hydrogen production from the biomass gasifier. The gasifier technology is based on GTI's RENUGAS® fluidization bed technology for biomass gasification. GTI was to make use of the experience learned from the existing mini-bench gasification equipment to construct a new unit or modify an existing one.

GTI has envisioned a 2" to 4" diameter bench-scale gasifier with operation capability up to 33 atm and 1000°C. To extend the duration of the gasification operation, a large batch capacity biomass feeding system was investigated. Either an oxygen supply system supposed to be procured or bottled gases were to be used. The gasification reactor is electrically heated by a multi-zoned furnace. Thermocouples are installed along the axis of the reactor for temperature measurement.

Syngas flow rates are measured by a dry test meter and directed to a gas chromatograph for determining the gas compositions. Design consideration also include steam/oxidant feeding arrangement, filtering, gasification reactor temperature/pressure ratings, heat insulation, cooling, instrumentation and control systems, etc.

GTI personnel evaluated potential sites for the new bench-scale biomass gasifier and reactor sizes and feed quantities needed to support the gasifier.

GTI personnel traveled to Auburn University to check the possibility of their biomass gasifier for use with GTI's membrane module. Discussions with personnel responsible for the Auburn gasifier and GTI personnel included such themes as safety of membrane unit and hydrogen-related safety regulations for the site, power requirements, conditioning of syngas after the gasifier, and ultimate quality of the feed to the membrane module. Maximum operating pressure of the gasifier is 150 psig. A compressor will be required to increase pressure and since no compressors work at high temperatures, cooling and reheating the gas may be required if the Auburn gasifier option is used. Another option is to use the syngas as "it is"- less hydrogen will be produced than originally was planned. Figure 60 shows the Auburn gasifier and a place where the membrane module can be located.

A second option for the membrane unit was GTI's gasifier at the Flex-Fuel Test Facility (FFTF). Due to a busy schedule of the gasifier, we need to identify an available timeslot when biomass gasification will occur so the proposed would "piggy back" on an existing project. Figure 61 shows 2 locations which can be used for membrane module if GTI's gasifier (FFTF) is used.

Figure 60. Auburn's gasifier (blue vessel) and a potential location for the membrane module.


Figure 61. Two sites in the FFTF where a membrane module can be located.

The current schedule for FFTF operations had a biomass test scheduled in the near future but since there was a no-go decision, this option was not utilized. The Auburn gasifier is not operational yet, but construction is progressing. Figure 62 shows Auburn gasifier in the process building.

Figure 62. Auburn's gasifier with instrumentation.

In conclusion, there were two potential locations to test hydrogen membrane integrated with gasifier: at the FFTF at GTI and at Auburn University, however due the "no-go" decision, these options were not tested with the candidate membrane.

**Task 4. Integrated testing of initial membrane with gasifier**

The objective of this task is to identify any issue that may surface from an early trial of gasifier testing with a membrane module. The membrane material will be selected based on the findings of Task 1.4. This task is further divided into three subtasks.

**Task 4.1 Design of Membrane Module Configuration**

The objective of task 4.1 "Design of membrane module configuration" is to design a membrane module that is compatible with the biomass gasifier. The module must be reliable, durable and cost effective. One of the major challenges of the proposed membrane reactor is that the hydrogen separation membrane module is exposed to an environment laden with particulate matter. Consequently, special care will be taken to minimize the interference of particulate materials with hydrogen separation, structural integrity and mechanical strength of the membrane. The major efforts of this task will involve the following:

- Conceptual design to identify the best configuration: tubular, planar or corrugated
- Modeling to determine the size and ideal flow pattern
- Sealing development in both material selection and mechanical design
- Design of manifold and gas flow channels to ensure uniform gas distribution

- Development of expansion-matched glasses and glass-ceramics to hermetically join materials such as metals and ceramics for the membrane module
- Development of compression sealing technique if the selected membrane has the required strength

| Parameters | Planar design | Tubular design |
|---|---|---|
| Fabrication of membrane | Easy to manufacture<br>Uniform metal deposition on a flat surface is relatively easy (electroless plating, electroplating) | Rolling of metal foils is more difficult.<br>For glass membranes tubular design is a challenging issue |
| Sealing options | Metal gaskets<br>Welding<br>Brazing | Sealing area per unit area of membrane surface is small<br>Brazing<br>Welding<br>Flexible graphite gaskets |
| Stresses | Deflection due to pressure is greater. Need for stronger support | Less mechanical deflection due to pressure, especially if feed side is inside tube |
| Cost | Stacked planar mechanical design is relatively inexpensive | Membrane surface area per unit volume is lower, therefore less quantity of expensive alloy is needed |

The hydrogen membrane module can be located in either of two places: inside the gasifier or outside and closely-coupled after the cyclone. Based on AMR reviewers' comments, the first configuration to be experimentally tested was closely-coupled placement of the membrane module, in which the module located after the cyclone so that the hydrogen membrane would not be exposed to particulate matter.

The initial candidate membrane was chosen on June, 2008 and it is the foil $Pd_{80}Cu_{20}$ by 100 microns thickness. The design of the membrane module was dictated by required membrane thickness and alloy properties.

*Planar or tubular design*

Planar design for membrane module was chosen due to ease of fabrication and relatively inexpensive cost. Stacked planar membrane modules with narrow and wide channels provide good mass transport of hydrogen while a tubular configuration does not allow this configuration for the feed channels. Table 15 shows the advantages for tubular or planar configuration.

Table 15. Design configuration of membrane module

Input from Wah Chang indicated that tubular designs require complex manufacturing techniques, and have difficult methods of sealing and maintenance/repair issues:

Metal seals are capable of producing high-quality sealing conditions provided the sealing surface that they contact is flat, supported uniformly and has the proper surface finish. They are reliable, stable and have no permeability issues. However, they are typically a one-time-use item and can have fairly long lead times. They can also be costly.

Fiber seals are inexpensive and easy to produce; however permeability (leakage) can be problematic particularly at high differential operating pressures.

The main requirements for the membrane module are:

1. Material of construction for membrane module- should be hydrogen sulfide-resistant, and be able to withstand high operating temperature and pressure (up to 850ºC and 30 atmospheres).
2. Support should be mechanically stable to withstand high pressures (30 atm), chemically stable in a reducing atmosphere (hydrogen) and have no transport resistance at operating conditions.
3. An intermetallic diffusion layer between membrane and metallic support should be inert at high temperature conditions and have no transport resistance for hydrogen.
4. Sealing between the feed and permeate sides is a critical issue. Sealing should be capable to withstand high pressures and temperature conditions, and be chemically stable.
5. Sizing of the membrane module should include an ideal flow pattern. Hydrogen diffusion to the membrane surface should not be a limiting step.
6. The membrane should be chemically and mechanically stable as well as durable at gasifier operating conditions and have high hydrogen permeability.
7. The membrane area should be calculated based on a commercial product gas (UGAS®) data (syngas flowrate, hydrogen content, selectivity, hydrogen permeability etc).

Based on these requirements material, size and sealing for membrane module were chosen:

1. **Hastelloy® C-276 for membrane module body.**

The feed gas mixture contains hydrocarbons together with hydrogen sulfide, and organosulfur species. Steel alloys with high concentrations of nickel and/or chromium are good selections (Inconel 600, Inconel 800). SS grades (316 and 304) are not good choices. Superalloys such as Hastelloy and Haynes are resistant to hydrogen sulfide and can be used in high temperature environment. Haynes is an expensive alloy for fabrication. Hastelloy® C-276 remains resilient in the most corrosive environments such as in chemical processing, pollution control, pulp and paper production, waste treatment and the recovery of "sour" natural gas. So, the initial material choice is Hastelloy® C-276 (supplied by Haynes Corporation).

2. **Hastelloy® C-276 for porous support and additional mechanical support.**

To have no transport resistance from porous support, substrate should have pores of 20 microns (from experimental work) and a thickness of about 1 mm. Also, chemical stability in reducing environment requires a support that is made from a higher grade of stainless steel. Hastelloy is a good choice. The membrane still needs additional support to avoid mechanical deformation. A perforated or corrugated support can be used. The selected material for substrate and additional support is Hastelloy to avoid problems that may appear due to a difference of thermal expansion coefficients. ACI Porous Technologies and Mott Corporation supplies porous supports in different shapes, pores sizes and various materials. So, our choice is that porous supports should be constructed from Hastelloy with 20 microns pore size and thickness of 1 mm. Mechanical support will be made from Hastelloy also.

**3. Cement layer (OmegaBond "400",Omega Engineering Inc) as intermetallic layer between membrane and porous support.**

Due to the high operating temperature, a layer between the metallic porous support and the metallic membrane is necessary to prevent intermetallic diffusion of one metal into another that causes a drop in hydrogen permeability of the membrane. A cement (OmegaBond "400",Omega Engineering Inc) layer was deposited on a metallic support (20 microns pore size); a subsequent test showed no resistance for hydrogen transport due to the addition of the cement.

4. **Copper gaskets coated by carbon spray**.

Table 16 shows different sealing options. Sealing by gaskets was chosen due to low cost and ease of application. Membrane sealing issues were resolved by using copper gaskets coated by sprayed carbon. Graphite gaskets (2 different thicknesses) leaked at high pressures. Copper gaskets, however, have also failed leak tests in our pressurized system. Also, hydrogen sulfide affects chemical stability of copper due to the copper sulfide formation. Carbon spray (Dry Film Lubricant 321, Dow Corning Corporation) was used as a coating for copper gaskets and provided the required adhesion and chemical stability. Tests at high pressures (up to 30 atmospheres) and temperatures (up to 850ºC) showed no leaks both external and between the feed and permeate sides. Also, experiments with hydrogen sulfide (1000 ppm) showed sealing integrity.

5. **Configuration of feed channel: length is 20 cm, width is 20 cm and height (distance between channels) is 5 cm.**

Regardless of membrane design, the mass transfer of hydrogen to the feed side of the membrane should be considered. If the membrane module is planar, a parallel feed design should be chosen to reduce pressure drop for the feed stream through the module. Gas flow should be in the turbulent regime to avoid diffusion which would be a limiting step in hydrogen transport from the feed side to the permeate side. At such parameters as 20x20x5cm (length, width, and height), hydrogen diffusion to the membrane won't be a limiting factor in the hydrogen permeation: hydrogen will diffuse to the membrane surface fast enough during the short time interval that the feed is flowing over membrane.

6. **An initial candidate membrane is $Pd_{80}Cu_{20}$ foil with thickness 100 microns.**

An initial candidate membrane was chosen in consultation with DOE. GTI demonstrated by a sequence of tests that $Pd_{80}Cu_{20}$ membrane is chemically stable, can operate at high temperatures and high pressures (supported) and has good hydrogen permeability.

**7. Total membrane area is 0.4 $m^2$ with 10 membranes of 0.04 $m^2$ of permeable area.**

Based on results of UGAS® modeling and calculation for flow distribution, a membrane area was calculated.

Membrane module will be capable to produce a minimum of two (2) lbs per day of $H_2$ (hydrogen) or 7.4 slpm.

Based on results obtained for typical biomass gasification modeling by using RENUGAS GTI-proprietary program and experimental results obtained for the initial candidate membrane ($Pd_{80}Cu_{20}$), we can calculate required membrane area to have hydrogen separation at least 2 lbs/day. Based on our calculations, the membrane with total area of 0.14 $m^2$ is capable to produce hydrogen with flowrate 7.4 slpm at operational conditions. The 10 membranes with dimensions 20 cm by 20 cm will have 0.4 $m^2$, which is about three times more than required for given hydrogen production rate. Due to possibility of unexpected problems during membrane fabrication, we decided to have 10 membrane pieces with 20 cm x 20 cm dimensions for each one.

Table 16. Membrane Sealing Options

| Membrane sealing options | Advantages | Disadvantages |
|---|---|---|
| Flexible graphite gaskets | • Versatility<br>• ease of application<br>• low cost | • Poor oxidation resistance at T>400°C<br>• Non-zero gas permeability<br>• Requires very smooth contact surface |
| Brazing | • Works well on thick membranes (>100μm) | • Limited application due to melting points<br>• Brazing should wet surfaces to be joined<br>• Dissolution of membrane into brazing alloy<br>• High cost<br>• Failure due to difference in thermal expansion coefficients |
| Welding | • Laser welding | • Overheating- should be localized |
| Metal gaskets | • Ease of application<br>• Low cost | • Chemical reactivity to poisons<br>• Limited application |

Design of the membrane module is shown in Figure 63. The membrane module consists of 10 membranes located in 5 channels. Syngas from the cyclone enters the membrane module and hydrogen will be collected from 5 streams shown on the right side of the figure.

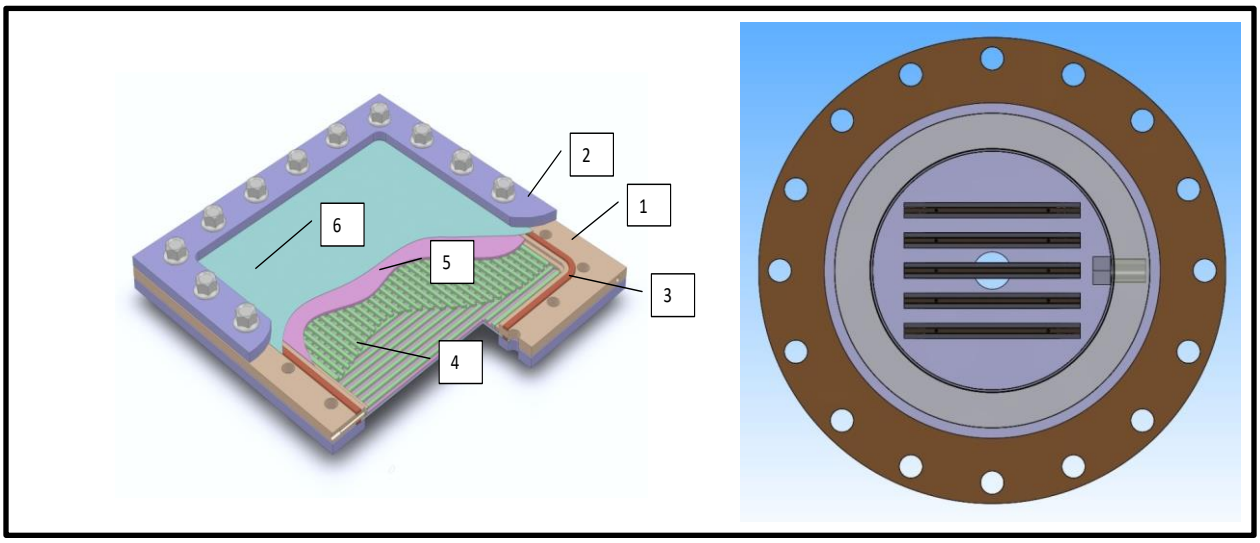


Figure 63. Design of membrane module: 1-base plate, 2-clamping frame, 3-copper gasket, 4-slotted metal support, 5-porous support, 6-membrane.

.

Next step of the project was fabrication of membrane module using initial candidate membrane. Some changes may be made due to limitation of fabrication methods which cannot be predicted at this stage of membrane module development.

In summary, GTI designed the membrane module in planar design for initial candidate membrane ($Pd_{80}Cu_{20}$). Calculations were made to have no diffusion limitation for hydrogen permeation process and have uniform gas distribution. Sealing was developed to withstand high temperatures and high pressures of operation. Support to have high mechanical stability was designed. Membrane module design is presented along with some drafting schemes. Wah Chang assisted in review of membrane module design. Changes to the membrane module design advised by Wah Chang were incorporated.

**Task 4.2 Membrane Module Fabrication**

*Task 4.2 Objective*: The module will be sized for integration with a bench scale biomass gasifier that is to be built in Task 3. All the required hardware such as support frame, casing, loading device, insulation, pipes, fittings, etc. will be specified and procured. GTI will make use of its experience and capability in high temperature fuel cell technology to assemble a workable membrane module. The unit will be tested first before it is close-coupled to the bench scale biomass gasifier.

The existing membrane module was designed for an operational pressure of 427 psig and for hydrogen production of 7.4 slpm. The membrane has an area of 0.4 $m^2$. Due to decreased feed

pressure, less hydrogen will be produced than was planned. If the biomass gasifier has a maximum operational pressure of 150 psig (11.2 atmospheres) then the partial pressure of hydrogen on the feed side will be approximately 2.2 atmospheres. Only hydrogen will be on sweep gas, so hydrogen partial pressure on sweep side is 1 atmosphere. It is feasible to use steam as a sweep gas for this application. For the commercial application, a steam sweep gas will likely be utilized.

Due to the low-quality of palladium-copper foils tested at GTI, a search for vendors to supply membranes of better quality was done. Five different membranes were ordered. Membranes obtained from 3 different companies (ACI Alloys, RSI and Tanaka Corporation) were tested for hydrogen flux. The foil purchased from Tanaka Corporation has higher hydrogen flux and looks more uniform and has less visible pits and other surface irregularities. Due to fabrication method of alloys, $Pd_{80}Cu_{20}$ foil can be purchased with width size no more than 20 cm. So, dimensions of the membranes planned for membrane module were reduced to accommodate that size. Porous supports made from SS316 were purchased from Mott Corporation: 12 pieces with a lead time of 4 weeks.

The membrane module designed was rated for pressure up to 30 atmospheres (427 psig). The flanges of the housing vessel were sized to a smaller diameter and thinner wall due to lower operating pressure. Figure 64 shows membrane module inside the pressure vessel.

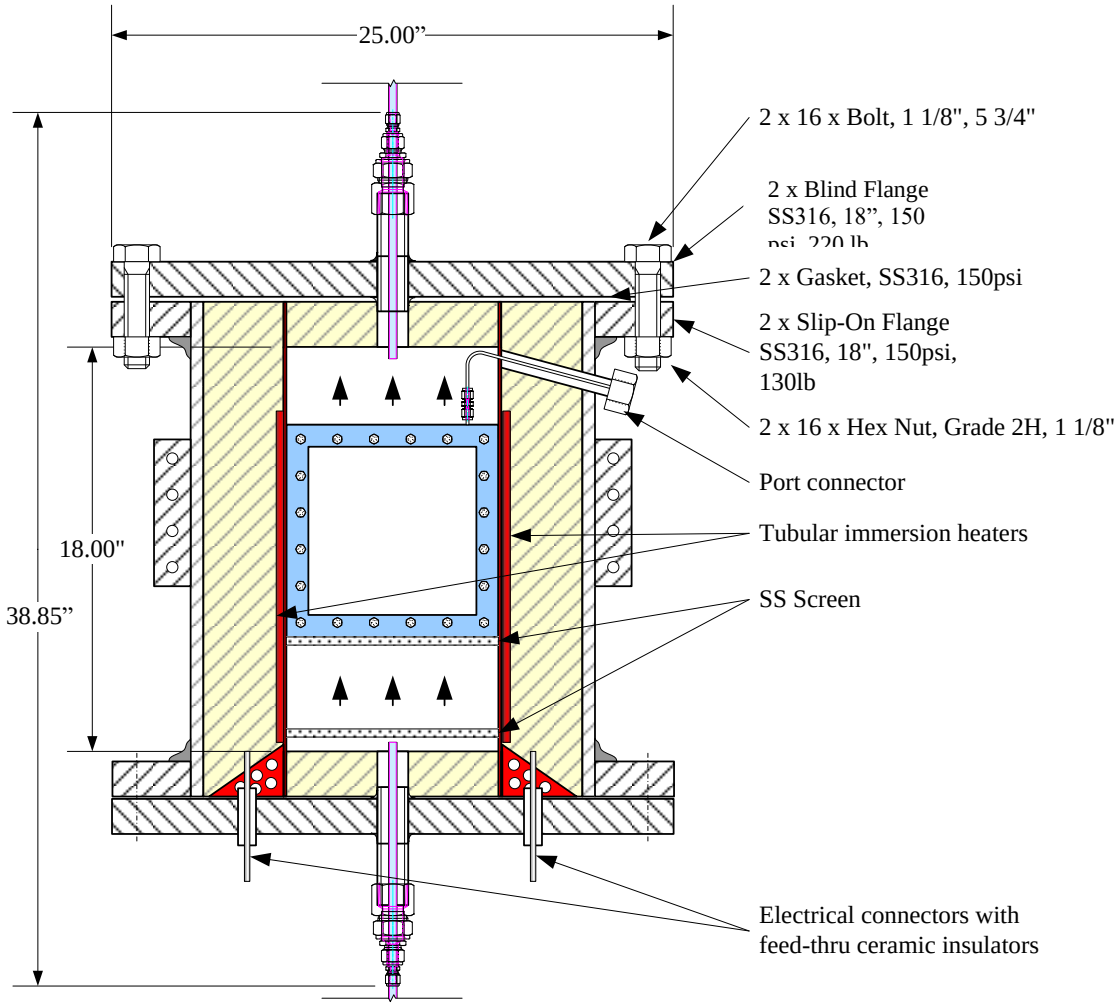


Figure 64. Membrane Module Unit in Pressure Vessel.

The membrane fabrication was initiated by GTI’s in-house Mechanical Shop. The Membrane module design is being modified due to fabrication issues. Redesign of the membrane module was finalized and fabrication of the module was in progress. The final design of the membrane module is shown in Figure 65 and area for reforming catalyst bed is illustrated in Figure 66.

.

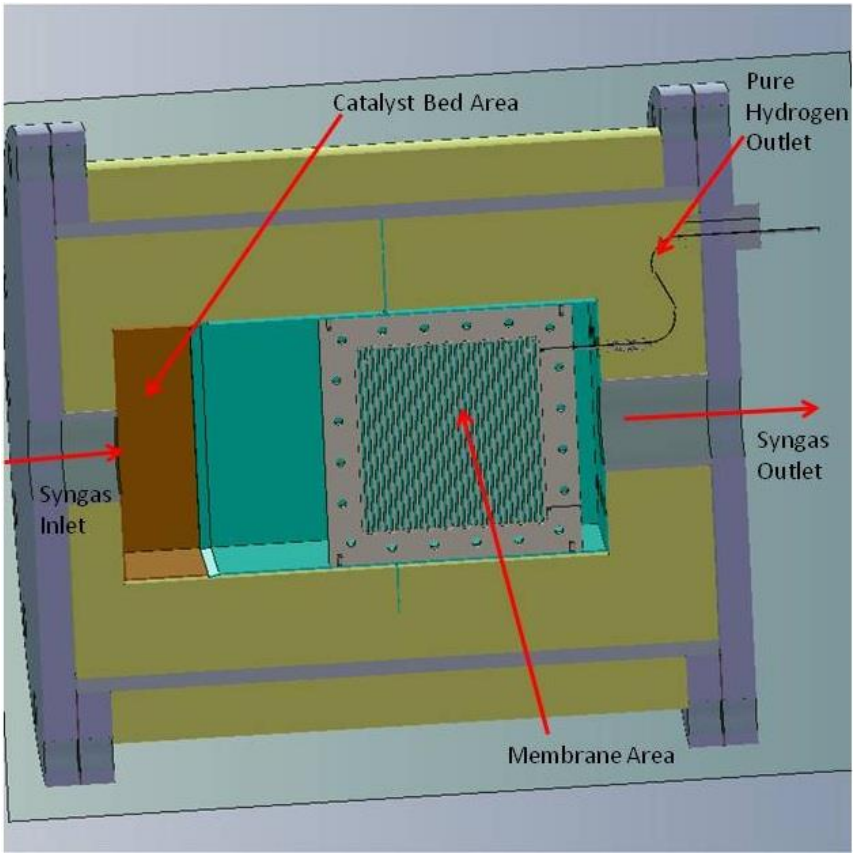


Figure 65. General view of membrane module.

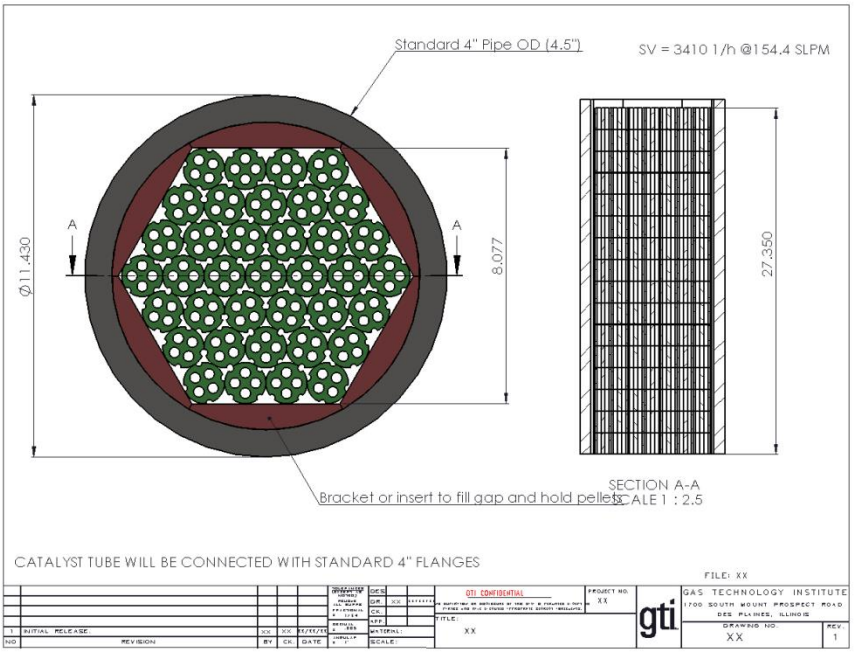


Figure 66. Engineering drawing of catalyst bed area.

All major design aspects for the membrane module have been completed. These include a detailed design of the membrane module flanges and gaskets, membrane module flow duct and internal insulation configuration, external insulation configuration, catalyst module and heater configuration, $H_2$ extraction plumbing, and external flanges.

The membrane module is being fabricated. All major parts such as heaters, catalysts, insulation, membranes, copper sheets, and alumina cloths were purchased. Ten inner membrane perforated mechanical supports have been machined and are ready for use. Two of ten reactor cover bodies have been rough water jetted and are being machined to final sizes. Parts machined are shown in Figure 67.

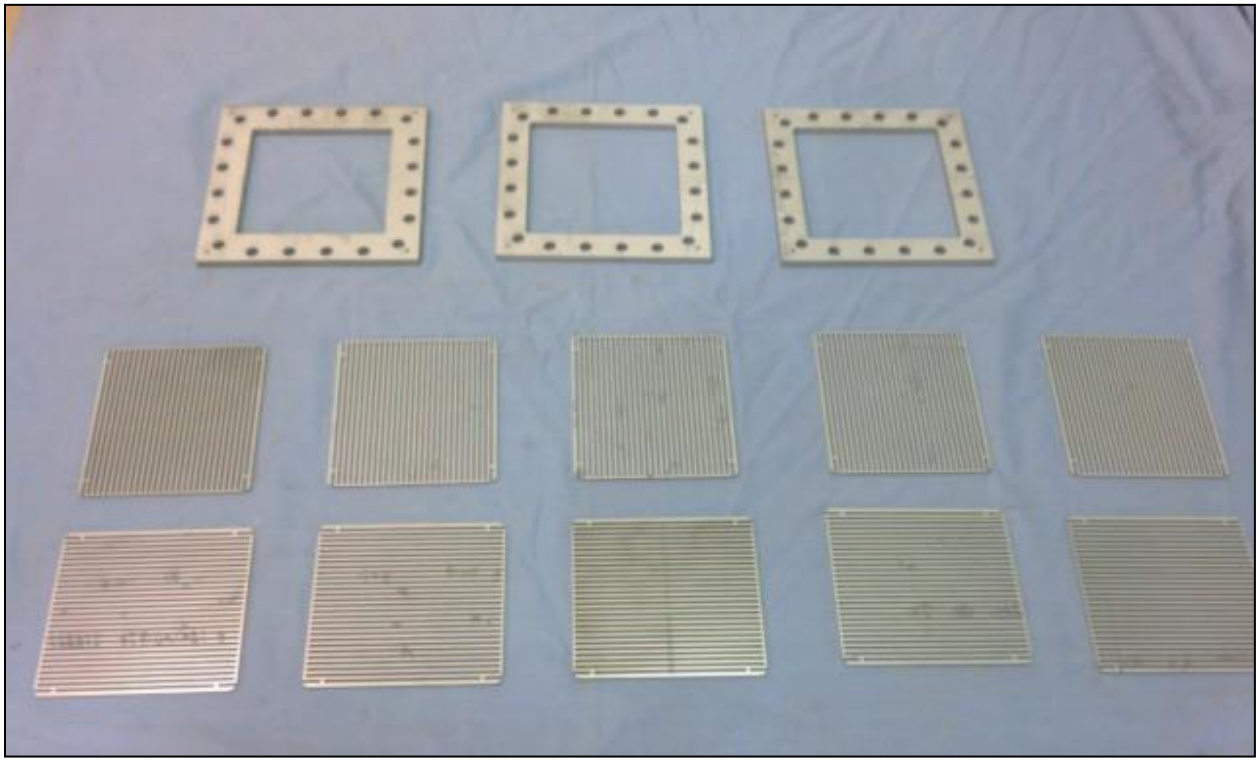

Figure 67. Machined parts of membrane module: perforated mechanical supports and reactor covers.

Machining of the first set of reactor frames and covers has been completed. After the material was roughed out with a water jet, they were surface ground to assure parallelism. Then a special fixture was made which utilized the same hole locations for bolts to simulate the clamping and distortional forces put upon the body so that the machined sealing surfaces would not be distorted in actual use in the actual set up. This will also ensure repeatability in the upcoming modules to be machined. Figure 68 show the first machined set of membrane module with a special fixture.

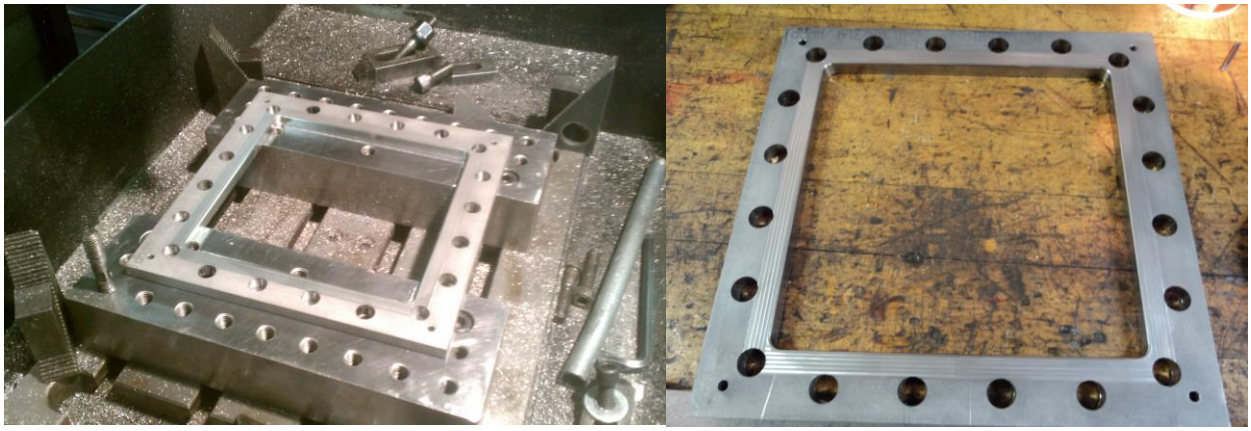

Figure 68. Module cover with special fixture.

Due to the importance of membrane sealing, a spring energized seal was considered. Figure 69 shows the sealing located on body of membrane module. Also, copper gaskets were cut and are ready for testing (see Figure 70).

Figure 69. Module body with a spring energized seal.

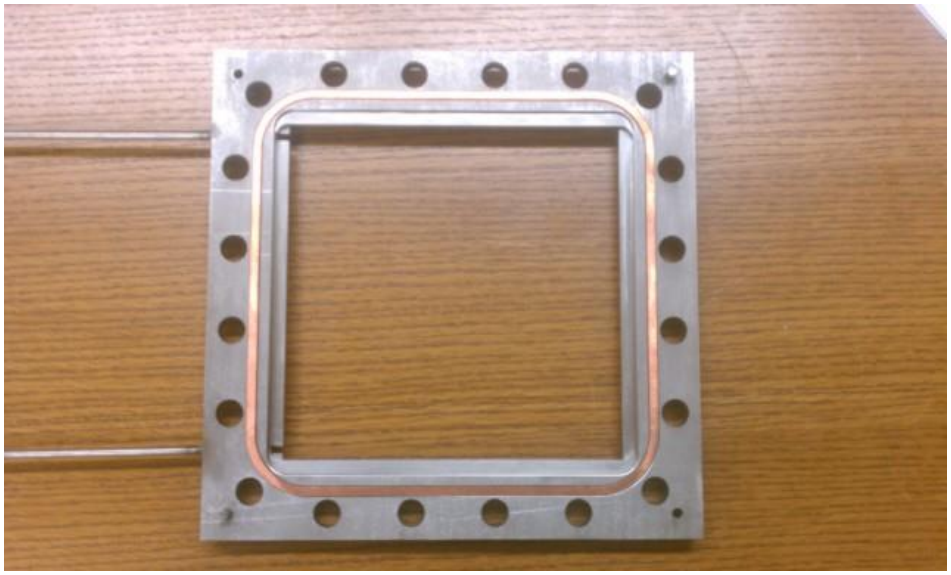

Figure 70. Module body with a copper gasket.

Membrane module fabrication was stopped due to the No Go decision.

**Task 4.3 Testing of a bench scale biomass gasification membrane reactor (Phase 1)**

*Task 4.3 Objective:* The bench scale biomass gasifier constructed in Task 3 will be commissioned as part of this subtask. The required amounts of biomass feedstock will be procured and prepared for feeding to the gasifier. The membrane module will then be installed to the gasifier unit.Initially the membrane module will be close-coupled next to the gasifier for ease of installation. Post test analysis of the membrane will be conducted. Catalysts may not be incorporated into the support system of the selected membrane at this stage of testing. GTI will prepare a detailed test plan and conduct the testing. For the testing in this subtask, air instead of oxygen will be used first as an oxidant for the biomass gasifier. Enriched oxygen-blown operation may be tested depending on the readiness of an oxygen supply system or bottled gases for the gasifier. The targeted duration of operation is 8 hours or longer for this task.

The focus of this initial testing activity is on the issues of particulate erosion on the membrane, material compatibility of the membrane module in the close-coupled mode, and other operation issues that may appear. Improved design and operation protocol will be developed to address all the issues at the end of this task.

Due to No Go decision no work was done.

**Task 5. Integrated testing of best candidate membrane with gasifier**

Due to No Go decision, GTI didn't perform this task. To approach this task, following plans were made.

**Subtask 5.1 Design of membrane module configuration (Phase 1)**

The general approach in this task is similar to subtask 4.1. If the same membrane material as in Task 4 is selected for this task, an improved version of the membrane module will be designed. If the membrane materials are different, a new design of the membrane module will be developed. A better module design is expected from the valuable experience learned in the initial integrated testing of Task 4.

Although this task is mainly focused on the module design for a bench scale membrane gasification reactor that is to be tested in subtask 5.3, design considerations will also include future commercial fabrication methods and scale-up issues.

**Subtask 5.2 Membrane module fabrication (Phase 1)**

Based on the results from subtasks 1.1, 1.2, and 1.3, the optimal membrane material selected in subtask 1.5 will be fabricated into a module.

The module will be sized for integration with the bench scale biomass gasifier. All the required hardware such as support frame, casing, loading device, insulation, pipes, fittings, etc. will be specified and procured. The unit will be tested first before it is connected to the bench scale biomass gasifier.

**Subtask 5.3 Testing of a bench scale biomass gasification membrane reactor (Phase 2)**

The objective of this task is to demonstrate direct hydrogen production from the biomass gasifier and confirm the technical feasibility of the membrane gasification reactor concept. GTI will prepare a detailed test plan and conduct the testing. Tests will be conducted at pressures from 10 atm up to 30 atm. The gasifier may be operated in oxygen-blown mode, in addition to the air-blown operation. It is anticipated that both close-coupled membrane operation followed by in-situ reactor operation will be tested. Hydrogen production rate will be optimized by adjusting the gasifier operating conditions, steam/oxidant feed rates, biomass feed rates, sweeping gas flow rates for the non-permeable gas, etc. Detailed mass and energy balances will be developed when the system reaches steady-state operation. Post-test analysis for the membrane material will be conducted. The performance data and operating experience will be used to optimize the selected membrane material in subtask 1.6, and module design. For demonstration purposes, a commercial wood-filled pellet will be used as the biomass fuel for its superior handling characteristics. The gasifier will be able to process approximately 2-10 kg/hr of biomass for hydrogen production. The targeted duration of operation is 24 hours or longer.

**Task 6. Project management and reporting (All Phases)**

This task is devoted to the overall technical, fiscal and administrative management of the proposed project. The major activities include coordination and communication with the project team members, preparation of the Progress Reports, Annual Reports, Topical Reports and other Annual Project Review information. GTI, as the prime contractor, will have the responsibility for all the required project deliverables.

**Management Accomplishments**

- Made project status presentation at DOE Annual Hydrogen Meeting 2008 in Washington DC
- Hosted kick-off meeting for project participants at GTI headquarters in Des Plaines, IL
- Provided project input for annual hydrogen report
- Generated quarterly reports to DOE
- Distributed Quarterly Project reports to project partners and maintained contact to provide updates on project progress
- Initiated and coordinated a project review meeting in Chicago to review initial candidate membranes.
- Participated in DOE Peer Review Meeting 2010 in Washington DC
- Provided input for DOE Annual Report
- Presented membrane status update for Hydrogen Production Technical Team Meeting at Argonne National Laboratory and toured their laboratory facilities at DOE request
- Participated in DOE Peer Review Meeting 2011 in Washington, DC.
- Submitted report for 2010 Annual Progress Report for the DOE Hydrogen Program
- Submitted Milestone reports for Task 4.1 “Membrane Module Design“and Task 2 “Process Development & Economic Analysis”.
- Initiated and coordinated a project review meeting in Chicago to review Go/No Go decision.

## CONCLUSIONS

The main conclusions from the project are:

From all synthesized membranes (glass, ceramic and metallic), the best membrane is $Pd_{80}Cu_{20}$ alloy membrane. $Pd_{80}Cu_{20}$ showed a flux of 47.2 SCFH/$ft^2$. It has a good thermal, mechanical and chemical stability. But the membrane performance is still lower than DOE targets.

Based on H2A analysis, results indicated a $1.96 cost per gge (in comparison, the future PSA case yielded a $2.00/gge) $H_2$ based on a 5µm thick Pd-Cu membrane. In comparison, the future PSA case yielded a $2.00/gge $H_2$.

## REFERENCES

1. http://www.hydrogen.energy.gov/h2a_production.html
2. X. Qi and Y.S. Lin, Electrical conduction and hydrogen permeation through mixed proton-electron conducting strontium cerate membranes, Solid State Ionics 130 (2000) 149.
3. C. Zuo, S.E. Dorris, U. Balachandran, M. Liu, Effect of Zr-doping on the chemical stability and hydrogen permeation of Ni-$BaCe_{0.8}Y_{0.2}O_{3-\alpha}$ mixed protonic-electronic conductor, Chem Mater 18 (2006) 4647.
4. Shelby, J.E., and J. Vitko, Hydrogen Transport in a machinable Glass-Ceramic, *Journal Of Non-Crystalline Solids*, *45* (1), 83-92, 1981.
5. Tuzzolo, M.R., and J.E. Shelby, Hydrogen-Induced Formation of Colloids of Arsenic, Antimony, and Bismuth in Oxide Glasses, *Journal Of Non-Crystalline Solids*, *143* (2-3), 181-190, 1992.
6. Shelby, J.E., *Handbook of Gas Diffusion in Solids and Melts*, 240 pp., ASM International, 1996.
7. Chun, S.Y., K. Shinozaki, and N. Mizutani, Electrically active grain boundaries in ZnO varistors by liquid-infiltration method, *Journal Of Materials Science-Materials In Electronics*, *11* (1), 73-80, 2000.
8. Juradoegea, J.R., A.E. Owen, and A.K. Bandyopadhyay, Electronic Conduction In Basalt Glass And Glass-Ceramics - Correlation With Magnetite Crystallization, *Journal Of Materials Science*, *22* (10), 3602-3606, 1987.
9. Yoshino, T., M.J. Walter, and T. Katsura, Connectivity of molten Fe alloy in peridotite based on in situ electrical conductivity measurements: implications for core formation in terrestrial planets, *Earth And Planetary Science Letters*, *222* (2), 625-643, 2004.
10. Das, G.C., T.K. Reddy, and D. Chakravorty, Electro-Conducting Glass-Ceramics Produced By Ion-Exchange And Reduction Treatments, *Journal Of Materials Science*, *13* (10), 2211-2216, 1978.
11. Conzone, S.D., U.O. Hafeli, D.E. Day, and G.J. Ehrhardt, Preparation and properties of radioactive rhenium glass microspheres intended for in vivo radioembolization therapy, *Journal Of Biomedical Materials Research*, *42* (4), 617-625, 1998.
12. Borisov, A. Y., Lahaye, and Palme, H., *American Mineralogist*, ***89 (4),*** 564, 2004.

13. Capobianco, C. J., and Drake, M. J., *Geochimica Et Cosmochimica Acta*, **54 (3)**, 869, 1990.

14. Rindone, G. E., Rhoads, J. L., *Journal of the American Ceramic Society*, **39 (5)**, 173, 1956.

15. Schreiber, H. D., Harville, T. R., and Damron, G. N., *Journal of the American Ceramic Society*, **73 (5)**, 1435, 1990.

16. Burggraaf, A.J. and Cot, L. (Eds), Fundamentals of Inorganic Membrane Science and Technology, Elsevier, Amsterdam (1996).

17. Hsieh, H.P. Inorganic Membranes for Separation and Reaction, Elsevier, Amsterdam (1996)

18. S.Adhikari and S.Fernando, "Hydrogen Membrane Separation Techniques", Ind Eng Chem Res (2006) 45, P875.

19. Shu J., Grandjean B.P.A., Van Neste A., Kaliaguine S., "Catalytic Pallaium-Based Membrane Reactors: A Review", The Canadian Journal of Chemical Engineering 69 (1991) 1036-1060.

20. Kulprathipanja A., Alptekin G.O., Falconer J.L., Way J.D., "Effects of water gas shift gases on Pd-Cu alloy membrane surface morphology and separation properties", Ind.Eng.Chem.Res.2004,43, 4188-4198.

21. Mardilovich P.P., She Y., Ma Y.H.,"Defect-free palladium membranes on porous stainless-steel support", AIChE, 44 (1998) 310-322.

22. Roa F., Block M.J., Way J.D., "The influence of alloy composition on the H2 flux of composite Pd-Cu membranes", Chem. Eng. Sci. 54 (1999) 3369-3377.

23. S.E. Nam, K-H Lee, "Hydrogen separation by Pd alloy composite membranes: introduction of diffusion barrier", J. Mem Sci. 192 (2001) 177

24. Shih, D.S., Robertson, I.M., and Birnbaum, H.K., *Acta Metall*, ***26*** **(1),** 111, 1988.

25. Shih, D. S., Birnbaum, H. K., *Scripta Metall*., **20,** 1261, 1986.

26. Spath, P., Aden, A., Eggeman, T., Ringer, M., Wallace, B., and Jechura, J., "Biomass to Hydrogen Production Detailed Design and Economics Utilizing the Battelle Columbus Laboratory Indirectly-Heated Gasifier," NREL/TP-510-37408, May 2005.